UNIVERSITI TEKNOLOGI MARA

LACCASE IMMOBILIZATION IN ZEOLITIC IMIDAZOLATE METAL-ORGANIC FRAMEWORKS FOR WATER MICROPOLLUTANT REMOVAL VIA BIOCATALYSIS AND ADSORPTION

AMIRAH SYAKIRAH BINTI ZAHIRULAIN

MSc

June 2026

UNIVERSITI TEKNOLOGI MARA

LACCASE IMMOBILIZATION IN ZEOLITIC IMIDAZOLATE METAL-ORGANIC FRAMEWORKS FOR WATER MICROPOLLUTANT REMOVAL VIA BIOCATALYSIS AND ADSORPTION

AMIRAH SYAKIRAH BINTI ZAHIRULAIN

Thesis submitted in fulfilment
of the requirements for the degree of
Master of Science
(Chemical Engineering)

Faculty of Chemical Engineering

June 2026

CONFIRMATION BY PANEL OF EXAMINERS

I certify that a Panel of Examiners has met on 10 December 2025 to conduct the final examination of Amirah Syakirah binti Zahirulain on her Masters of Science thesis entitled "Laccase Immobilization in Zeolitic Imidazolate Metal-Organic Frameworks for Water Micropollutant Removal via Biocatalysis and Adsorption" in accordance with Universiti Teknologi MARA Act 1976 (Akta 173). The Panel of Examiners recommends that the student be awarded the relevant degree. The Panel of Examiners was as follows:

Najmiddin Yaakob, PhD
Associate Professor
Faculty of Chemical Engineering
Universiti Teknologi MARA
(Chairman)

Harumi Veny, PhD
Senior Lecturer
Faculty of Chemical Engineering
Universiti Teknologi MARA
(Internal Examiner)

Nabila A. Karim, PhD
Senior Lecturer
Cell Fuel Institute
Universiti Kebangsaan Malaysia
(External Examiner)

PROFESSOR DR HJH ZURAEDA IBRAHIM
Dean
Institute of Postgraduates Studies
Universiti Teknologi MARA

Date: 11 June 2026

AUTHOR'S DECLARATION

I declare that the work in this thesis was carried out in accordance with the regulations of Universiti Teknologi MARA. It is original and is the results of my own work, unless otherwise indicated or acknowledged as referenced work. This thesis has not been submitted to any other academic institution or non-academic institution for any degree or qualification.

I, hereby, acknowledge that I have been supplied with the Academic Rules and Regulations for Postgraduate, Universiti Teknologi MARA, regulating the conduct of my study and research.

Name of Student	:	Amirah Syakirah binti Zahirulain
Student ID. No.	:	2021358645
Programme	:	Master of Science (Chemical Engineering) – EH750
Faculty	:	Chemical Engineering
Thesis Title	:	Laccase Immobilization in Zeolitic Imidazolate Metal-Organic Frameworks for Water Micropollutant Removal via Biocatalysis and Adsorption
Signature of Student	:	……..
Date	:	June 2026

ABSTRACT

The increasing presence of micropollutants in aquatic environments, originating from diverse industrial sources, poses severe risks to human health, animal life, and ecosystems, even at trace concentrations. Enzyme-based biocatalysis offers a promising green strategy for mitigating these contaminants due to enzymes' high selectivity and ability to catalyze specific reactions without generating harmful by-products. However, the practical application of free enzymes is often limited by their instability under environmental stressors such as extreme pH and temperature, which leads to denaturation and reduced catalytic performance. To address these challenges, this study investigates the *in-situ* encapsulation of laccase from Trametes versicolor within metal–organic frameworks (MOFs), specifically Zeolitic Imidazolate Frameworks (ZIF-8, ZIF-67, and ZIF-7). Aqueous-based synthesis was employed, replacing conventional organic solvents with water, thereby emphasizing a green and sustainable approach to MOF fabrication. The crystallization of ZIFs followed a common pathway involving rapid coordination of metal cations (Zn^{2+} or Co^{2+}) with imidazolate linkers, nucleation, and subsequent crystal growth governed by metal-to-ligand ratios. This process enabled simultaneous enzyme encapsulation during framework formation, yielding L@ZIF composites. Characterization using FESEM, XRD, FTIR, TGA, BET, and particle size analysis confirmed distinct morphologies, with truncated rhombic dodecahedra in ZIF-8 (1:16), leafy and rod-like crystals in ZIF-67 (1:8 and 1:12), and amorphous spheres in ZIF-7 across all ratios. Laccase loading efficiencies were 65.44% for L@ZIF-8, 81.01% for L@ZIF-67, and 70.74% for L@ZIF-7, where high loading is crucial for maximizing catalytic activity and material efficiency. Enzyme kinetics of free laccase, determined via Hanes-Woolf plot using ABTS as substrate, showed K_m = 0.27 mM and V_{max} = 0.0031 mM/min, indicating slight low substrate affinity and catalytic turnover to the relative literature, serving as benchmarks to evaluate the performance of the immobilized counterparts. The adsorption rate for ZIF-8 and ZIF-67 was typically faster at the beginning of the adsorption process and started to level off after 240 min (58.1% for ZIF-8 and 6.3% for ZIF-67). The sorption kinetic data for both ZIF-8 and ZIF-67 was observed fitted to the pseudo-first-order kinetics model ($R2 > 0.91$). ZIF-8 obeyed the Langmuir isotherm model adsorption behaviour, while ZIF-67 Freundlich followed model. These results indicates that ZIF-8 go through monolayer adsorption in homogenous surface while ZIF-67 undergoes multilayer adsorption. Biocatalytic performance tests revealed that L@ZIF-8 achieved over 90% methylene blue degradation within four weeks, surpassing other composites. L@ZIF-8 have higher methylene blue removal compared to its pristine; 92.31% and 85.81% respectively after 4 weeks. Meanwhile, L@ZIF-67 have lower methylene blue removal of 48.78% compared to pristine of 53.36% due to enzyme high confinement that reduce the enzyme reaction. This study establishes a sustainable synthesis route for enzyme-MOF composites using water as a green solvent, avoiding hazardous organic systems. By combining high enzyme loading more than 60% and preserved catalytic activity up to 92% when encapsulate in ZIF, the findings demonstrate the potential of aqueous-synthesized enzyme-MOF composites as eco-friendly and efficient materials for micropollutant remediation, contributing to global sustainability goals such as SDG 6 (Clean Water and Sanitation) and SDG 12 (Responsible Consumption and Production).

ACKNOWLEDGEMENT

In the name of Allah, The Most Gracious and The Most Merciful.

All my praises and gratitude are to Him for giving me perseverance and patience throughout this master's journey and with His will, allowing me to complete a long and challenging master's successfully.

Secondly, my gratitude and thank you to my supervisor Assoc. Prof. Ir. Ts. Dr. Fauziah Marpani for her advice, knowledge, and financial support along the way in finishing this master's. My appreciation also to my co-supervisors, Assoc. Prof. Ts. Dr. Nik Raikhan Nik Him and Prof. Ts. Dr. Norazah Abd Rahman for their encouragement and support.

My appreciation also goes to the Faculty of Chemical Engineering, Faculty of Mechanical Engineering, and Faculty of Civil Engineering, Universiti Teknologi MARA for the support and assistance of staff and technicians in preparing and analyzing the sample in completing the research. My gratitude to Mr. Jefri Saman from Alma Resources for his assistance in preparing the FESEM result. Special thanks to my colleagues and friends for helping and giving courage in completing this master's.

Finally, this thesis is dedicated to my husband, Dr. Luqmannulhakim Mohammad Ikhram, and my daughter, Sumayyah Luqmannulhakim for knowledge, and physical, understanding and moral support. This thesis is also dedicated to my parents; Zahirulain Mohamed Anuar and and parents-in-law; Mohammad Ikhram Ishak and for their encouragement, financial support, and determination to educate me. This piece of victory is dedicated to all of you. Alhamdulilah.

TABLE OF CONTENTS

LIST OF TABLES

LIST OF FIGURES

LIST OF ABBREVIATIONS

Abbreviations

ABTS	2,2'-azino-bis(3-ethylbenzothiazoline-6-sulfonic acid)
AOP	Advanced Oxidation Process
BET	Brunauer-Emmett-Teller
BIEX	Biological Ion Exchange
BPA	Bisphenol A
CPA	Carboxypeptidase A
Cu-BDC	Copper-benzene-1,4- dicarboxylic acid
DEA	Diethanolamine
DMF	Dimethylformamide
E-MOF	Enzyme-Metal Organic Framework
EE2	17α-ethynylestradiol
FESEM	Field Emission Scanning Electron Microscopy
FTIR	Fourier Transform Infrared Spectroscopy
GOx	Glucose Oxidase
HRP	Horseradish Peroxidase
IEX	Ion Exchange
MB	Methylene Blue
MOF	Metal-Organic Framework
OpdA	Organophosphohydrolase

OPP	Orange Peel Peroxidase
PFO	Pseudo-First Order Model
PSO	Pseudo-Second Order Model
TGA	Thermogravimetric Analysis
XRD	X-ray Diffraction
ZIF	Zeolitic Imidazolate Framework
ZIF-L	Zeolitic Imidazolate Framework-Leaf like Structure

LIST OF NOMENCLATURES

Nomenclatures

K_m	Michaelis Menten Constant
V_{max}	Maximum Rate of Enzyme Reaction
V_o	Initial Rate of Enzyme Reaction
K_1	Pseudo-First Order Constant (1/min)
K_2	Pseudo-Second Order Constant (g/mg.min)
qe	Amount of the Adsorbate Adsorbed by Adsorbent at Equilibrium (mg/g)
qt	Amount of the Adsorbate Adsorbed by Adsorbent at Relative Time (mg/g)
Ce	Final Concentration of the Adsorbate (mg/L)

CHAPTER 1
INTRODUCTION

1.1 Research Background

The increasing presence of micropollutants in aquatic systems, largely originating from industrial discharges and anthropogenic activities, has become a pressing global concern due to their persistence and bioactivity even at trace concentrations (ng L^{-1}–µg L^{-1}) (Zdarta et al., 2022). Compounds such as endocrine-disrupting chemicals (EDCs), pharmaceuticals, pesticides, and personal care products have been widely detected in surface waters and groundwater, where chronic exposure has been associated with carcinogenicity, endocrine disruption, genetic perturbations, and ecological imbalance (Kim & Zoh, 2016). Their high chemical and thermal stability render them recalcitrant to conventional treatment technologies (Tarigan et al., 2025; H. Zhang et al., 2021). Current methods including adsorption (Guillossou et al., 2020; Marszałek et al., 2022), advanced oxidation processes (Dogruel et al., 2020; Liang et al., 2019), ion exchange (Chu et al., 2023), and membrane separation (Aldana et al., 2024), can effectively reduce micropollutant concentrations but often face significant drawbacks, such as secondary waste generation, limited substrate selectivity, and performance inhibition in the presence of natural organic matter (Rego et al., 2021). These limitations highlight the urgent need for alternative, selective, and sustainable water treatment strategies.

Enzyme-based catalysis has emerged as a promising solution due to the inherent chemo-, regio-, and stereoselectivity of enzymes, which enable the transformation of water micropollutants into specific and typically non-toxic products without undesirable by-products (Mu et al., 2020). Laccase (EC 1.10.3.2), a multicopper oxidase derived from Trametes versicolor, contain four copper ions which are responsible for the oxidation of a wide spectrum of phenolic and non-phenolic pollutants, including bisphenol A, triclosan, dyes and pharmaceutical residues (Arregui et al., 2019; Bilal, Iqbal, et al., 2019). The enzyme is widespread in nature and found in plants, fungi, insects, yeast and bacteria (Shraddha et al., 2011). Due to their broad substrate scope and ability to produce water as the only co-product laccases are considered potential biocatalysts for industrial processes in the food and textile industry, synthetic chemistry

and bioremediation (Mayolo-Deloisa et al., 2020; Moreno et al., 2020). Nevertheless, the practical application of free enzymes is limited by their instability in complex environments, as fluctuations in pH, temperature, and ionic strength readily induce denaturation and activity loss (da Silva et al., 2012; Kabir & Ju, 2023).

To increase the enzyme robustness for the purpose, Laccase is encapsulated within metal organic framework (MOF) (Han et al., 2022). Also known as porous coordination polymers (PCP), MOF is a porous, crystalline material constructed from the coordination of organic ligands and metal clusters (Zhou et al., 2012). Due to the wide spectrum of organic linkers with varying size and structure, the properties and architecture of MOFs can easily be controlled and thereby provide perfect carrier materials for various enzymes (Mehta et al., 2016; Rogacka & Labus, 2024). Comprehensive justifications of MOF as a host matrix for Laccase includes (Hu et al., 2018; X. Wang et al., 2020): 1) The high surface area and porosity facilitate a high loading of enzyme, especially for the fact that many MOFs with large cavities; 2) MOFs exhibit open architectures. Substrates and products can transport from the pores, so encapsulated enzyme could interact with external environment; 3) The metal nodes, ligands as well as topological structures of MOFs are with high variety; 4) Various active groups can be uniformly distributed both in the pore and on the surface of MOFs, which could interact with enzymes to eliminate or reduce their leaching; 5) The high crystallinity of MOFs provides defined networks and clear structural information, which is critical when investigating the interaction/mechanisms with guest molecules. The encapsulation should result in enzyme-MOF composites with size dependent substrate specificity, improved thermal and process stability and prolonged retention of catalytic ability (X. Wang et al., 2020). Additionally, enzyme-MOF materials can easily be retrieved by centrifugation or filtration and are thereby usable as heterogeneous catalysts, preventing protein contamination of the samples (Knedel et al., 2019).

Recent advances in MOF synthesis have emphasized the replacement of toxic organic solvents such as N,N-dimethylformamide (DMF) and dimethylacetamide (DMA) with greener alternatives, particularly water, to improve sustainability and reduce environmental impact (Kumar et al., 2020). Water-based synthesis not only eliminates the hazards associated with volatile organic solvents but also offers unique advantages in controlling nucleation and crystal growth through hydrogen bonding and polarity effects (Akhundzadeh Tezerjani et al., 2021). For example, ZIF-8 and other zeolitic imidazolate frameworks have been successfully synthesized in purely aqueous

systems under ambient conditions, producing high-crystallinity materials with well-defined morphologies and tunable particle sizes (Jian et al., 2015). The use of water as a solvent enables rapid and scalable MOF production while maintaining structural integrity, surface area, and porosity comparable to those obtained from conventional solvothermal approaches. Furthermore, aqueous synthesis facilitates compatibility with biomolecules, making it particularly suitable for enzyme encapsulation strategies where mild conditions are required to preserve enzymatic activity (Kushch et al., 2024; Mahfudz et al., 2024). Thus, water-mediated MOF synthesis represents a sustainable and biocompatible pathway that aligns with green chemistry principles and enhances the feasibility of enzyme–MOF composites for water treatment applications.

In this research, three ZIFs are selected; ZIF-8, ZIF-67, and ZIF-7 due to their structural and functional relevance to micropollutant degradation and enzyme immobilization. ZIF-8, constructed from zinc ions and 2-methylimidazolate linkers, possesses sodalite topology with ~11.6 Å cages and ~3.4 Å pore apertures, offering suitable confinement for small aromatic molecules and protective microenvironments for enzymes. ZIF-67, the cobalt analogue of ZIF-8, exhibits similar topology but with distinct redox activity at the Co nodes, which can synergistically enhance the catalytic interactions of redox enzymes such as laccase. ZIF-7, composed of zinc and benzimidazolate linkers, is a flexible framework with dynamic gate-opening behavior that allows selective uptake of aromatic micropollutants, particularly those with larger molecular dimensions. Importantly, all three ZIFs can be synthesized in water without organic solvents, aligning with sustainable green chemistry principles.

The integration of enzymes with MOFs, leading to enzyme–MOF (E-MOF) composites, has recently gained momentum as a transformative platform for water purification. Immobilization techniques, including adsorption, covalent attachment, and in-situ biomimetic mineralization, enable the encapsulation of enzymes within MOFs while preserving their native conformations (Mehta et al., 2016). These E-MOFs exhibit enhanced tolerance to extreme pH and temperatures, improved storage stability, and recyclability over multiple catalytic cycles. Recent advances demonstrate that E-MOF systems combine the adsorptive preconcentration of pollutants by MOFs with the selective degradation activity of enzymes, offering dual-function remediation. For example, laccase@ZIF-8 composites have shown significantly improved bisphenol A degradation efficiency and operational stability compared to free laccase (Sun et al., 2023). Furthermore, E-MOF composites have been successfully integrated into

continuous-flow reactors and catalytic membranes, demonstrating long-term activity and high micropollutant removal efficiency under realistic conditions.

Building on these advances, the present study focuses on the aqueous synthesis of ZIF-8, ZIF-67, and ZIF-7 at varying metal-to-ligand ratios, followed by immobilization of laccase from *T. versicolor*. The resulting L@ZIF composites are thoroughly characterized in terms of physicochemical and thermal properties and enzyme loading. Their adsorption and enzymatic kinetics are systematically investigated, alongside their degradation performance against representative micropollutant, methylene blue. This approach aims to provide a sustainable, efficient, and scalable strategy for clean water reclamation, offering a new perspective on the integration of MOF-based materials with biocatalysis for environmental remediation.

In summary, this research is significant as it pioneers the integration of enzyme biocatalysis with green-synthesized MOFs to address the pressing issue of micropollutant removal. The development of laccase–MOF composites not only enhances catalytic stability and recyclability but also promotes the sustainable production and reclamation of clean water, reducing dependence on conventional treatment methods that often generate secondary waste. By advancing eco-friendly material synthesis and high-efficiency pollutant degradation, the study directly supports global sustainability efforts, particularly SDG 6 (Clean Water and Sanitation), SDG 12 (Responsible Consumption and Production), and SDG 14 (Life Below Water).

1.2 Problem Statement

The widespread presence of micropollutants in water bodies, including dyes, pharmaceuticals, and agrochemicals, has become a pressing environmental concern due to their persistence, toxicity, and resistance to conventional wastewater treatment methods. Among these, methylene blue is frequently studied as a model dye pollutant because of its environmental relevance and chemical stability. Even at trace levels, methylene blue can adversely affect aquatic ecosystems and human health, underscoring the need for innovative treatment strategies that are both sustainable and efficient (Oladoye et al., 2022).

Enzyme-based biocatalysis has emerged as a promising alternative to conventional treatment technologies, offering high selectivity, mild operating conditions, and eco-friendly degradation pathways. Laccase, a multicopper oxidase, is

particularly attractive due to its ability to catalyze the oxidation of a wide range of phenolic and non-phenolic pollutants, including dyes such as methylene blue, into less harmful or mineralized products. However, the industrial application of laccase remains limited because the free enzyme suffers from poor operational stability, susceptibility to denaturation under changing pH and temperature, and difficulties in recovery and reuse (Chen et al., 2022). These challenges necessitate the development of robust immobilization strategies to preserve enzyme activity.

Metal–organic frameworks (MOFs), and more specifically Zeolitic Imidazolate Frameworks (ZIFs), have recently been explored as advanced supports for enzyme immobilization due to their tunable porosity, high surface area, and chemical robustness (X. Wang et al., 2020). ZIFs not only provide a protective microenvironment for enzymes but also exhibit inherent adsorption capabilities, which may synergistically enhance pollutant removal. Importantly, synthesizing ZIFs in aqueous media represents a unique green chemistry strategy, eliminating the reliance on toxic organic solvents and aligning with sustainable material development (Kumar et al., 2020). However, despite these advantages, several knowledge gaps persist: the optimal synthesis and characterization of ZIFs for laccase encapsulation, the adsorption–desorption kinetics of pollutants on pristine MOFs, and the catalytic performance of enzyme–MOF composites in dye degradation remain insufficiently understood. Addressing these challenges is crucial to bridging the link between adsorption-driven removal and biocatalytic degradation, thereby advancing the design of efficient, sustainable enzyme–MOF systems for micropollutant treatment.

1.3 Objectives of the Study

The main objective of this research is to find better L@ZIF in biocatalysis from various concentration ratio of metal to organic ligand of ZIF. The specific objectives are drawn out based on the main objective.

a) To synthesize a tailored Zeolitic Imidazolate Framework (ZIF) and its L@ZIF composite, and to systematically characterize their structural and physicochemical properties.

b) To evaluate the enzyme kinetics of free laccase and L@ZIFs & adsorption behaviour of pristine ZIF through adsorption kinetic and isotherm analysis.

c) To assess the catalytic performance of the L@ZIF composite in degrading methylene blue.

1.4 Scope and Limitation of the Study

The scope and limitation in this research are outlined by several considerations. The synthesis formulation of the MOF is based on the established procedure that reported in the literature. The concentration ratios of the metal ions to organic ligand of the MOF are varied at 1:8, 1:12 and 1:16 to evaluate their influence on the framework formation. During the synthesis, ZIF-8 and ZIF-67 were synthesized at room temperature and ZIF-7 was synthesized at 35 °C, which is close to room temperature. Only commercial enzyme with control concentration were utilized in this research during synthesis of all E-MOFs to secure consistency.

The physiochemical and thermal properties of MOFs and E-MOFs were characterized by using X-ray Diffraction (XRD), Fourier-Transform Infrared Spectroscopy (FTIR), and Thermogravimetric Analysis (TGA). Their morphology, particle distribution, surface area was examined by using Field Emission Scanning Electron Microscopy (FESEM), Brunauer–Emmett–Teller (BET) analysis, and particle size analysis. The enzyme loading of the E-MOFs is determined by using UV-Vis spectrophotometer. The enzyme kinetics of free laccase and E-MOFs were determined using a UV-Vis spectrophotometer. Same with enzyme kinetics, the adsorption kinetics of the MOFs were analyzed with the same UV-Vis spectrophotometer technique. Finally, the biocatalytic reduction of E-MOFs were analyzed by using methylene blue as model substrate for duration of four weeks.

1.5 Significance of Study

The significance of this research lies in advancing sustainable solutions for water pollution management through the integration of biocatalysis and advanced material design. By encapsulating laccase within Zeolitic Imidazolate Frameworks (ZIFs), the study addresses the major limitations of free enzymes, particularly their poor stability under fluctuating environmental conditions. The resulting enzyme–MOF

composites are expected to demonstrate improved robustness, recyclability, and prolonged catalytic activity, thereby offering an efficient and eco-friendly alternative to conventional water treatment technologies. Unlike physical adsorption or advanced oxidation processes, which often require harsh operating conditions and generate secondary waste, the enzyme–MOF approach facilitates selective biotransformation of micropollutants into less harmful compounds under mild conditions. This not only enhances treatment performance but also minimizes resource consumption and operational costs, aligning with the principles of green chemistry and sustainable engineering.

From a broader perspective, the outcomes of this research contribute directly to global sustainability agendas by promoting safe, clean, and affordable water treatment technologies. The adoption of water-based MOF synthesis further reinforces the eco-compatibility of the system, reducing reliance on hazardous organic solvents and enabling scalable, green production routes. Importantly, the development of enzyme–MOF composites supports the production and reclamation of clean water by enabling the reuse of treated wastewater, thus reducing freshwater extraction and alleviating stress on natural water bodies. By combining environmentally benign synthesis with high-efficiency pollutant degradation, the study supports United Nations Sustainable Development Goals (SDGs), particularly SDG 6 (Clean Water and Sanitation) by enabling access to clean water and promoting water reuse, SDG 12 (Responsible Consumption and Production) through green material synthesis, and SDG 14 (Life Below Water) by mitigating the ecological risks of persistent micropollutants. Thus, this research not only advances scientific understanding of enzyme–MOF composites but also aligns with urgent societal needs for sustainable clean water production, reclamation, and resilient purification strategies. This study also supporting Malaysian policy on water pollution in Environmental Quality Act 1974, Department of Environmental and The National Standard for Drinking Water Quality, Ministry of Health.

CHAPTER 2
LITERATURE REVIEW

2.1 Micropollutant in Water

Issues regarding micropollutants emerge rapidly as various industries operate these days (Zdarta et al., 2022). Micropollutants are organic or synthetic chemical contaminants that can be detected in very low concentrations, in the range of microgram per liter (μg/L) to nanogram per liter (ng/L) (Kim & Zoh, 2016; Yang et al., 2022). Micropollutants are commonly anthropogenic chemicals (chemicals produced from human activity) that come from pharmaceuticals, personal care products, industrial chemicals, and pesticides (Zdarta et al., 2022). Examples of micropollutants are antibiotics, hormones, painkillers, dyes and pigments, fragrances, insecticides, cosmetics, herbicides, solvents, plastics, estrogenic compounds, thyroid disruptors, and androgenic compounds that come from various sources of industries (Zdarta et al., 2022).

Urbanization causes emerging a huge amount of micropollutants in the environment and ecosystem (Mutzner et al., 2022). This is because of the high dependence on the products and lack of education in managing the products and their waste (Zulkifli & Abd Manaf, 2024). Micropollutants that come from wastewater treatment give the highest contribution (El Hammoudani et al., 2024; Santhi et al., 2012). Due to their high stability, and high resistance to physiochemical degradation, micropollutants are difficult to remove from water and wastewater even in low concentrations (Zdarta et al., 2022; H. Zhang et al., 2021). Micropollutants can change their chemistry as surroundings and temperature change due to their active molecules (Belete et al., 2023). Micropollutants easily pass into surface water, groundwater, and marine water and thus the water that contains micropollutants can go into the human body and ecosystem such as marine and soil (Zdarta et al., 2022).

Figure 2.1 show the micropollutant compounds such as estradiol & equivalent, bio-& pesticides, and pharmaceuticals chemical compound having a low concentration that below microgram per liter (μg/L) (red line) (Stamm et al., 2016). Even though, the concentration is low (which make up a very tiny fraction of the organic matter), can have a huge impact on the biological system of humans and the environment (Stamm et

al., 2016). J. Zdarta et al. (2022), stated the impact of the micropollutant in every source toward human and marine health (Zdarta et al., 2022). Li Y. et al (2023) reported the impact of the micropollutant on oxidation stress, DNA damage, organ dysfunctions, metabolic disorder, immune response, neurotoxicity, reproductivity and development toxicity in cells, organoids and animals. (Li et al., 2023).

Every source of the micropollutants can give various negative biological impact to human and other organisms as stated in Table 2.1. The antibiotics, hormones and painkillers that come from pharmaceutical interfere the cell development, inhibit growth, disrupt hormones control such as feminine hormone especially in fish (Patel et al., 2019; H. Wang et al., 2021; Zdarta et al., 2022). Personal hygiene products such as fragrances, dye, and cosmetics lead to human cancer, harming reproductive or development system and endocrine disruption (Chaturvedi et al., 2021; Johnson et al., 2022; H. Wang et al., 2021). The table also outline the industrial chemicals including solvents, plastics and dyes or pigments, trigger human's asthma, allergic, and causing eyes watery (Chowdhary et al., 2020; Rovira & Domingo, 2019; Zdarta et al., 2022). This industrial chemical such dyes and pigments can causing low photosynthesis for aquatic life due to limitation sunlight penetration. Low photosynthesis causing low oxygen in water, thus lowering life duration expectancy for aquatic life (Islam et al., 2023; Zdarta et al., 2022). The pesticides consist of herbicides, insecticides and fungicides effecting human genetic disorder and physiological changes to respiratory problem (Ahmad et al., 2024; Zdarta et al., 2022). Overall, the diverse sources of micropollutant and their ecological and health impact, strengthen the importance of sustainable water treatment technologies for micropollutant removal.

Table 2.1
Example of The Micropollutants from The Sources and Its Effects

Sources	**Example micropollutants**	**Effect**	**References**
Pharmaceutical	Antibiotics Hormones Painkillers	Negative impact on embryonic cells Growth inhibition Feminine features highly developed in fish	(Chaturvedi et al., 2021; Patel et al., 2019; H. Wang et al., 2021; Zdarta et al., 2022)
Personal hygiene products	Fragrances Dyes Cosmetics	Cancer Reproductive or development harm	(Chaturvedi et al., 2021; Johnson et al., 2022; H. Wang

		Endocrine disruptor	et al., 2021)
Industrial chemicals	Solvents Plastics Dyes and pigments	Allergic skin Asthma Watery eyes Limit sunlight penetration for photosynthesis of aquatic life	(Chowdhary et al., 2020; Islam et al., 2023; Rovira & Domingo, 2019; Zdarta et al., 2022)
Pesticides	Herbicides Insecticides Fungicides	Human genetic disorder Physiology changes that affect life expectancy Respiratory problem	(Ahmad et al., 2024; Dhankhar & Kumar, 2023; Kumar et al., 2019; Zdarta et al., 2022)

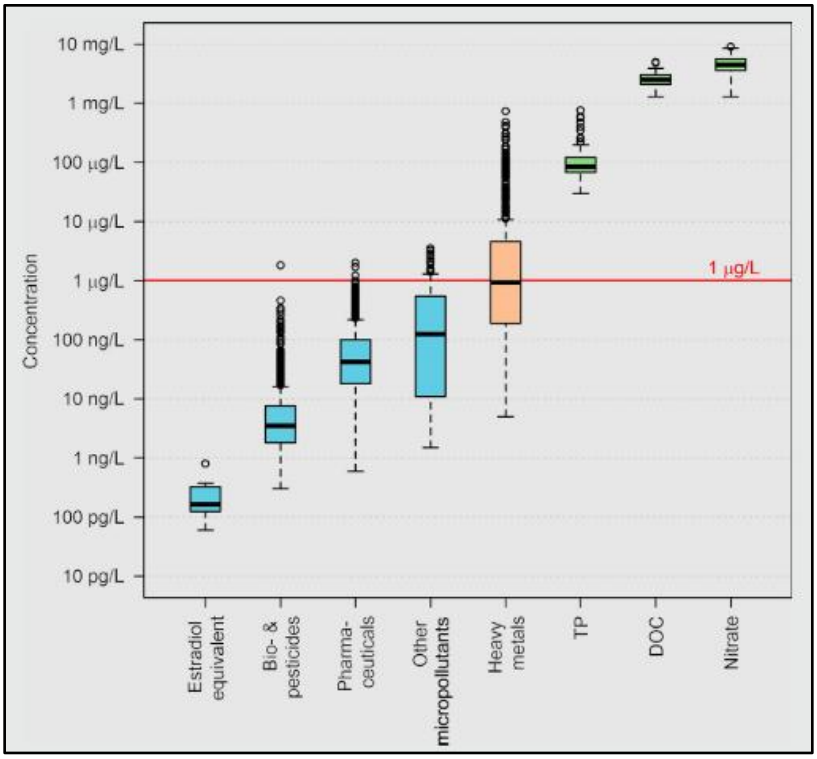

Figure 2.1 The Concentration of The Pollutants

Note/Source: Unravelling The Impacts of Micropollutants in Aquatic Ecosystems: Interdisciplinary Studies at The Interface of Large-Scale Ecology (Stamm et al., 2016). Reprinted with permission from Elsevier.

2.2 Conventional Treatment of Water Micropollutant

There are many methods for treating the micropollutant in water and wastewater (Bhatt et al., 2022; Gulia et al., 2024). These reliable methods of micropollutant

treatment are commonly used to reduce the micropollutant to the permissible limit before release to the water bodies (Rego et al., 2021). Figure 2.2 shows the method used in treating the micropollutant in water. This section will discuss the overview of each of the methods for treating the micropollutant in water.

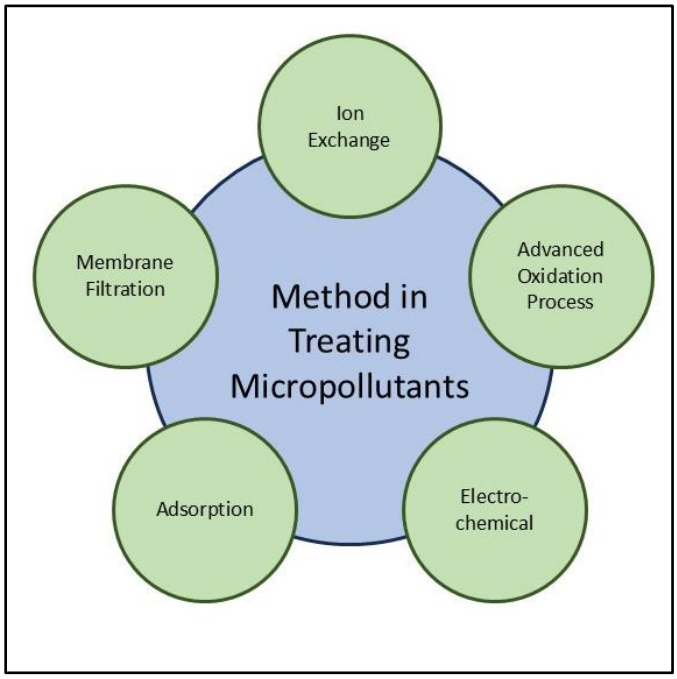

Figure 2.2 Method in Treating Micropollutant

Adsorption is a physio-chemical method in removing micropollutants. That are many materials that used as adsorbents; carbo-based (activated carbon), carbon nanotube, and hydroxides-based. Activated carbon is a porous carbon structure with a high surface area. Its characteristics of porosity and hydrophobic, help in adsorbing a significant number of impurities from water. Activated carbon is cost effective, easy operation and high removal efficiency. There are two types of activated carbon; powdered (PAC) and granule carbon (GAC). Activated carbon is also versatile by adsorbing various types of water micropollutants by using one type of activated carbon (powdered activated carbon) (Sher et al., 2021). A study by Guillossou R. et al. (2020) stated that the adsorption of the organic micropollutants by PAC can be disrupted with the presence of the dissolved organic matter (Guillossou et al., 2020). Mailler R. et al. (2016) stated that the activated carbon structural characteristic give impact to the adsorption efficiency (Mailler et al., 2016). They also stated that the presence of the FeCl2 did not give negative impact to the adsorption process.

Carbon nanotube (CNT) is also common material that use adsorption method in reducing the micropollutant. The characteristic of CNT that high porosity and and tuneable make it one of the favourable materials. There are two types of the carbon nanotube (CNTs); i) single-walled CNTs, which are formed by rolling a single graphene sheet into a cylinder, and ii) multi-walled CNTs, which consist of multiple concentric rolled graphene cylinders (Solorio-Rodriguez et al.). Nowadays, CNT are combined with membrane or CNT based membrane to improve the usage efficiency (Heo et al., 2011; Khan et al., 2021). CNT-based membrane is modified with bentonite can remove more than 90% of the zinc and lead (Marszałek et al., 2022). Instead of using for adsorption, CNT also being used in electrochemical method with combination of membrane (Chu et al., 2023; Liu et al., 2024). Diclofenac, anti-inflammatory medicine and one of the micropollutant from pharmaceutical industry can be reduce by using modified CNT based membrane (CeO2-N@CNT-based membrane) using electrocatalytic method (Chu et al., 2023).

Ion exchange is a method in exchanging ions with other ions by using ion exchange resin; an insoluble material that can substitute desire ions; cations or anions. In removing micropollutant, the ions from the ion exchange resins release to the water and the micropollutant bind to the resin. Most of the researcher use cation exchange resins in heavy metal removal (Bhatt et al., 2022). These days, not only synthetic resins used in water treatment, but biological ion exchange also used in promoting the environmental friendly process (Liu et al., 2022). Biological Ion Exchange (BIEX), a combination of ion exchange resins and microbe used in remove micropollutant like atrazine and thiamethoxam (Liu et al., 2022). Trihalomethane (THM) reduced more than 50% by using different kinds of anion exchange resins (Li et al., 2021). A hybrid system of IEX and membrane can removed various type of the micropollutant such as paracetamol and ketoprofen (Devaisy et al., 2023).

Advanced oxidation process (AOP) is a water treatment that goes through a chemical process by using oxidants such as ozone, hydrogen peroxide, or ultraviolet to generate hydroxyl radicals to remove organic and sometimes inorganic compounds. These radicals compound oxidating the toxic micropollutant. The drawback, in chlorination of sewage, this reaction can produce unwanted disinfection by-products such as halo-acetic acid and trihalomethane which these chemicals are cytotoxic and genotoxic (Han et al., 2021). Liang J. et al. (2019) reported that using AOP by combining ultrasound-Mn(II) in sludge in degrading 3,3′-dimethoxybenzidine (Liang et

al., 2019). Wang B. et al. (2024) using method of nanobubble-based AOP in reducing 98% of Rhodamine B (Wang et al., 2024).

Ozonation and UV-based AOP also under the same method of AOP; produce radicals' compound in removing micropollutant. The ozonation process uses ozone to become ozone radicals in treating micropollutants in water. The ozonation is one part of the advanced oxidation process but the ozonation specifically uses ozone as an oxidation agent in water treatment (Bhatt et al., 2022). Dogruel S. et. al (2020) reported that they use ozonation process in treating secondary waste treatment, reduced 55% of the micropollutants at original ozone pH (Dogruel et al., 2020). Malvestiti J. et al. (2019) use combination of metal ion and ozonation process in inactivation the microorganisms and pesticide removal (Malvestiti et al., 2019). However, the presence of the organic matter quantity give impact on the ozonation performance (van Gijn et al., 2022).

Ultraviolet based Advanced Oxidation Processes (UV-based AOP) is a process under AOP which the ultraviolet light combines with other oxidants of AOP like ozone, hydrogen peroxide and chlorine in treating micropollutant (Hübner et al., 2024). This UV irradiation will make the oxidants become radicals and the oxidation process take place by oxidizing substrate by oxidant radicals (Hübner et al., 2024). For example, UV is used to produce hydroxyl radicals (from hydrogen peroxide) in treating real wastewater that contain up to 30 chemical compound of pharmaceutical (Cibati et al., 2022). But some of the wastewater hindering UV from photo reacting the H_2O_2. Wang C. et al. (2019) use combination of UV and chlorine of UV based AOP in reducing 12 micropollutant from local wastewater treatment plant's water (C. Wang et al., 2019). But the some wastewater compound can reduce the UV fluence in converting oxidants to radicals which can reduce the micropollutant reduction (Yin et al., 2024).

Electrochemical oxidation is a process in treating micropollutant by using electricity in producing oxidant and/or reductant. The redox of the reaction happen at anode and cathode which anode go through electrochemical oxidation in reducing micropollutant and/or cathode go through electrochemical reduction in reducing by products (Gamoń et al., 2024; Yang & He, 2025). Yang K. and He Z. conducted the study of the electrochemical oxidation and electrochemical reduction simultaneously of the wastewater by reducing micropollutant from anode and byproducts from cathode (Yang & He, 2025). The metal use for the electrode plays roles in reducing the micropollutant. For example, boron-doped diamonds (BDD) electrodes are commonly

used in electrochemical oxidation as it is hardly to fouling (Barrios et al., 2015; Barrios et al., 2016; Gamoń et al., 2024).

Membrane separation is a process that use a semi-permeable material with induced pressure in filtering the water from certain or selected compound in physically or chemically properties (Ezugbe & Rathilal, 2020). There are many types of membrane used in membrane separation process especially in treating micropollutant such as ultrafiltration, microfiltration and nanofiltration (Aziz et al., 2024; Ezugbe & Rathilal, 2020). Aldana J. et al. (2024) conducted study on micropollutant rejection by using ultrafiltration and nanofiltration membrane with combination of pretreatment of PAC and/or coagulation-flocculation (Aldana et al., 2024). They found that straightforward ultrafiltration membrane gives the best adsorption of organic micropollutants (Aldana et al., 2024). There are also various types of materials used as membrane such as ceramics, silica and polymers (Ezugbe & Rathilal, 2020). Nowadays, the membrane also used in hybrid with other method like combining electrochemical with membrane and adsorption process with membrane (Aldana et al., 2024; Khan et al., 2021; H. Li et al., 2024). Li H. et al. (2024) stated a few configurations of the electrochemical anionic oxidation based-membrane system in removing micropollutant; flow-by and flow-through for electrochemical configuration and using flat sheet and hollow fibre membrane in the combination (H. Li et al., 2024).

In conclusion, these conventional methods have significantly good results in treating water micropollutants. On the other side, these methods also have limited effectiveness in reducing micropollutants. There are methods such as ion exchange that selective with the pollutants and methods of adsorption and membrane separation process that produce secondary waste that needs to retreat again.

2.3 Overview of Enzyme-Metal-Organic Framework (E-MOF) for Enzymatic Remediation

Metal-Organic Framework (MOF) is a porous crystal material that consist of metal ions and coordinating organic linkers (Wang & Astruc, 2020; Yusuf et al., 2022). Most of the organic linker that make MOF structure are carboxylate linker. There are thousands type of MOFs synthesized up todays research such as, Zeolitic Imidazolate Framework (ZIF), Universitetet I Oslo (UiO), Hong Kong University of Science and Technology (HKUST) and Porous Coordination Network (PCN) (Yusuf et al., 2022).

Furthermore, these MOF can be synthesized in various method such as hydrothermal/solvothermal, microwave, sonochemical, mechanochemical and electrochemical (Raptopoulou, 2021; Yusuf et al., 2022). In this study, the MOF, specifically ZIF is synthesis in one-pot synthesis by using water as solvent at room temperature and pressure. The MOF characteristics of high porosity, high surface area and stable in thermal and chemical condition give huge benefit in applications such as absorption, catalysis, sensor and biological and medical usage (Ahmadi et al., 2021; Ding et al., 2019). Xu G. et al. (2021) reported that bulk MOF can remove heavy metals such as lead, chromium and mercury (G. R. Xu et al., 2021). Rego R. et al. (2021) reported the ability of various MOF in water remediation from various pollution such as heavy metals, dyes, and antibiotics (Rego et al., 2021).

Table 2.2 show the summary of various MOFs with their synthesis method and applications across biomedical, environmental, sensing, and food technology. This table demonstrates the different preparation routes such as solvothermal, hydrothermal, electrochemical and one-pot synthesis which tailored to achieve functional properties and applications. For biomedical application, NO@HKUST-1 is synthesized by using water-ethanol mixture under liquid nitrogen condition has reported for diabetic wound healing (P. Zhang et al., 2020). There are several MOFs that shown in the table below to be applied in food technology. For example, Ag-MOF@CS and curcumin-loaded MIL-101@CMFP are utilized to extend fruit shelf life and food preservation, respectively. In sensing and detection applications, UiO-66-NH_2 through electrochemical synthesis and UiO-66 synthesized by solvothermal method demonstrate effective performance in fluorescence and hydrogen peroxide detection, highlighting the microporous MOF that increasing the chemical detection (Huang et al., 2021; Zhang et al., 2022). The table also illustrates the effectiveness of MOFs in environmental remediation. In pharmaceutical contaminant removal, Zr-MOF-NH_2 and Cu(II)-MOF are employed for adsorption of ibuprofen and diclofenac sodium (Alkhathami et al., 2023; Liu et al., 2019). Meanwhile, MIL53(Al)@TiO_2 is used to remove naproxen via photodegradation (Murtaza et al., 2022). The addition of TiO_2 in MOF enhances the pharmaceutical contaminant through photocatalysis. Meanwhile, gelatin/UiO-66-NO2 has been used for Pb(II) removal from apple juice (W. Yang et al., 2021). In energy related application, Ce-MOF-808 and MOF-5 is used for aqueous-based supercapacitor and nanogenerator respectively (Shaukat et al., 2022; Shen et al.,

2021). Overall, this Table show broad applications of MOFs with synthesis strategy and structural functional.

Zeolitic Imidazolate Framework (ZIFs) is one family type of the MOF synthesized. ZIFs as its name, constructed by using imidazolate ligand and various type of metal ion. Zinc, cobalt, copper, iron and nickel are some of the metals that used in the ZIFs. ZIFs characteristic of high porosity, high surface area, tuneable pore, stable in various chemical dan thermal condition, give ZIFs a lot of application such as gas storage, catalysis, environmental remediation, drug delivery and enzyme immobilization (S. Chen et al., 2023; Ebrahimipour et al., 2025; Nazir et al., 2025; Sankar et al., 2020; Tran et al., 2011).

Table 2.2
MOF and Its Applications

MOF	**Synthesis Method**	**Application**	**References**
NO@HKUST-1	Mixture water & ethanol as solvent in -60℃ of liquid nitrogen	Diabetic wound healing	(P. Zhang et al., 2020)
UiO-66-NH_2	Electrochemical	Fluorescence detection	(Wei et al., 2019)
Ce-MOF-808	Solvothermal	Aqueous-based supercapacitor	(Shen et al., 2021)
UiO-66	Solvothermal	H_2O_2 detection	(Q. Wang et al., 2021)
Zr-MOF-NH_2	Hydrothermal	Ibuprofen adsorption	(Alkhathami et al., 2023)
MIL-53(Al)@TiO2	Infiltration of TiO2 into ready-made MIL-53(Al)	Naproxen photodegradation	(Murtaza et al., 2022)
Cu(II)-MOF	One-pot synthesis at 120℃	Adsorption diclofenac sodium	(Liu et al., 2019)
Gelatin/UiO-66-NO_2	Solvothermal	Remove Pb(II) in apple juice	(W. Yang et al., 2021)
MOF-5	Hydrothermal	Electric nanogenerator	(Shaukat et al., 2022)
Ag-MOF@CS	One-pot synthesis at 50℃	Fruit shelf life	(Zhang et al., 2022)
Curcumin-loaded into MIL-101@CMFP	Infiltration curcumin to MIL-101@CMFP (through one pot synthesis at 50℃)	Food preservation	(Huang et al., 2021)

Enzyme is a biocatalyst that consists of protein molecules that use in biochemical reaction. Enzyme is a greener catalyst as it promotes regio- and specific selectivity reaction, which produce specific product without side products that need to remove and treated. Like chemical catalyst, enzyme can be reuse until its structure altered (can be degraded or denatured) that causing loss of the enzyme's catalytic capability due to the harsh surrounding such as high temperature and extreme pH levels or presence of molecules that disturbed the enzyme's molecules. The presence of the inhibitors that blocking the enzyme's active site also can reduce the enzyme capability in catalyst the substrate. Every enzyme in this world has categorises based on their reaction in the Enzyme Commission number (E.C), which have 7 classifications (oxidoreductase, transferases, hydrolases, lyases, isomerases, ligases and trasolases).

Laccase is one of the many enzymes that presence in this world. Laccases is a metal-contain enzyme which contain 4 copper atoms in 1,4-benzenediol, which show as oxygen oxidoreductase (EC 1.10.3.2) (one type of the enzyme reaction). The laccase that can oxidase without mediator and work as electron acceptor (Chen et al., 2022). Laccases commonly use in industries such as pulp and paper, textile, food and bioremediation (Mayolo-Deloisa et al., 2020; Moreno et al., 2020; Zhu et al., 2011). Laccase works as an oxidase, polymer degrader, and participate in cross-linking of monomer and cleaving the aromatic ring compound. Therefore, laccase can oxidase phenolic and non-phenolic compound (Upadhyay et al., 2016). Laccase is one of oxidoreductase enzymes that commonly use in reducing micropollutants especially pharmaceutical products, make it highly demand for enzymatic reduction (Bilal et al., 2022; Chen et al., 2022; Sharma et al., 2023).

The each of the four copper atoms in laccase play main roles in biocatalysis as shown in Figure 2.3 (Arregui et al., 2019). These metals are categorized into 3; T1 (Cu1 - one atom), T2 (Cu2 - one atom) and T3 (Cuα3 & Cuβ3 - two atoms). T1 works as oxidation agent for the substrate and T2 and T3 works as reduction agent for the oxygen to turn into water. The electron is move from the substrate to the T3 copper atoms. The T3 copper atom move the electron to the T2 copper atom to donate the electron to the oxygen to produce water (Arregui et al., 2019). Laccase which oxidoreductase, oxidase the compounds (commonly substrate) by moving the electron to the oxygen to reduce it into water (Arregui et al., 2019). The oxidised substrate later goes for cleavage or demethylation into less- or nontoxic product.

Even though laccase widely needed in the industries, laccase sometimes need mediator to effective biocatalysis, low stability in complex environment and highly production cost for high uses (Chen et al., 2022). Immobilization of laccase is one of the solutions in overcome the laccase limitations (Chen et al., 2022).

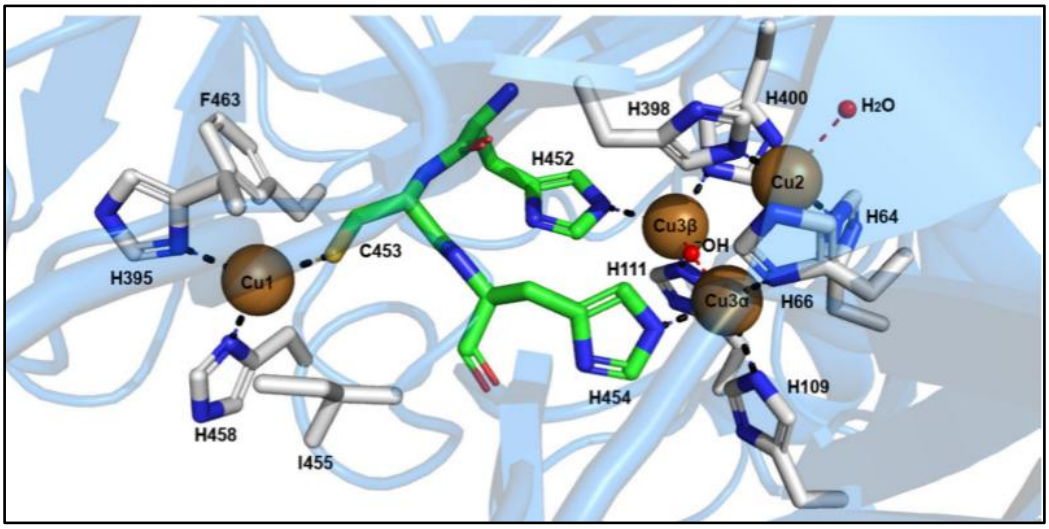

Figure 2.3 The Copper Position in Laccase Structure

Note/Source: Laccase: Structure, Function, and Potential Application in Water Bioremediation (Arregui et al., 2019). Open Access.

The incorporation of enzyme and MOF produces an Enzyme-Metal-Organic Framework (E-MOF). This combination is done by immobilizing the enzyme to the MOF which works as a platform matrix for the enzyme (S. Liu et al., 2021). There are several methods for immobilizing the enzyme to the MOF as shown in Figure 2.4; i) adsorption, ii) chemical linking, iii) *in situ* encapsulation, and iv) infiltration (Bilal, Adeel, et al., 2019; Han et al., 2022).

Adsorption method goes through physical immobilization which enzyme adsorb on the ready-made MOF and rely on the weak interaction like Van Der Waals and electrostatic interaction to "hook" on the MOF (Han et al., 2022). Infiltration also goes through physical immobilization like adsorption but with ready-made mesoporous MOF which the enzyme easily diffuses into the MOF (adsorption happen with microporous MOF) (Han et al., 2022). Chemical linking method is using functional additives such as EDC/NHS and glutaraldehyde (GA) that work with carboxyl group from MOF linker to produce carbodiimide binding. This chemical will "glue" the enzyme to the MOF (Han et al., 2022). In-situ encapsulation is the only method that

immobilized the enzyme with MOF during MOF synthesis (Han et al., 2022).

In this research, *in situ* encapsulation is used in immobilizing the enzyme to MOF. *In situ* encapsulation or by another name, one-pot synthesis is where metal ions, organic ligands, and enzymes are added together, and synthesis occurs in one pot/container. *In situ* encapsulation method is the only method where the synthesis of MOF and enzyme immobilization occurs simultaneously. The other methods like adsorption, chemical linking, and infiltration, the MOF is synthesized first, and the enzyme is immobilized to ready-made MOF. *In situ* encapsulation method is helpful to the enzyme in maintain its structure and activity by providing barrier and block the fragile enzyme segment from high temperature, inhibitors, and various pH (X. Wang et al., 2020; Xia et al., 2020). The MOF structure that porous make the only substrate reach to the enzyme active site without bring out the enzyme to the surrounding (Liang & Liang, 2020).

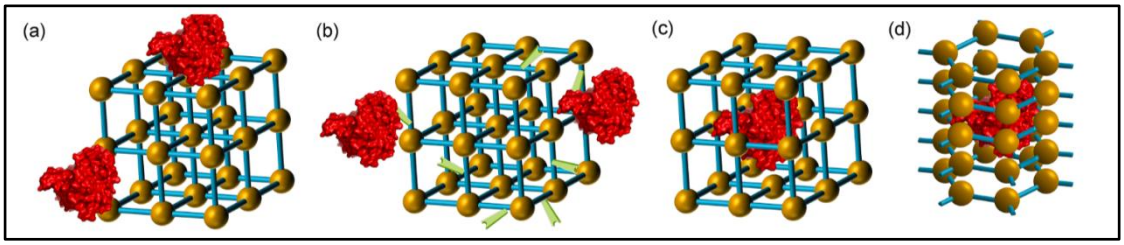

Figure 2.4 Enzyme Immobilization Method; a) Adsorption, b) Chemical linked, c) *In situ* Encapsulation and d) Infiltration

Note/Source: Metal-Organic Frameworks (MOFs): A Novel Platform for Laccase Immobilization and Application (Han et al., 2022). Reprinted with permission from Elsevier.

2.3.1 Green Synthesis Approach

The green synthesis approach in synthesis MOF getting the eye of the researchers as today's target in improving the environment situation toward minimum pollution and better health (Dai et al., 2021; Kumar et al., 2020). This green synthesis approach is one of the 12 principles of green chemistry as it covers less hazardous chemical synthesis, safer solvents & auxiliaries, energy efficiency, renewable feedstock, waste prevention, and degradable final product (Julien et al., 2017; Kumar et al., 2020). Furthermore, in reducing the micropollutant by using enzymes which safer and biologically catalyzed, the MOF that is used together with the enzyme (becoming

E-MOF) also needs to go through environmentally safe synthesis. This approach is suitable for medical and environmental applications (Binaeian et al., 2023).

Attentions are given to some parameters when constructing green MOF; i) solvents, ii) metal ions, and iii) organic linkers. In this research, water is used as a solvent in the synthesis of MOF and E-MOF. Traditionally, MOFs are synthesized by using organic solvents such as dimethylformamide (DMF), methanol, and N,N-diethylformamide (DEF). Gao J. and team (2020) used DMF in synthesizing ZIF-7 before immobilizing it to the membrane (Gao et al., 2020). Ta D. et al. (2018) used methanol in constructing nano-ZIF-8 with high yield (Ta et al., 2018). Albeit these chemicals are common in MOF synthesis, these organic solvents are dangerous to the environment. Water is safe, readily available, cheap, and the simplest post-synthesis method. Yang C. and team synthesized MIL-100(Fe) (C. Yang et al., 2021). This green synthesis powder can adsorb tetracycline hydrochloride, an antibiotic up to 72% (C. Yang et al., 2021). Diab K. et al. (2021) synthesized MIP-202 bio-MOF (using organic bio-ligand) in deionized water in hydrothermal method to be used as dye adsorbent (Diab et al., 2021).

This approach is also suitable especially for enzyme immobilization on/in MOF by one-pot synthesis/ *in situ* encapsulation method. This is because harsh solvents such as organic solvents can reduce the enzyme activity (Kushch et al., 2024; Mahfudz et al., 2024).

The Table 2.3 represents a list of MOFs that synthesized using water or water-based solvent systems, highlighting on the environmentally benign and sustainable routes. Deionized water or water mixed with mild acids such as acetic or formic acid is employed as the primary solvent, replacing conventional toxic solvent (Nimbalkar & Bhat, 2019; Shortall et al., 2022). Furthermore, small amounts of mild acids in water help in metal-ligand coordination as desired applications (hierarchically porosity) (Yuan et al., 2017). Hydrothermal synthesis is commonly used method as reflecting its suitability for aqueous system and its ability to promote crystal growth. In addition, one-pot synthesis approaches are reported for several MOFs, showing simplified and scalable preparation strategies.

The table shows the water-synthesized MOFs exhibited diverse and practical applications. MOF-303, CAU-23 and MOF-801 are highlighted for water harvesting, indicating the environmentally friendly synthesis does not compromise functional performance (Aghajani Hashjin et al., 2023; Zheng et al., 2023). Al-MOF have

anticancer properties that can use for cancer treatment (Zeraati et al., 2021). As MOFs characteristics of high porosity and high surface area; thus, MOFs have good capability in adsorption for removal and recovery of chemical compound. For example, PNC-25-Fe and Fe-MIL-127 are applied in toxic gas capture, sulphur dioxide and ammonia (Chen et al., 2020). Sr-MOF and UiO-66-NO_2 demonstrated adsorption capabilities for organic compound and dyes (Chen et al., 2019; Ibrahim et al., 2021). Meanwhile, Bio-MOF that synthesize in water is reported for vitamin B recovery (Pérez-Cejuela et al., 2020). Overall, these water-based MOFs can achieve high functionality while aligning with green chemistry principles, making them particularly attractive to environmental, biomedical, adsorption and water related applications.

Table 2.3
List of MOF that Synthesis with Water as Solvent

MOF	Solvent	Synthesis Method	Application	Reference
MOF-303	Deionized water	Hydrothermal	Water harvesting	(Zheng et al., 2023)
CAU-23	Deionized Water	Hydrothermal	Water harvesting	(Zheng et al., 2023)
UiO-66$(COOH)_2$	Water & acetic acid mixture	Hydrothermal	-	(Nimbalkar & Bhat, 2019)
PCN-25-Fe	Water & acetic acid mixture	Hydrothermal	Toxic gas capture	(Chen et al., 2020)
Fe-MIL-127	Water & acetic acid mixture	Hydrothermal	Toxic gas capture	(Chen et al., 2020)
UiO-66-NO_2	Water & acetic acid mixture	One-pot synthesis at 100℃	Water & ethanol adsorption	(Chen et al., 2019)
Al-MOF	Deionized water	Hydrothermal	Anticancer treatment	(Zeraati et al., 2021)
ZIF-zni	Water & sodium acetate mixture	One-pot synthesis	-	(Shortall et al., 2022)
MOF-801	Water/formic acid mixture	One-pot synthesis	Water harvesting	(Aghajani Hashjin et al., 2023)
Sr-MOF	Deionized water	Hydrothermal	Crystal violet adsorption	(Ibrahim et al., 2021)
Bio-MOF	Water	Hydrothermal	Vitamin B recovery	(Pérez-Cejuela et al., 2020)

2.3.2 Enzyme-Metal-Organic Framework (E-MOF) Application on Water Micropollutants

Integrating enzyme with MOF becoming E-MOF give enzyme a new level in promoting the enzyme activity. This E-MOF help in combating the micropollutant as these micropollutants give negative impact toward humans' health, animals and ecosystem (Zdarta et al., 2022). The function of the MOF in the integration of the E-MOF is to protect the enzyme from changes of its conformation due to extreme condition, different pH and elevated temperature since the MOF itself is robust in that condition (Han et al., 2022). The conformation changes of the enzyme can cause the degradation of the enzyme, thus reduce the enzyme biocatalysis of the substrate.

Table 2.4 summarises the recent application of E-MOF for removal and degradation of water micropollutant from various sources by highlighting the type of MOF support, type of enzyme immobilized, enzyme immobilization strategy, target pollutant, and E-MOF degradation efficiency. This table is providing an overview of hybrid E-MOFs systems have been developed as advanced materials for micropollutant remediation.

This table demonstrate that oxidoreductase enzymes, particularly laccase and horseradish peroxidase (HRP) are the most widely employed toward water micropollutant removal due to their strong catalytic ability toward phenolic compounds, dyes, endocrine-disrupting chemicals and pharmaceuticals. For example, HRP-based MOFs demonstrated high performance by achieving up to 100% for 2,4-dichlorophenol and attain up to 98% for BPA removal (Gao et al., 2023; Y. Liu et al., 2021; S. Xu et al., 2021). Laccase-based E-MOFs were employed for the removal of reactive dyes, estrogen (EE2) and phenolic compounds such as 2,4-dichlorophenol, with efficiencies typically ranging from 81% to 96% and obtained up to 100% for BPA removal, indicating strong catalytic activity and suitability for endocrine-disruptor removal (Amari et al., 2021; Peng et al., 2021; Rybarczyk et al., 2025; Wu et al., 2019; Yang et al., 2023; R. Zhang et al., 2020). Multi enzyme such as HRP/GOx@NZIF-7, also included, indicating the potential of synergistic catalytic pathways to enhance pollutant degradation (Babaei et al., 2023).

Various immobilizations method is reported, including *in-situ* encapsulation, adsorption, chemical linking, infiltration, coprecipitation and metal-ion affinity interaction. In-situ encapsulation is frequently used and generally yield high

degradation efficiencies (80%-100% removal) because enzyme is protected within the MOF pores, enhancing enzyme stability against pH, temperature and solvent effects. For example, laccase@HKUST-1 achieved complete degradation of BPA (100%) (R. Zhang et al., 2020). Chemical linking provides covalent attachment, reducing enzyme leaching and improving the reusability (Mahmoodi & Abdi, 2019; Y. Zhang et al., 2021). Meanwhile, adsorption is a simpler method in enzyme immobilization but effecting in enzyme leaching due to weak interaction from purely physical adsorption system. For example, degradation of 2,4-dichlorophenol and Reactive Black 5 achieve 87% and 81% respectively after immobilizing laccase via adsorption (Amari et al., 2021; Wu et al., 2019). Organophosphorus degradation obtains 89.26% after OpdA go through adsorption immobilization on MIL@88A (Xue et al., 2019). Coprecipitation of CPA with PVP to ZIF-8 for ochratoxin A degradation only attain 71.37% which might be due to the substrate limitation by capping agent during synthesis (Ma et al., 2020). Advanced approaches such as metal-ion affinity interactions (100% degradation 2,4-dichlorophenol) can further enhance enzyme loading and catalytic stability (Gao et al., 2023).

The table further illustrates that E-MOFs are effective against a wide range of micropollutant such as synthetic dyes (Reactive Deep Green KE-4BD, Acid Blue 92 and Reactive Black 5), pesticides (organophosphorus), endocrine disruptor (BPA and EE2), pharmaceutical (2,4-dichlorophenol) and mycotoxin (ochratoxin A) with degradation efficiencies exceeding 80%.

Overall, this table highlights the versatility of E-MOF as hybrid biomaterials that integrate high enzyme catalytic selectivity with MOFs features of high surface area, tunable porosity and stable structure. These E-MOFs attributes make it promise candidates for advanced water treatment applications targeting persistent micropollutant.

Table 2.4
E-MOF Applications Towards Water Micropollutants

E-MOF	Enzyme	Immobilization Method	Application	Degradation	Reference
LAC@Cu-ZIF-90	Laccase	In-situ encapsulation	Reduction of reactive deep green KE-4BD	73%	(Yang et al., 2023)
FL@ZIF-8 (PA)	Laccase	Infiltration	Reduction BPA	90.28%	(Sun et al., 2023)
HRP@ZIF-8	HRP	In-situ encapsulation	BPA removal	98%	(S. Xu et al., 2021)
Laccase on Cu-BDC	Laccase	Adsorption	Removal estrogen (EE2)	96%	(Rybarczyk et al., 2025)
MIL-68(Al)/PVA/Lac	Laccase	Chemical linking	Decolorization of Alizarin green	95.86%	(Peng et al., 2021)
Laccase on Fe3O4-NH2@MIL-101(Cr)	Laccase	Adsorption	Removal 2,4-dichlorophenol	87%	(Wu et al., 2019)
Laccase on Fe3O4-NH2@MIL-101(Cr)	Laccase	Absorption	Removal of Reactive Black 5	81%	(Amari et al., 2021)
Laccase on ZIF-8	Laccase	Chemical linking	Acid Blue 92 removal	90%	(Mahmoodi & Abdi, 2019)
Laccase on NH2-MIL88(Fe)	Laccase	Chemical linking	Decolourization Remazol Brilliant Blue R	92%	(Y. Zhang et al., 2021)
HRP/GOx@NZIF-8	HRP & GOx	In-situ encapsulation	BPA removal	80%	(Babaei et al., 2023)
OpdA@MIL-88A	OpdA	Adsorption	Removal organophosphorus (pesticide)	89.26%	(Xue et al., 2019)
HRP-ZIF-8@P1	HRP	In-situ encapsulation	Degradation BPA	94.7%	(Y. Liu et al., 2021)
laccase@HKUST-1	laccase	In-situ encapsulation	BPA degradation	100%	(R. Zhang et al., 2020)
HRP@HP-Zr-MOF@Fe_3O_4	HRP	Metal-ion affinity interaction	Degradation 2,4-dichlorophenol	100%	(Gao et al., 2023)
CPA/PVP/ZIF-8	CPA	Coprecipitation	Ochratoxin A degradation	71.37%	(Ma et al., 2020)

The integration laccase and MOF have the commonly used materials in micropollutant removal as laccase are versatile enzyme and MOF help laccase in biocatalyst in harsh condition (Han et al., 2022). However, there still lacking in incorporation laccase with ZIF-67 and ZIF-7.

2.4 Kinetic Study of Enzyme-Metal-Organic Framework (E-MOF)

The study of enzyme kinetic is to determine the rate of enzyme biocatalysis toward substrates. The free laccase and immobilized enzyme to the MOF have different enzyme kinetics due to the interaction of the enzyme's active site and substrates. The rate of enzyme catalysis is plotted by using the Michaelis Mentens kinetics model, a model that is used to determine the biocatalysis rate. This model shows the K_m value (Michaelis Menten constant), the half of the Vmax value (the maximum rate of the enzyme biocatalysis). K_m (Michaelis Menten constant) indicates the affinity of the enzyme to the substrate. The higher the enzyme affinity, the higher the enzyme attraction to the substrate, thus highly likely to form enzyme-substrate complex and biocatalysis. Alternately to lower affinity it has a lower enzyme attraction to the substrate, thus a low tendency to form enzyme-substrate complex and biocatalysed. The equation of the Michaelis Menten model:

$$V_o = \frac{V_{max}\,[S]}{K_m + [S]} \tag{2.1}$$

From the equation (2.1), V_o is the initial reaction rate of the enzyme, V_{max} is the maximum reaction rate of the enzyme, $[S]$ is the substrate concentration, and K_m is the Michaelis Menten constant.

From the Michaelis Menten kinetic model, the graphical presentation of the enzyme kinetic is plotted. There are three types of graphical presentation of the enzyme kinetics: i) Lineweaver-Burk plot, ii) Eadie-Hofstee plot, and iii) Hanes-Woolf plot. These graphical presentations are easier to read and analyze because these graphical presentations are plotted in linear graphs compared to the Michaelis Menten model plotted in exponential graphs. In all the graphical presentations, the Lineweaver-Burk plot is the common graph that is used in presenting the enzyme kinetics.

The Lineweaver-Burk plot shows the linear equation (y=mx+c). This plot is commonly used to graphically show how the enzyme work (J. Chen et al., 2023; Ezike

et al., 2021; Isanapong et al., 2024; Panwar et al., 2023). The steeper the plot, the faster the enzyme react to the substrate and vice-versa of the plot. Equation 2.2 show the linear equation of Lineweaver-Burk plot. From this equation, the V_{max} and the K_m can be obtained from the plotted graph of 1/Vo and 1/[S].

$$\frac{1}{V_o} = \frac{K_m}{V_{max}} \cdot \frac{1}{[S]} + \frac{1}{V_{max}} \tag{2.2}$$

The table below (Table 2.5) show the reported kinetic parameters of free laccase and laccase immobilized in ZIFs, focusing on the Michaelis-Menten (K_m), maximum reaction rates (V_{max}) and experimental conditions. This table is used to compare the catalytic behaviour of free and immobilized laccase and to evaluate the impact of performance when laccase immobilization in ZIFs.

The Michaelis-Menten constant (K_m) reflects the apparent affinity of the laccase toward the substrate (in this table towards the ABTS). The table shows the wide range of K_m values of free laccase as the K_m value influenced by the buffer type, pH, temperature and substrate concentration, indicating the laccase activity is highly sensitive to environmental conditions. The K_m value often increase slightly after immobilization, suggesting a reduce apparent affinity of substrate. The contributions of this value are mass transfer limitation, diffusion resistance within MOF pores and partial shielding of active sites caused by encapsulation (Knedel et al., 2019; Rybarczyk et al., 2025). The Vmax values represent the maximum catalytic rate of the enzyme system. In this table show the Vmax values of immobilized laccase reduces compared to free laccase (Dlamini et al., 2023; Zixuan Li et al., 2024). This reduction is due to restricted enzyme mobility and diffusional barriers within MOF structure (Knedel et al., 2019; Rybarczyk et al., 2025).

Overall, this table demonstrates that ZIF immobilization alters the kinetic behaviour of laccase by increasing K_m and reducing Vmax due to the diffusion and structural constraints but significantly enhancing enzyme stability and reusability. This trade-off is considered acceptable for environmental applications as immobilized laccase provides improved operational stability and suitability for continuous wastewater treatment targeting water micropollutants.

Table 2.5
Enzyme Kinetics for Free Laccase and Immobilized Laccase in ZIF

Enzyme/E-MOF Application	Immobilization method (for E-MOF)	Km	Vmax	Condition	Reference
Laccase	-	0.18mM	0.027mM/s	0.005-1.5 M of ABTS at 40℃	(Kołodziejczak-Radzimska & Jesionowski, 2020)
	-	14.2 μM	0.0487μM/s	0-0.8 mM/L of ABTS in phosphate buffer (pH 5)	(Iriarte-Mesa et al., 2019)
	-	0.0763mM	2.635μM/min.mg	50-500 μmol/L of ABTS in acetate buffer at room temperature	(Jiang et al., 2022)
	-	0.789 mM	0.0428 mM/min	0.1-2 mM of ABTS in citrate-phosphate buffer (pH 7) at room temperature	(Dlamini et al., 2023)
	-	0.18 mM	755.5 U/mg	0.1-2 mM of ABTS in sodium acetate (pH 4.5)	(Tülek et al., 2021)
	-	0.22 mM	3.78 μM/min	0.5-2 mM of ABTS in acetate buffer (pH 6) at 30℃	(Zixuan Li et al., 2024)
L@ZIF-8	In-situ encapsulation	0.998 mM	0.0205 mM/min	0.03g of L@ZIF-8 and 0.1-2 mM of ABTS in citrate-phosphate buffer (pH 7) at room temperature	(Dlamini et al., 2023)
	In-situ encapsulation	0.08 mM	3.55 μM/min	L@ZIF that contain 20 μg laccase/mL and 0.5-2 mM of ABTS in acetate buffer (pH 6)	(Zixuan Li et al., 2024)

2.5 Adsorption Kinetics and Isotherms of Metal-Organic Framework (MOF)

Adsorption and separation are some of the MOF applications as environment remediation toward toxic and micropollutant, gas storage and separation technology (Ding et al., 2019). MOF is effectively adsorbed many types of the compounds of adsorbate, in liquids and gases (Ding et al., 2019). This is because of the characteristics of the MOF that is high porosity and surface area make it good in adsorption. Adsorption kinetics is a rate of the molecules (adsorbate) taken by the adsorbent (in this study is MOF) with taking the factor of physical and chemical processes. Meanwhile adsorption isotherm explaining the interaction of the adsorbent and adsorbate during the adsorption.

There are a few models that used in determine the adsorption kinetics: pseudo-first order, pseudo-second order, Elovich model and Linear Driving Force (LDF) approach. For MOF, pseudo-first order (PSO) and pseudo-second order (PSO) are commonly used for adsorption kinetics due to the solid-liquid adsorption interaction (Feng et al., 2016; Younis et al., 2025; Yu & Wu, 2020). For the pseudo-first order model is showing the assumption physical adsorption (physisorption), meanwhile for the pseudo-second order model is showing the chemical adsorption (chemisorption). The MOF commonly favourable in pseudo-second order as its fitting line is same or more than 0.99 compared to the pseudo-first order (Feng et al., 2016; J. Li et al., 2020; K. Li et al., 2024; Yu & Wu, 2020). The linearization of pseudo-first order in equation (2.3) and pseudo-second order in equation (2.4) are:

$$\ln(q_e - q_t) = \ln q_e - K_1 t \tag{2.3}$$

$$\frac{t}{q_t} = \frac{1}{K_2 q_e^2} + \frac{1}{q_e} t \tag{2.4}$$

Where t (min) is time, qe and qt (mg/g) is amount of adsorbate adsorbed by adsorbent at equilibrium and at time t respectively. K_1 (1/min) and K_2 (g/mg.min) are pseudo-first order rate constant and pseudo-second order rate constant, respectively. In determine the pseudo-first order model, the graph is plotted log (qe-qt) versus t meanwhile for pseudo-second order model, the graph is plotted t/qt versus t. The rate constant of pseudo-first order model (K_1) is taken from the slope of the PFO graph as -

K_1. The graph pseudo-second order graph is determined by plotting t/qt versus t. The K_2 constant is taken from the slope of the pseudo-second order graph as positive K_2.

The adsorption isotherm commonly come together with adsorption kinetics in study the interaction between adsorbate and adsorption. The characteristic of the adsorbent (pore size and surface area) and the condition of the adsorbate (concentration and pressure) is taken in determine adsorption mechanism whether monolayer or multilayer and homogenous or heterogenous. The models that used in analysed the adsorption isotherm are Langmuir isotherm, Freundlich isotherm, BET isotherm, Elovich isotherm and Toth isotherm. The Langmuir isotherm and Freundlich isotherm are common isotherms used in determine the interaction between MOF and adsorbate. The Langmuir isotherm assumes the monolayer adsorption in homogenous surface. The Freundlich isotherm assumes the multilayer adsorption The linearized equation of the Langmuir and Freundlich isotherm are shown in equation (2.5) and (2.6) respectively.

$$\frac{C_e}{q_e} = \frac{1}{K_L q_{max}} + \frac{C_e}{q_{max}} \tag{2.5}$$

$$logq_e = logK_F + \ +\frac{1}{n} logC_e \tag{2.6}$$

Ce (mg/L) is the final concentration of the adsorbate at respective time, qe (mg/g) is the amount of the adsorbate adsorb by the weight of the adsorbent. K_L (L/mg) and K_F (mg/g)(L/mg)$^{(1/n)}$ is the Langmuir isotherm constant and Freundlich isotherm constant respectively. The graph of Langmuir isotherm is determined by plotting the Ce/qe versus Ce meanwhile Freundlich isotherm graph is determined by log qe versus log Ce.

In determine the isotherm behaviour (especially for Langmuir isotherm), the dimensionless separation factor, R_L in equation (2.7) is used.

$$R_L = \frac{1}{1 + K_L C_0} \tag{2.7}$$

Which R_L show the adsorption system in the situation of irreversible (R_L=0), in favourable (0<R_L<1), linear (R_L=1) or unfavourable (R_L>1) in the Langmuir isotherm.

2.6 Biocatalytic Productivity of Enzyme-Metal-Organic Framework toward Dye

Synthetic dye is one of the micropollutant that commonly used in industry especially in textile industry (Islam et al., 2023). There are many types of dyes and their applications (Al-Tohamy et al., 2022). For examples, aniline yellow come from azo dye type used for silk and cotton, dispersed red 60 from disperse dye type used for polyamide and plastic and acid blue 78 come from acid dye type used for leather, cosmetics and wool (Al-Tohamy et al., 2022).

Dye can reduce the water quality as it can reduce the light penetration, which can reduce photosynthesis of the water plant as dye have high colour intensity albeit of the low dye concentration (Uddin et al., 2021). Furthermore, dye can also release toxic compound such as heavy metals and azo dyes (Al-Tohamy et al., 2022; Islam et al., 2023). The small dye concentration can give high colour intensity. This condition can give bad quality of the water. The higher the dye intensity can reduce the sunlight penetration, which can reduce the marine plants' photosynthesis, causing low oxygen dilution in water, make the marine animals hard to survive like fishes due to lack of oxygen and food chain disturbance (Al-Tohamy et al., 2022; Islam et al., 2023; Soni et al., 2025).

In this study, laccase is used to oxidise methylene blue to less toxic or non-toxic products. Methylene blue is one of thiazine dye, go through a few steps mechanism in laccase biocatalysis. Reduction of methylene blue can go through reaction of N-demethylation, demethylation and ring cleavage in producing various intermediates and continue to final product of less or nontoxic product (Owen et al., 2013; Sánchez-Álvarez et al., 2024; Wu et al., 2022). Methylene blue produce intermediates of azure A to azure B to azure C and to thionine through N-demethylation (Sánchez-Álvarez et al., 2024). This is the only pathway reported directly reaction of methylene blue by enzyme laccase while others using fungus that contain laccase. Possible reaction is laccase can go through sulphur oxidation of methylene blue and ring cleavage to produce intermediates (Wu et al., 2022). This intermediates go through another oxidation in produce small molecules (Wu et al., 2022). Another possible pathway of demethylation of thionine to thionol and from azure A to thionoline (Owen et al., 2013).

E-MOF one of the methods in dye remediation and has proven its effectives in dye removal as the enzyme like laccase versatile in biocatalysis various substrates.

Mahmoodi and Abdi (2019) synthesized E-MOF which integrating laccase with ZIF-8 through process chemical linking by using glutaraldehyde (GA) that use as linker in between ZIF-8 and laccase (Mahmoodi & Abdi, 2019). This E-MOF can reduce the Acid Blue 92 by 90% for duration of 120 minutes after optimized the parameters.

Orange peel peroxidase (OPP) is immobilized in the MOF (they using ZIF-8 precursors) by using in-situ encapsulation method in reducing methylene blue and congo red (Salgaonkar et al., 2019). OPP-MOF effectively reduce the methylene blue and congo red 85.6% and 89.9%, respectively even though not high as free enzyme 88.3% for methylene blue and 93.2% for congo red. These results obtained might be due to the enzyme active site being block by certain structure of the MOF, that causing the mass transfer hindering then lowering the interaction in between enzyme and substrate (in this case methylene blue and congo red).

Table 2.6
The Dye Degradation by E-MOF

E-MOF	Enzyme	Immobilization Method	Dye Type	Degradation	Concentration	Time	Reference
HRP@SOM-ZIF-8	HRP	Infiltration	Methyl Orange	80%	37.5 μM	2 minutes	(S. F. Li et al., 2020)
HRP on ZIF-8	HRP	Adsorption	Methyl Orange	60%	25 μM	2 minutes	(S. F. Li et al., 2020)
MIL-68(Al)/PVA/Lac	Laccase	Adsorption	Alizarin Green	>93%	10 mg/L	12 hours	(Peng et al., 2021)
FE_3O_2@ZIF-8-Lac	Laccase	Adsorption	Indigo carmine	90%	25 mg/L	15 minutes	(J. Wang et al., 2019)
Laccase on Fe3O4-NH2@MIL-101(Cr)	Laccase	Adsorption	Reactive Black 5	81%	5 mg/L	24 hours	(Amari et al., 2021)
laccase@MMOF	Laccase	In-situ encapsulation	Crystal violet	93%	-	20 minutes	(Ladole et al., 2020)
OPP-MOF	OPP	In-situ encapsulation	Methylene blue	85.6%	100 ppm	1 hour	(Salgaonkar et al., 2019)
HRP@UiO-66-NH_2	HRP	Infiltration	Methylene blue	45%	10 ppm	60 minutes	(Kurtuldu et al., 2022)
laccase@MMOF	Laccase	In-situ encapsulation	Methylene blue	91%	-	20 minutes	(Ladole et al., 2020)
OPP-MOF	OPP	In-situ encapsulation	Congo red	89.9%	100 ppm	1 hour	(Salgaonkar et al., 2019)
Laccase on NH2-MIL88(Fe)	Laccase	Chemical linking	Remazol Brilliant Blue R	92%	20 mg/L	-	(Y. Zhang et al., 2021)
LAC@Cu-ZIF-90	Laccase	In-situ encapsulation	Acid Red 18	85.7%	50 mg/L	4 hours	(Yang et al., 2023)
LAC@Cu-ZIF-90	Laccase	In-situ encapsulation	Reactive Deep Blue B-2GLN	68.3%	50 mg/L	4 hours	(Yang et al., 2023)
Laccase on ZIF-8	Laccase	Chemical linking	Acid Blue 92	90%	20 mg/L	120 minutes	(Mahmoodi & Abdi, 2019)

2.7 Summary

This chapter discussed the occurrence of water micropollutants, their environmental and health impacts, and the limitations of the conventional treatment technologies. Micropollutants from pharmaceuticals, pesticides, personal care products and dyes are hardly removed by traditional wastewater treatment processes, demanding the development of advanced and sustainable remediation approaches. MOFs have emerged as promising materials due to their high surface area, tuneable porosity, and able to integrate with enzyme (E-MOF) for enzymatic catalytic functions.

This literature highlight that the selection of ZIF types, synthesis methods and enzyme immobilization strategies plays a critical role in determining the performance of E-MOF systems. ZIFs is one of the MOFs that commonly used integrating with enzyme. Various immobilization techniques, such as adsorption, chemical linking, *in-situ* encapsulation, and infiltration has been reported with *in-situ* encapsulation showing superior enzyme stability and protection against harsh environmental condition. Green synthesis using water as solvent has been demonstrated to improve sustainability which align with green chemistry principles and enhance the applicability of MOFs and E-MOFs for water-related applications. Kinetics and adsorption studies show that immobilization can slightly reduce the enzyme affinity due to the diffusion limitations but significantly enhanced enzyme stability.

Overall, E-MOFs exhibited high potential for water micropollutant degradation through synergistic adsorption and biocatalysis, although challenges such as enzyme leaching and scalability remain. This thesis focuses on synthesizing and evaluating laccase-immobilized ZIF-based MOFs for efficient water micropollutant degradation.

CHAPTER 3
RESEARCH METHODOLOGY

3.1 Introduction

The research framework shows three mains of the experiments. The first main experiment focuses on the synthesis and characterizing of the ZIFs; ZIF-8, ZIF-67, and ZIF-7. The ZIFs is synthesized by using one pot synthesis method and using water as solvent at room temperature (except for ZIF-7 and L@ZIF-7 at 35℃) and at room pressure. The ratio of metal ion to organic ligand concentration of ZIFs are manipulated from 1:8 to 1:16. The second main experiment evaluates the enzyme kinetics of free laccase and L@ZIFs from selected ZIF and analyse by using UV-Vis spectrophotometer. The adsorption kinetics of the pristine of selected ZIFs is conducted and analysed its adsorption by using UV-Vis spectrophotometer. The third main experiment is to investigate the performance of the biocatalytic oxidation of L@MOF in reducing methylene blue as micropollutant in water.

3.2 Chemicals and Materials

Zinc nitrate ($Zn(NO_3)_2$) (R&M), cobalt nitrate (R&M), 2-methylimidazole (M50850, Sigma Aldrich), benzimidazole (R&M). These chemicals are used as the precursor for ZIF8, ZIF-67, and ZIF-7. Methylene blue (0264-00, R&M) is used as a dye and decomposed by Laccase from *Trametes Versicolor* (38429, Sigma Aldrich) enzyme. Potassium phosphate monobasic (KH_2PO4) (Merck) and Potassium hydrogen phosphate (K_2HPO4) (Merck) are mixed and diluted with ultrapure water to make phosphate buffer pH 7. This buffer is used to make laccase solution.

3.3 Synthesis ZIF-8, ZIF-67 and ZIF-7 Particles

3.3.1 Synthesis ZIF-8 with Different Concentration Ratios of Metal ions to Organic Ligand

1mL 0.05M zinc nitrate aqueous solution is added into 10mL 0.4M 2-methylimidazole aqueous solution. The ratio of this zinc ion to 2-methylimidazole

molarity is 1:8. The mixture is stirred at 300 rpm for 2 hours at room temperature. The solution turned from yellowish-transparent to opaque milky white. The mixed solution is then centrifuged at 5000 rpm for 15 minutes. The mixed solution will split into supernatant and precipitate (ZIF-8) after being centrifuged. The supernatant of the solution is removed, and the precipitate is rinsed and dried at 60℃. The precipitate is ZIF-8 becoming a powder is then brought for morphology and characterization analysis. The experiment was repeated to ensure reproducibility. The experiment is repeated by using different ratios of zinc ion to 2-methylimidazole molarity as shown in Table 3.1 below:

Table 3.1
The Ratio of Zinc to 2-methylimidazole Molarity for ZIF-8

Ratio zinc to 2-methylimidazole	Molarity of zinc ion (M)	Molarity of 2-methylimidazole (M)
1:8	0.05M	0.4M
1:12	0.05M	0.6M
1:16	0.05M	0.8M

3.3.2 Synthesis ZIF-67 with Different Concentration Ratios of Metal Ion to Organic Ligand

5mL 0.045M cobalt nitrate aqueous solution and is added into 5mL 0.36 M 2-methylimidazole aqueous solution. The ratio of this cobalt ion to 2-methylimidazole molarity is 1:8. The mixture is stirred at 300 rpm for 2 hours without any heating. The solution turned from brick red of cobalt to purple. the solution is stayed overnight for 18 hours at ambient temperature. The mixed solution is then centrifuged at 5000 rpm for 15 minutes. The mixed solution will split into supernatant and precipitate (ZIF-67) after being centrifuged. The supernatant of the solution is removed and the precipitate is rinse and dried at 60℃. The ZIF-67 powder is then brought for characterization analysis. The experiment was repeated to ensure reproducibility. The experiment is repeated by using different ratios of cobalt ion to 2-methylimidazole molarity as shown in Table 3.2 below:

Table 3.2
The Ratio of Zinc to 2-methylimidazole Molarity for ZIF-67

Ratio cobalt to 2-methylimidazole	Molarity of cobalt ion (M)	Molarity of 2-methylimidazole (M)
1:8	0.045M	0.36M
1:12	0.045M	0.54M
1:16	0.045M	0.72M

3.3.3 Synthesis ZIF-7 with Different Concentration Ratios of Metal Ion to Organic Ligand

50mL of 0.32M benzimidazole solution is sonicate and dissolve at 35℃. 50mL of 0.04M zinc nitrate aqueous solution and is added into benzimidazole aqueous solution. The ratio of this zinc ion to benzimidazole molarity is 1:8. The mixture is stirred at 300 rpm for 6 hours at 35℃. The solution turned from colorless to opaque white. The mixed solution is then centrifuged at 5000 rpm for 15 minutes. The mixed solution will split into supernatant and precipitate (ZIF-7) after being centrifuged. The supernatant of the solution is removed and the precipitate is rinsed and dried at 60℃. The ZIF-7 powder is then brought for characterization analysis. The experiment was repeated to ensure reproducibility. The experiment is repeated by using different ratio of zinc ions to benzimidazole molarity as shown in Table 3.3 below:

Table 3.3
The Ratio of Zinc to 2-methylimidazole Molarity for ZIF-7

Ratio zinc to benzimidazole	Molarity of zinc ion (M)	Molarity of benzimidazole (M)
1:8	0.04M	0.32M
1:12	0.04M	0.48M
1:16	0.04M	0.64M

3.4 Synthesis L@ZIF-8, L@ZIF-67 and L@ZIF-7 Particles

3.4.1 Synthesis L@ZIF-8 Particle from Selected Concentration Ratio

10mL 0.8M 2-methylimidazole aqueous solution and 1 mg/mL (1mL) of laccase are added into 1mL 0.05M zinc nitrate aqueous solution. The mixture is stirred at 250 rpm for 2 hours without any heating. The solution turned from yellowish-transparent to opaque milky white. Small amount of the solution is taken after synthesis for calculate enzyme immobilization. The mixed solution is then centrifuged at 5000 rpm for 15 minutes. The mixed solution will split into supernatant and precipitate (L@ZIF-8) after being centrifuged. The supernatant of the solution is taken for enzyme leakage calculation, and the precipitate is rinsed and dried at 60℃. The L@ZIF-8 powder is then brought for characterization analysis. The experiment was repeated to ensure reproducibility.

3.4.2 Synthesis L@ZIF-67 Particles from Selected Concentration Ratio

5mL 0.54M 2-methylimidazole aqueous solution and 1 mg/mL (1mL) of laccase are added into 5mL 0.045M cobalt nitrate aqueous solution. The mixture is stirred at 250 rpm for 2 hours without any heating. The solution turned from brick red of cobalt to purple. The mixed solution is stayed overnight for 18 hours at ambient temperature. Small amount of the solution is taken after synthesis for calculate enzyme immobilization. The mixed solution is then centrifuged at 5000 rpm for 15 minutes. The mixed solution will split into supernatant and precipitate (L@ZIF-67) after being centrifuged. The supernatant of the solution is taken for enzyme leakage calculation, and the precipitate is removed from the centrifuge tube rinsed and dried at 60℃. The L@ZIF-67 powder is then brought for characterization analysis. The experiment was repeated to ensure reproducibility.

3.4.3 Synthesis L@ZIF-7 Particle from Selected Concentration Ratio

5mL of 0.32M The benzimidazole solution is sonicate and dissolve at 35℃. 5mL of 0.64M zinc nitrate aqueous solution and 1 mg/mL (1mL) of laccase are added into benzimidazole aqueous solution. The mixture is stirred at 300 rpm for 6 hours at 35℃.

The solution turned from colorless to opaque white. Small amount of the solution is taken after the synthesis for calculate enzyme immobilization. The mixed solution will split into supernatant and precipitate (L@ZIF-7) after being centrifuged. The supernatant of the solution is taken for enzyme leakage calculation, and the precipitate is removed from the centrifuge tube, rinsed and dried at 60℃. The L@ZIF-7 powder is then brought for characterization analysis. The experiment was repeated to ensure reproducibility.

3.5 Characterization of ZIF-8, L@ZIF-8, ZIF-67, L@ZIF-67, ZIF-7 and L@ZIF-7 Particles

The structure, physiochemical and thermal properties of synthesized ZIF-8, ZIF-67, and ZIF-7 with different concentration ratios and L@ZIF-8, L@ZIF-67, and L@ZIF-7 are characterized by using Field Emission Scanning Electron Microscopy (FESEM), X-ray diffraction (XRD), Fourier Transform Infrared (FTIR), Thermogalvanic Analysis (TGA), Brunauer-Emmett-Teller (BET) analyses and particle analyzer.

3.5.1 Field Emission Scanning Electron Microscopy (FESEM)

The morphology of the ZIF8, ZIF-67, and ZIF-7 with different concentration ratios and L@ZIF-8, L@ZIF-67, and L@ZIF-7 are studied by using the FESEM by using Zeiss Supra VP FESEM model that operated at 10 kV. The sample is prepared by sprinkle on the sample holder and the sample go through platinum sputter coating to prevent charging during viewing.

3.5.2 X-Ray Diffraction (XRD)

The XRD analysis is using Rigaku Ultima IV model to study of the crystal structure and crystallinity of synthesized ZIF8, ZIF-67, and ZIF-7 with different concentration ratios and L@ZIF-8, L@ZIF-67, and L@ZIF-7. The XRD analysis uses Cu Kα radiation with diffraction angle 2θ in range of 5° to 50° with a scanning rate of 2° min^{-1} and width step of 0.02° at voltage of 40kV and current of 40mA.

3.5.3 Fourier Transform Infrared (FTIR)

FTIR spectrophotometer analysis with transmission configuration using instrument Perkin-Elmer model, used to identify the functional group of the synthesized ZIFs (ZIF8, ZIF-67, and ZIF-7) and L@ZIF-8, L@ZIF-67, and L@ZIF-7. The FTIR spectrophotometer analysis is recorded the wavenumber pattern from 515 cm^{-1} to 4000 cm^{-1}.

3.5.4 Thermogravimetric Analysis (TGA)

The thermal study of ZIF-8, ZIF-67, ZIF-7, L@ZIF-8, L@ZIF-67, and L@ZIF-7. are evaluated by using thermogravimetric analysis (TGA). TGA measurement is conducted on the Mettler Toledo TGA/DSCI STAR System model with N2 atmosphere gas at temperatures from 25℃ to 700℃ with a heating rate of 10℃/min.

3.5.5 Brunauer-Emmett-Teller (BET) Analysis

The surface area, pore volume and pore size of the ZIF-8, ZIF-67, ZIF-7 L@ZIF-8, and L@ZIF-67, L@ZIF-7 are evaluated by using Brunauer-Emmett-Teller (BET) analysis. The BET analysis is performed by using model Micromeritic 3Flex 3500 by starting with degassed the sample at temperature of 150℃ for 3 hours before the analysis.

3.5.6 Particle Analysis

ZIF-8, ZIF-67, ZIF-7, L@ZIF-8 from selected pristine ZIF-8, L@ZIF-67 from selected pristine ZIF-67 and L@ZIF-7 from selected pristine ZIF-7 are go through particle analysis by using model Malvern Instruments, Mastersizer 2000 to identify the particle size of these particles.

3.6 Enzyme Encapsulation and Enzyme Leakage Calculation

The solution of the synthesized L@MOF is taken to calculate enzyme immobilization during the synthesize. The supernatant that produced after centrifuge of

L@MOF is taken to calculate enzyme leakage due to centrifuge. The percentage enzyme immobilization and enzyme leakage in the MOF is calculated as below:

$$enzyme\ immobilization\ (EI)\ (\%) = \frac{m - (C_s V_s)}{m} \times 100 \quad (3.1)$$

$$enzyme\ leakage\ (EL)\ (\%) = EI - \left(\frac{m - (C_l V_l)}{m} \times 100\right) \quad (3.2)$$

$$Total\ immobilization\ (\%) = EI - EL \quad (3.3)$$

C_s and V_s are concentration and volume of the mixed solution of the synthesized L@MOF and C_l and V_l are concentration and volume of the supernatant of L@MOF after centrifuge, respectively. m is the mass of the enzyme in the solution during immobilization.

3.7 Enzyme Activity of Free Laccase and L@ZIFs

The enzyme activity protocol for free laccase is referred from published paper (Z. Wang et al., 2020; Yang et al., 2023). The enzyme activity of free laccase and selected L@ZIFs was measured spectrophotometrically with ABTS as substrate at wavelength 420nm by using UV-vis spectrophotometer (Shimadzu UV-1280). 0.1 mL of laccase solution (1mg/mL) or 10 mg of selected L@ZIFs that contain 1mg laccase was mixed with 2.9mL of ABTS solution (pH 7) at room temperature. Laccase oxidized the ABTS to ABTS·+ (ABTS positive radical). The ABTS·+ at 420nm have higher absorption coefficient compared to ABTS. The reaction rate of enzyme (V) is determined by the amount of ABTS oxidized (into green colour) and measured by UV-Vis spectrophotometer (Shimadzu UV-1280) for every 5 second for 500 seconds. One unit of laccase activity was defined as the amount of enzyme that needed to oxidize 1 μmol of ABTS per minute. The experiment was repeated to ensure reproducibility.

3.8 Enzyme Kinetics of Free Laccase and L@ZIFs

The enzyme kinetics of free laccase and selected L@ZIFs was measured spectrophotometrically with ABTS as substrate at wavelength 420nm by using UV-vis spectrophotometer (Shimadzu UV-1280). 0.1 mL of laccase solution (1mg/mL) or 10

mg of selected L@ZIFs that contain 1mg laccase was mixed with 2.9mL of ABTS solution (pH 7) at room temperature with different concentration of 0.2-1.0 mM. Laccase oxidized the ABTS to ABTS· + (ABTS positive radical). The ABTS· + (green colour) at 420nm have higher absorption coefficient compared to ABTS. The reaction rate of enzyme (V) is determined by the amount of ABTS oxidized (into green colour) and measured by UV-Vis spectrophotometer (Shimadzu UV-1280) for every 5 second for 500 seconds. The experiment was repeated to ensure reproducibility. The initial reaction rate of the enzyme (V_0) is determined by equation 3.4.

$$V_o = \frac{V_{max}\,[S]}{K_m + [S]} \tag{3.4}$$

V_{max} is the maximum rate of the enzyme. K_m is the Michaelis-Menten constant and [S] is the concentration of the substrate. The kinetics parameters (V_o, K_m and V_{max}) are calculated by using Shimadzu UV-1280 software for Lineweaver-Burk (equation 3.5), Hanes-Woolf (equation 3.6) and Eadie-Hofstee (equation 3.7) plots.

$$\frac{1}{V_o} = \frac{K_m}{V_{max}\,[S]} + \frac{1}{V_{max}} \tag{3.5}$$

$$\frac{[S]}{V_o} = \frac{[S]}{V_{max}} + \frac{K_m}{V_{max}} \tag{3.6}$$

$$V_o = -K_m \frac{V_o}{[S]} + V_{max} \tag{3.7}$$

3.9 Adsorption Kinetics and Isotherms of ZIF-8, ZIF-67 and ZIF-7 Particles

20 mg of the particles (ZIF-8, ZIF-67 and ZIF-7) is added into 60mL of methylene blue solution of at room temperature and pressure. The mixture is stirred at 100 rpm. The 4mL of the mixture is taken for every 1-hour interval to observe the reduction of methylene blue by using UV-Vis Spectrophotometer at wavelength of 665 nm. The experiment was repeated to ensure reproducibility. The amount of the adsorbate adsorbed by adsorbent at relative time (mg/g) is calculated by using the equation 3.8.

$$q_t = \frac{(C_o - C_t)V}{m} \tag{3.8}$$

q_t is an amount of the adsorbate (methylene blue) adsorbed by adsorbent (ZIFs) at relative time. C_o and C_t are the initial concentration of adsorbate and concentration at relative time, respectively. m is the mass of the adsorbent and V is the volume of the solution.

The adsorption kinetics of pristine ZIFs are determined by using pseudo-first order (equation 3.9) and pseudo-second order (equation 3.10):

$$\ln(q_e - q_t) = \ln q_e - K_1 t \tag{3.9}$$

$$\frac{t}{q_t} = \frac{1}{K_2 q_e^2} + \frac{1}{q_e} t \tag{3.10}$$

Where t (min) is time, qe and qt (mg/g) is amount of adsorbate adsorbed by adsorbent at equilibrium and at time t respectively. K1 (1/min) and K2 (g/mg.min) are pseudo-first order rate constant and pseudo-second order rate constant, respectively.

The adsorption isotherm of pristine ZIFs is determined by using Langmuir isotherm (equation 3.11) and Freundlich isotherm (equation 3.12):

$$\frac{C_e}{q_e} = \frac{1}{K_L q_{max}} + \frac{C_e}{q_{max}} \tag{3.11}$$

$$log q_e = log K_F + + \frac{1}{n} log C_e \tag{3.12}$$

Ce (mg/L) is the final concentration of the adsorbate at respective time, qe (mg/g) is the amount of the adsorbate adsorb by the weight of the adsorbent. K_L (L/mg) and K_F (mg/g)(L/mg)$^{(1/n)}$ is the Langmuir isotherm constant and Freundlich isotherm constant respectively.

The percentage methylene blue removal by pristine ZIFs is calculated using equation 3.13.

$$MB\ removal\ (\%) = \frac{\left([MB]_{initial} - [MB]_{final}\right)}{[MB]_{initial}} \times 100 \tag{3.13}$$

3.10 Biocatalytic Oxidation of Methylene Blue

The biocatalytic oxidation of the methylene blue is conducted by using selected ZIF from each of the ZIFs type. Small amount of weight of the selected L@ZIF that contain 1mg of laccase or close of it is added into the 10mL of 0.05mM methylene blue solution. The intensity of the methylene blue solution colour is observed by using UV-Vis spectrophotometer at wavelength of 665nm for every 7 days. The experiment was repeated to ensure reproducibility. The methylene blue (MB) degradation is calculated by using this equation 3.14 (Yang et al., 2023):

$$MB\ degradation\ (\%) = \frac{\left([MB]_{initial} - [MB]_{final}\right)}{[MB]_{initial}} \times 100 \quad (3.14)$$

CHAPTER 4
RESULTS AND DISCUSSIONS

4.1 Introduction

In this chapter, the results and findings obtained from the experiments were analyzed and discussed. First, the physiochemical properties of ZIF-8, ZIF-67, ZIF-7, with different ratio concentrations of metal ions to organic ligand are discussed. These particles were characterized by using various instruments such as field emission scanning electron microscopy (FESEM), x-ray diffraction (XRD), Fourier transform infrared spectroscopy (FTIR), Thermogravimetric analysis (TGA), Brunauer-Emmett-Teller analysis (BET), and particle analysis. Each of these pristine ZIFs particles is selected based on their characteristics to be used to enzyme encapsulation (L@ZIF-8, L@ZIF-67, L@ZIF-7). This L@ZIFs were also characterized by using same instrument as pristine particles and UV-VIS spectrometer to determine enzyme loading. This chapter also discussed the enzyme kinetic of free laccase, L@ZIF-8, L@ZIF-67, and L@ZIF-7 by using UV-Vis spectroscopy. The selected pristine of ZIF-8, ZIF-67 and ZIF-7 go through adsorption kinetic and isotherm experiment. Lastly, biocatalytic oxidation of methylene blue of L@ZIF-8, L@ZIF-67, and L@ZIF-7 were conducted and analysed by using UV-Vis spectrophotometer.

4.2 Physicochemical Properties of MOF with Different Concentration Ratios of Metal Ions to Organic Ligands

ZIF-8, ZIF-67, and ZIF-7 are synthesized by mixed metal ions (zinc or cobalt) and imidazolate ligand (2-methylimidazolate or benzimidazole) in ultrapure water for all concentrations ratios. The detailed methodology for the synthesis of the respective MOF can be referred to section 3.3.1, 3.3.2 and 3.3.3. Briefly, the solution is centrifuged and the obtained precipitates are rinsed and then dried. Physically observed, ZIF-8 powder is obtain in milky-white color, ZIF-7 in white color while ZIF-67 powder in purple color as shown in Figure 4.1.

Figure 4.1 Sample of ZIF-7, ZIF-8 and ZIF-67

4.2.1 Zeolitic Imidazolate Framework-8 (ZIF-8)

Figure 4.2 shows the images of the ZIF-8 with different ratios of concentration between metal and organic ligand from field emission scanning electron microscopy (FESEM). Different concentration ratios of the precursor of ZIF-8 show different morphology (Jian et al., 2015). In ratio of 1:8 (Figure 4.2(a)), there is agglomerate with no definite structure of ZIF-8 and for ratio 1:12 (Figure 4.2(b)), there are a various crystal structure, mostly are getting to the standard structure of rhombic dodecahedron of ZIF-8 with crystal size in range of 1.25-3.4 µm. ZIF-8 shows a truncated edge of a rhombic dodecahedron for a ratio of 1:16 (Figure 4.2(c)) with crystal size in the range of 0.9-2µm. From these images, the structure size decreases as the ratio concentrations increase as correspond to the particle size (Table 4.2); 316.28 μm for ratio 1:8, 1.096 μm for ratio 1:12 and 0.724 μm for ratio 1:16. The higher 2-methylimidazole concentration ratio to zinc ion, the smaller the particle size, as reported by Zhang Y. et al. (2018) (Y. Zhang et al., 2018).

2-methylimidazole play a main role in the formation of the ZIF-8 crystal. The nucleation of the ZIF-8 is started with deprotonation of the ligand by removing the H^+ from the compound (Akhundzadeh Tezerjani et al., 2021). Since the ligand and the ZIF-8 synthesis is in water, the water reacts first to the ligand through hydrolysis (H^+ move to the ligand) instead of the ligand deprotonation, causing the ligand positively charged. Due to this, the reaction with the Zn^{2+} hard, and lowering the ZIF-8 formation (Akhundzadeh Tezerjani et al., 2021). Due to that, ligand need to be in high concentration, as the higher the ligand concentration, the higher the potential of ligand to react with Zn^{2+} since there are excess of the ligand that are not hydrolyse with water

(Allegretto et al., 2024). Furthermore, the higher the ligand concentration, the better the deprotonation of the ligand as the ligand itself is base (Shi et al., 2017).

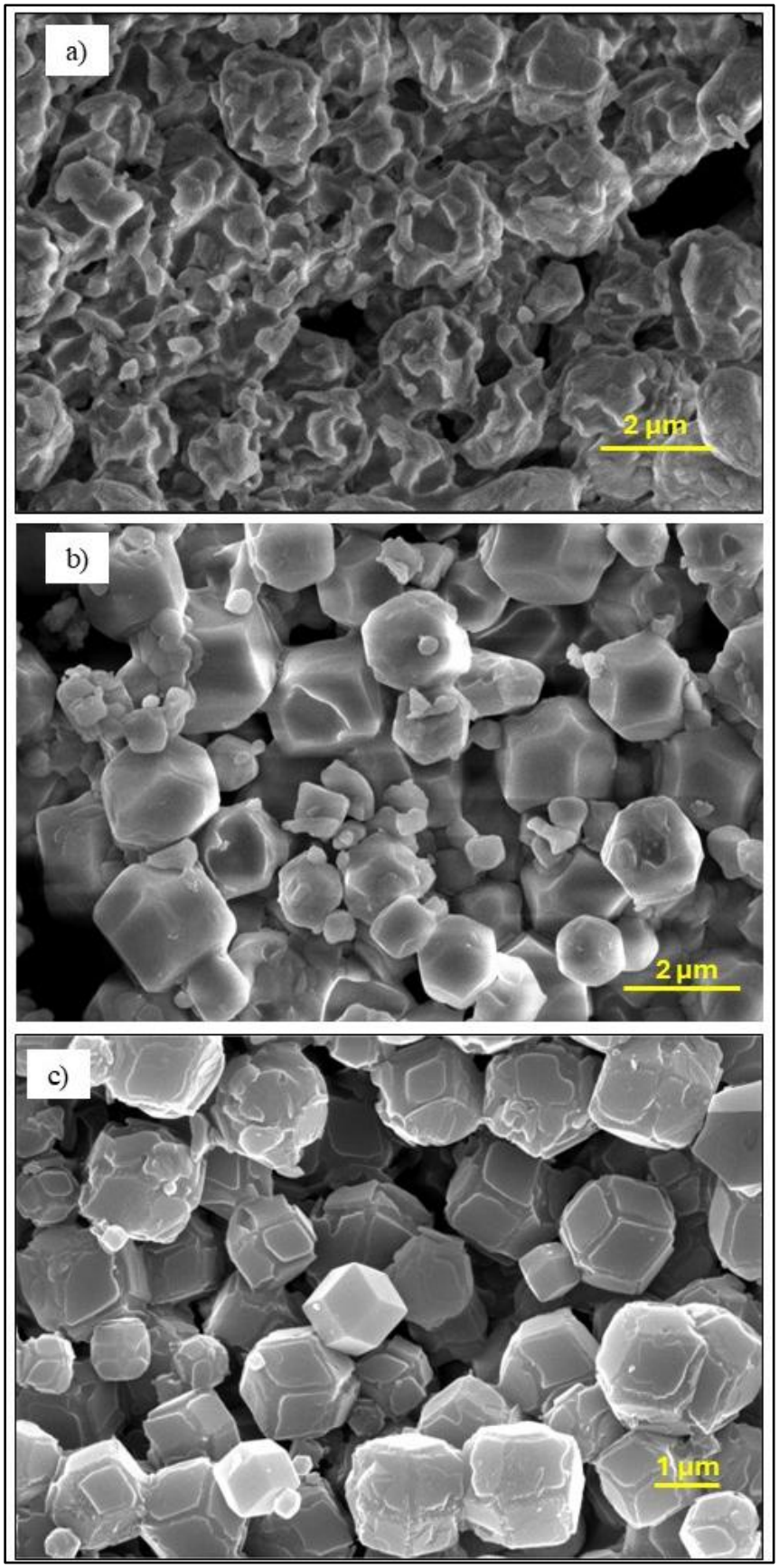

Figure 4.2 FESEM Images of ZIF-8 (Magnification x10k) with Respective Metal:Ligand Ratio; (a) 1:8 (b) 1:12 (c) 1:16

The ZIF-8 XRD pattern in Figure 4.3 exhibits the same pattern as the JCPDS card of ZIF-8 (00-062-1030) and as reported by Zhuo Shi et. al (Shi et al., 2017). The ZIF-8 peaks found at 2θ and its Miller indices from JCPDS card are 7.14° (110), 10.16° (200), 12.52° (211), 14.58° (220), 16.24° (310), 17.82° (222), 19.46° (321), 22.06° (411), 24.42° (332), 25.28° (422), 26.6° (431), 28.44° (521), 29.6° (440), 30.56° (433), 31.22° (442), 32.1° (611), 33.2° (620), 34.64° (622). Miller indices from the JCPDS cards show the orientation of the plane from the crystal. The XRD also shown that the higher the 2-methylimidazole concentration, the clearer and better the peak, which show the better sodalite features (Shi et al., 2017).

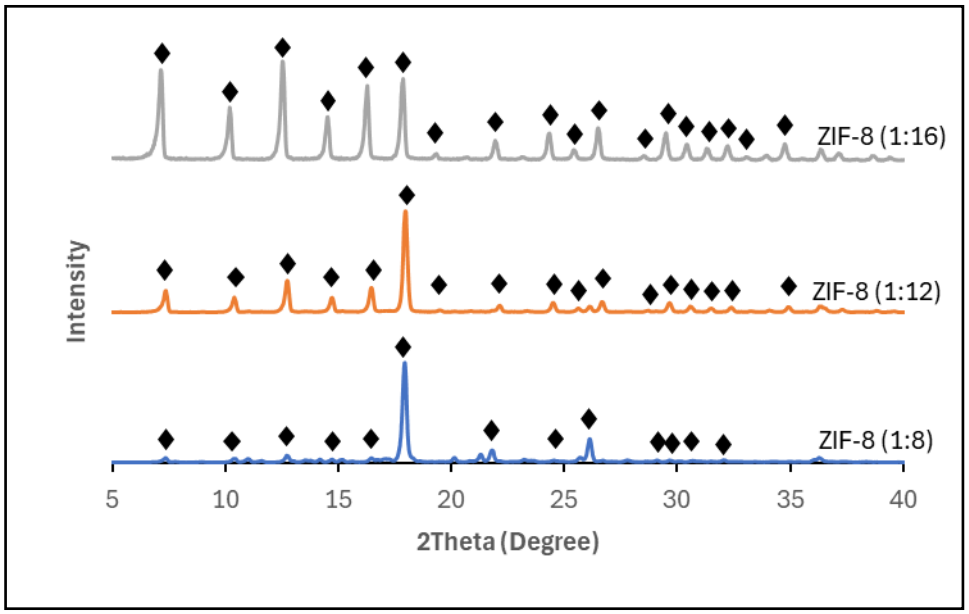

Figure 4.3 XRD Pattern for ZIF-8 with A Different Concentration Metal to Organic Ligand Ratio

Fourier Transform Infrared (FTIR) spectroscopy analysis is used to identify and verify the chemical functional group of the samples. Figures 4.4 show the FTIR spectra pattern of ZIF-8. The FTIR spectra pattern for each ZIF-8 shows similar patterns through different ratio concentrations, showing they have similar particle interactions. These FTIR spectra patterns also show similarity such as there is no band of stretch mode of N-H bond of raw material 2-methylimidazole appearing at the range of 2250-3250 cm^{-1} (Ulu, 2020). Peak at lower wavelength spectra around 750cm^{-1} and 700cm^{-1} show Zn-O and Zn-N bond of ZIF-8 (Jamil et al., 2019). The band at 697cm^{-1} and 756cm^{-1} (wavelength lower than 800cm^{-1}) indicate the out-of-plane of bending of

imidazole ring (Jian et al., 2015). The stretch of C-N shown at wavelength 990cm^{-1} and 1144cm^{-1} (Jofrishal et al., 2020). The peak at 1412cm^{-1} attribute the stretch of the entire ring (Bergaoui et al., 2021; Jian et al., 2015).

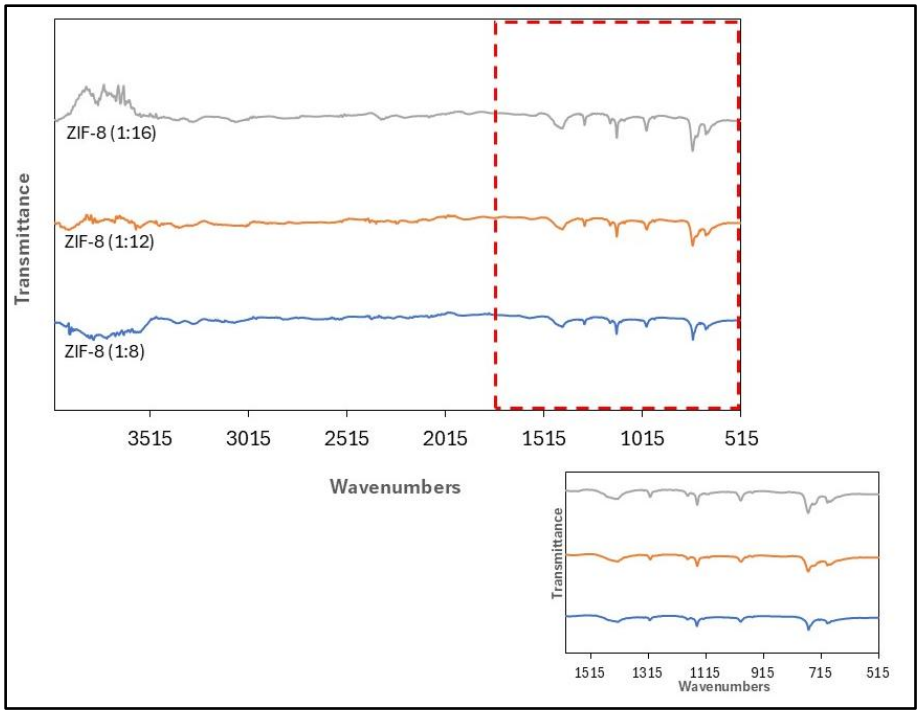

Figure 4.4 FTIR Spectra of ZIF-8 with Different Concentrations Metal:Organic Ligand

Figures 4.5 presents the thermogravimetric (TGA) profiles of ZIF-8 samples and Table 4.1 summarizes the corresponding total weight losses for different metal-to-organic ligand concentration ratios. All samples were subjected to heating up to 700℃ at constant ramp rate of 10℃/min. The thermal degradation proceeded through two distinct stages. The first stage, occurring at lower temperatures, is associated with the removal of physically adsorbed water molecules and residual unreacted precursors, indicating the degree of purity and solvent retention in the ZIF-8 framework. The second stage, observed at higher temperatures, corresponds to the decomposition of the organic linker and the subsequent collapse of the MOF crystalline structure, marking the breakdown of the imidazolate coordination network. The temperature range and extent of each degradation step provide insight into the thermal stability of ZIF-8 and how it varies with the metal-to-ligand ratio (Shi et al., 2017; X. Zhao et al., 2014). Between the two thermal degradation stages, a plateau region was observed in the TGA

curves, indicating the structural stability of ZIF-8 over a certain temperature range. For all concentration ratios, the first weight loss attributed to the removal of adsorbed water and residual precursors which occurred below 250℃. In the case of ZIF-8 (1:8), no clear plateau was observed, as the second degradation stage commenced immediately after the first, suggesting a lower resistance to the thermal stress. In contrast, ZIF-8 (1:12) and ZIF-8 (1:16) exhibited a pronounced plateau between approximately 250℃ and 600℃, signifying enhanced thermal stability and a delayed onset of framework collapse. Furthermore, ZIF-8 (1:12) show higher drop at second degradation due to high 2-methylimidazole residue contain in the sample. At the end of the heating cycle (700℃), ZIF-8 (1:16) retained a larger fraction of its initial mass compared to ZIF-8 (1:8) and ZIF-8 (1:12), indicating less structural destruction. This improved thermal resistance can be attributed to its denser and more compact crystalline structure, which is associated with smaller pore sizes. The reduced pore volume limits heat penetration into the internal framework, thereby slowing the degradation process (Mandal et al., 2023). Additionally, the higher degree of crystallinity and stronger coordination between zinc ions and the 2-methylimidazolate ligands in ZIF-8 (1:16) further contribute to its superior structural integrity under elevated temperatures (52% weight loss compared 55% of ZIF-8 (1:8) and 59% of ZIF-8 (1:12)). This suggests that the metal-to-ligand ratio plays a pivotal role in optimizing the packing density and coordination strength, both of which are critical factors in determining the thermal stability of ZIF-8.

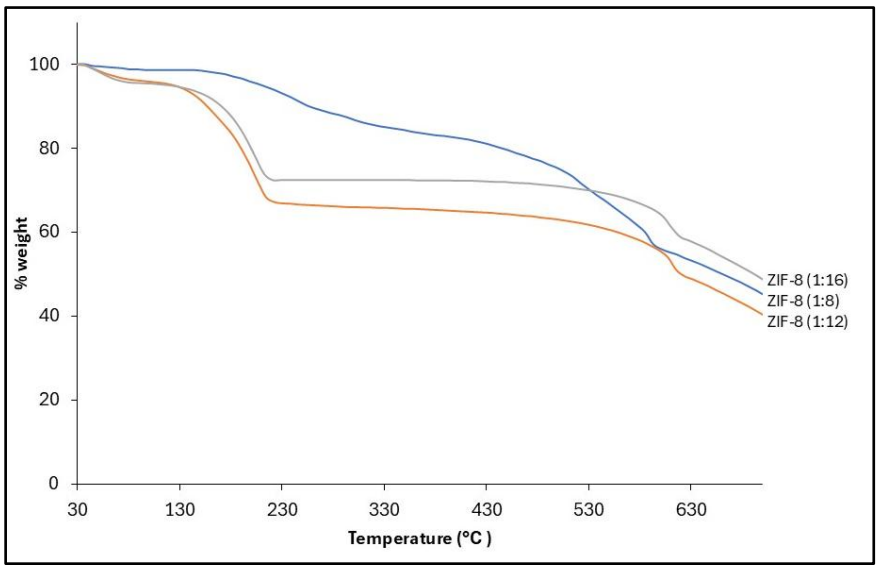

Figure 4.5 Thermogram of ZIF-8 with A Different Concentration Metal:Organic Ligand Ratio

Table 4.1
The Total Weight Loss of ZIF-8 with Different Concentration Ratio of Metal:Organic Ligand

ZIF	Ratio metal to ligand	Total weight loss (%)
ZIF-8	1:8	55
	1:12	59.8
	1:16	52.05

The BET surface area, pore volume and pore size of ZIF-8 with different metal-to-ligand ratios are summarized in Table 4.2. BET analysis shows that surface area and pore volume increase markedly from 76.25 m^2/g and 0.067 cm^3/g in ZIF-8 (1:8) to 552.59 m^2/g and 0.312 cm^3/g in ZIF-8 (1:16). Conversely, the pore size decreases from 3.534 nm to 2.260 nm with increasing ratio, which can be attributed to the development of a more well-defined rhombic dodecahedron morphology (Bergaoui et al., 2021). This compact crystalline structure, with closely packed atoms and stronger interparticle interactions, leads to a reduction in pore diameter while enhancing structural rigidity. FESEM images further confirm these trends, showing large, agglomerated particles in ZIF-8 (1:8) and small, uniform particles in ZIF-8 (1:16). The smaller particle size in ZIF-8 (1:16) (0.724 μm) correlates with its high surface area and pore volume, both of which contribute to better framework stability under heat.

Table 4.2
The BET Surface Area, Pore Volume and Pore Size of ZIF-8 With Different Concentration Ratios

ZIF-67 (metal:ligand)	BET surface area (m^2/g)	Pore volume (cm^3/g)	Pore size (nm)	Particle size (μm)
1:8	76.25	0.067	3.534	316.28
1:12	124.74	0.118	3.676	1.096
1:16	552.59	0.312	2.260	0.724

4.2.2 Zeolitic Imidazolate Framework-67 (ZIF-67)

Figure 4.6 show FESEM of ZIF-67 with different concentration ratio. Figure 4.6(a) shows the morphology of leafy-like for a ratio of 1:8, Figure 4.6(b) show Figure 4.6(c) show mixed polyhedral for a ratio of 1:16 with crystal size in the range of 2-8μm,

3-6μm and 2-5.5μm respectively. Like ZIF-8, ZIF-67 also show different morphology when different concentration ratios of precursor are used.

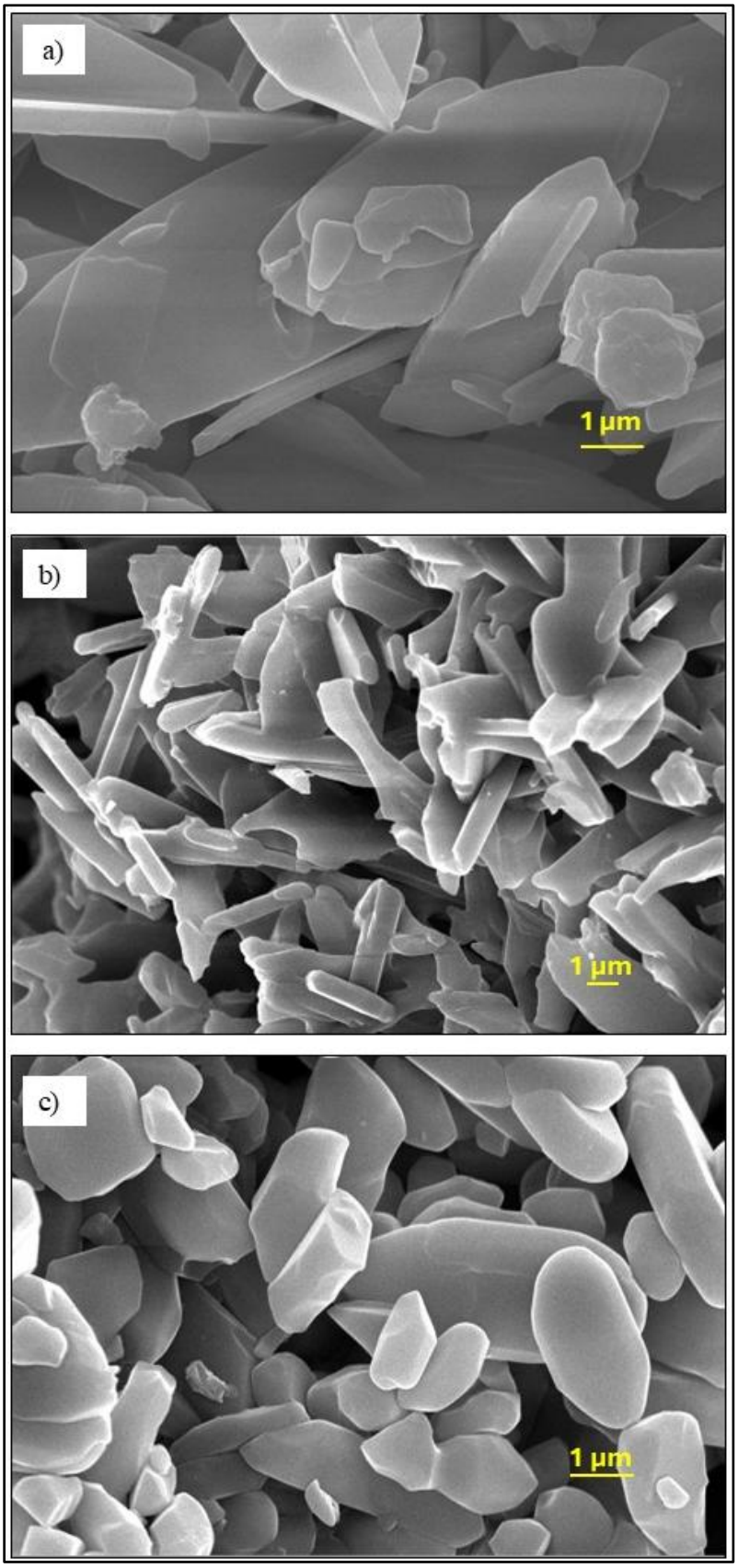

Figure 4.6 FESEM Images of ZIF-67 (Magnification x10k) with Respective Metal:Ligand Ratio; (a) 1:8 (b) 1:12 (c) 1:16

Traditionally, ZIF-67 is synthesized by using organic solvent such as DMF, DEA and methanol producing standard rhombic dodecahedron. In this study, when ZIF-67 is synthesized by using water as solvent, the different structure is constructed and none of it a standard rhombic dodecahedron. Furthermore, these images show the transitional structure of ZIF-67 to getting into standard structure of rhombic dodecahedron as reported by Zhang J. et al. (2015) (Zhang et al., 2015). This nucleation growth of the ZIF-67 is different with ZIF-8 might be due to the different metal ion and its interaction with water as solvent which ZIF-8 have much easier to getting into standard rhombic dodecahedron as ratio concentration metal:ligand 1:16 meanwhile in same ratio concentration, ZIF-67 still not getting into standard structure.

The construction of the ZIF-8 and ZIF-67 in water solvent is starting with the 2-methylimidazole linking with the water. In this case, different with other solvent (which other solvent will deprotonate the imidazole), 2-methylimidazole protonated by the water, and producing hydroxide (from water) (Akhundzadeh Tezerjani et al., 2021). The zinc ions have higher tendency in linking to the hydroxide ion compared to the imidazole (due to the charges). This interaction between zinc ions and hydroxides lowering the likelihood in making 3D ZIF-8 crystal compared to other solvent such as DMF and methanol (Akhundzadeh Tezerjani et al., 2021). These statements also supported by Ghosh T. et al. (2022) (Ghosh et al., 2022). They stated that the possibility of the ZIF-67 form in 2-dimensional like the result of the FESEM images is due to the high hydrolysis of 2-methylimidazole in water, the use of the water as solvent, polarity, viscosity and the interfacial surface tension (Ghosh et al., 2022).

Furthermore, the different between ZIF-8 and ZIF-67 is the metal ion used in constructing the ZIFs (with same organic ligand of 2-methylimidazole), might give effect of the constructing the structure. The reason why ZIF-8 can achieve faster toward standard structure of rhombic dodecahedron (both ZIF-8 and ZIF-67 producing standard structure of rhombic dodecahedron in organic solvent, as in conventional method) in increasing the concentration ratio of metal to ligand compared to ZIF-67 is due to the metal ion used. ZIF-8 used zinc meanwhile ZIF-67 using cobalt. Both metals can form metal-imidazole complexes in aqueous solution in constructing the ZIFs, but zinc ions stronger and more stable in interact with imidazole compared to cobalt ions. This is due to the zinc have electron configuration of d10 which more favour in interact with imidazole compared to cobalt that have electron configuration of d7 (Zhen Li et al., 2024).

The ZIF-67 XRD patterns in Figure 4.7 show similarity to the simulated pattern of ZIF-L reported by Yiwen Hu et. al (2019) (Hu et al., 2019). The characteristic peak of ZIF-67 like ZIF-L at 2θ are 7.36°, 7.68°, 8.86°, 10.4°, 11.1°, 11.56°, 13.1°, 13.5°, 14.88°, 15.22°, 15.52°, 16.66°, 17.3°, 18.1°, 19.28°, 21.28°, 21.86°, 23.58°, 25.1°, 27.76°, 29.06°, 29.56°. XRD pattern of these ZIF-67 in Figure 4.7 showing no significant different as reported by Jingcheng Zhang et al. (2015) (Zhang et al., 2015). This XRD pattern of ZIF-L correlated with FESEM result that show the leafy-like as the L term named Leaf-like structure in ZIF-L.

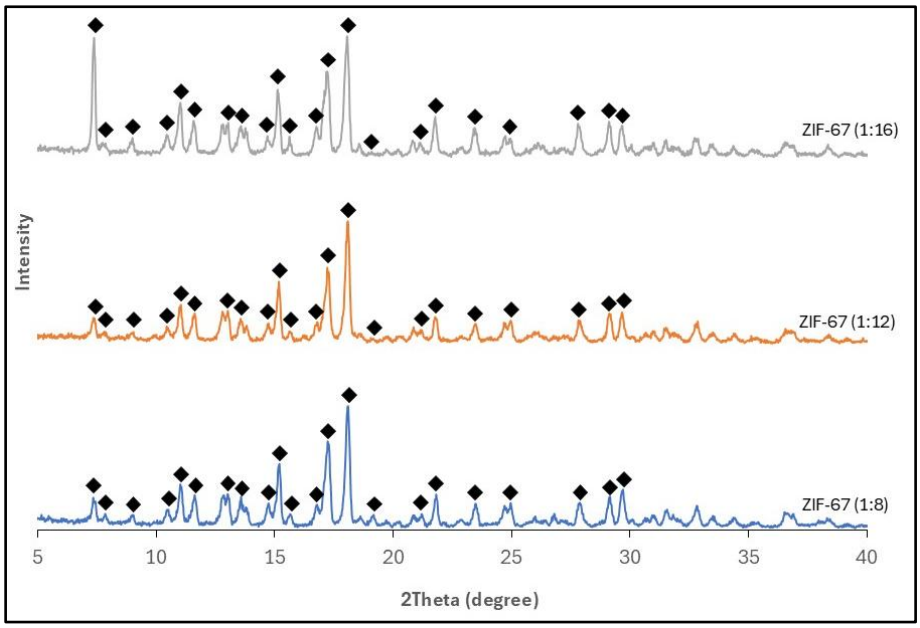

Figure 4.7 XRD Pattern for ZIF-67 with Different Concentration of Metal to Organic Ligand Ratio.

Figure 4.8 show the FTIR spectra pattern of the ZIF-67 with different concentration ratios. Each of different concentration ratios of ZIF-67 show similar FTIR spectra pattern. The significant peak of FTIR appears in range of 515cm-1 to 1700 cm^{-1}. These FTIR pattern also show no peak in range of 2000 cm^{-1} to 3500 cm^{-1} showing no N-H···N from imidazole ring appear due to the bonding to the cobalt (Bakar et al., 2024). The peak below 800cm^{-1} (747, 688 and 672 cm^{-1}) show the characteristic of the out-of-plane bending mode of the imidazole ring (Hu et al., 2019). The peak in range of 600-1500cm^{-1} show the characteristic of stretch and bending modes of imidazole ring where the peak 991, 1142, and 1303 cm^{-1} show the in-plane vibration of imidazole ring and 1415cm^{-1} show the skeletal vibration of imidazole ring (Bakar et al., 2024; Lei et

al., 2023; Rafiei et al., 2018). The peak of 1566 cm^{-1} of the spectra show the stretch mode of the C-N bond from imidazole ring (Rafiei et al., 2018).

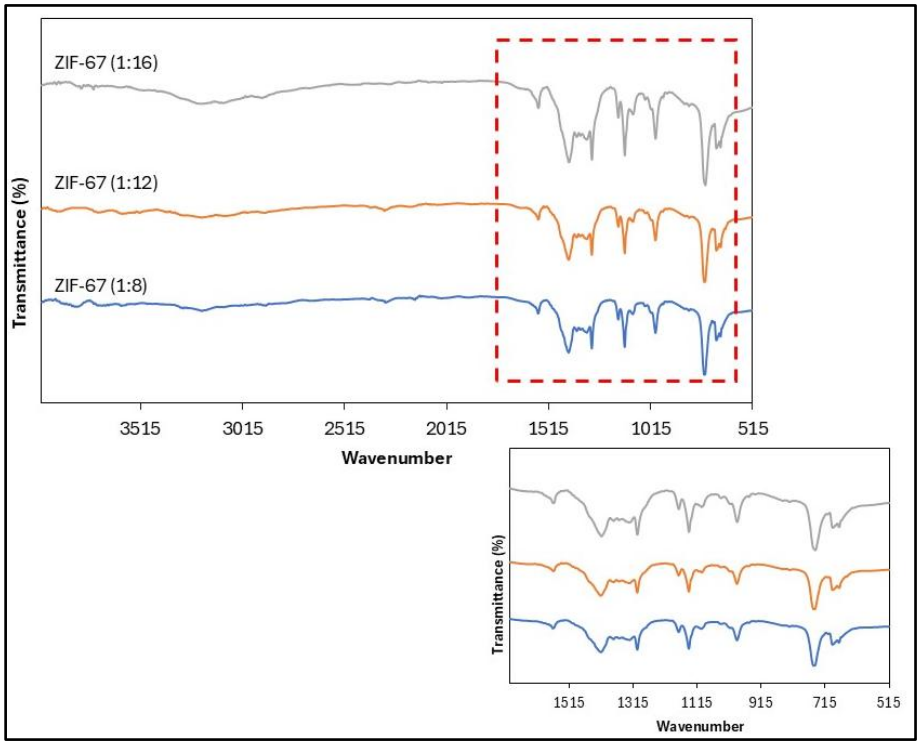

Figure 4.8 FTIR Spectra Pattern of ZIF-67 with Different Concentration Ratios (Metal:Ligand)

The thermogravimetric pattern of ZIF-67 with different concentration ratio of metal to organic ligand show in Figures 4.9. Table 4.3 show the total weight loss of ZIF-67s. Like ZIF-8, these ZIF-67s are heated up to 700℃ with a ramp rate of 10℃/min. As the result, these ZIF-67 samples are gone through three stages of thermal degradation: 1) first small of degradation due to removal of water, 2) second degradation because of 2-methylimidazole removal and 2) third degradation because of MOF structure collapse. The first small weight degradation happens around temperature 100℃ as the water vapourise at that temperature. The significant weight loss of second thermal degradation for all ZIF-67 concentrations ratio happen around 250℃ as the degradation of 2-methylimidazole can happen in between melting point and boiling point at range of 142℃-268℃. In between these second and third thermal degradation, a long plateau stage showing the structure stability toward increasing temperature. The thermogram show all ZIF-67s have a plateau, in range of 280℃ to 500℃ for ZIF-67 (1:12) and ZIF-67 (1:16) and short plateau of ZIF-67 (1:8) in range of 316℃ to 480℃.

At the end of the of the 700℃ thermogram, ZIF-67 (1:12) have less structural destruction compared to ZIF-67 (1:8) and (1:16). ZIF-67 (1:12) have better thermal degradation structure because of the structure of the ZIF-67 that have small pore size compared to other ZIF-67s and have rod-like structure that control heat from entering the structure.

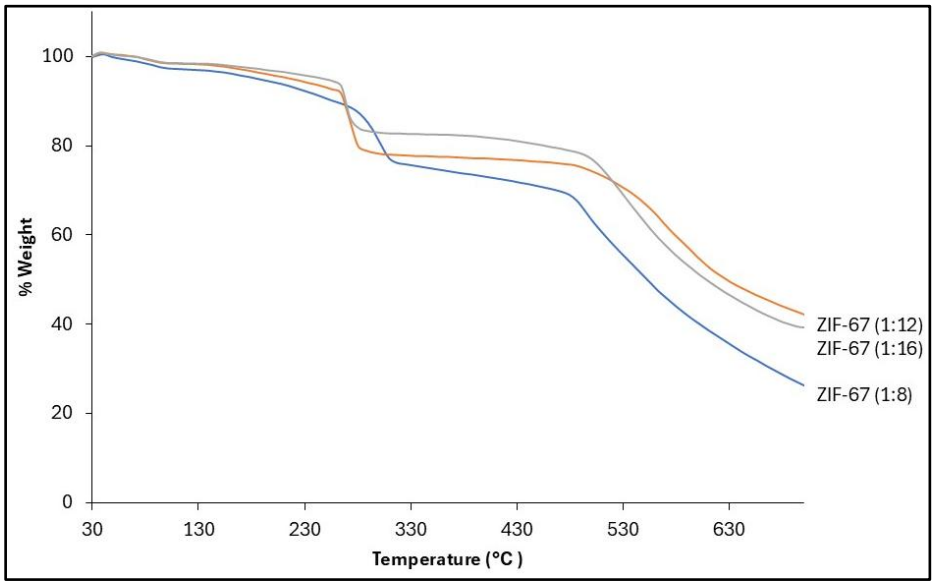

Figure 4.9 The Thermogram of ZIF-67 with Different Concentration Ratios (Metal:Ligand)

Table 4.3
The Total Weight Loss of ZIF-67 with Different Concentration Ratio of Metal:Organic Ligand

ZIF	Ratio metal to ligand	Total weight loss (%)
ZIF-67	1:8	74.0
	1:12	57.8
	1:16	60.7

Table 4.4 show BET surface area, pore volume, pore size and particle size of ZIF-67 with different concentration ratios. For ZIF-67, the BET surface area corresponds to the FESEM images as the concentration ratio of 1:8 has a higher surface area due to its structure that is leafy-like structure (wide and thin like a leaf to absorb light for photosynthesis) compared to the concentration ratio of 1:12 and 1:16 with the structure of rod-like and polyhedral, respectively. The particle size of the ZIF-67 with

different concentration ratios (metal:ligand) show lowest particle size comes to the ratio 1:12 and the highest is ratio 1:8. Like ZIF-8, particle size of the ZIF-67 ratio 1:8 is due to the agglomerates of particle.

Table 4.4
The BET Surface Area, Pore Volume, Pore Size and Particle Size of ZIF-67 with Different Concentration Ratios

ZIF-67 (metal:ligand)	BET surface area (m^2/g)	Pore volume (cm^3/g)	Pore size (nm)	Particle size (μm)
1:8	2.525	0.004	5.162	416.78
1:12	1.71	0.002	4.565	0.832
1:16	1.33	0.002	6.404	17.37

4.2.3 Zeolitic Imidazolate Framework-7 (ZIF-7)

Figure 4.10 show the FESEM images of ZIF-7 with different ratio concentration precursors use. These ZIF-7s (ratio concentration metal:ligand of 1:8 (Figure 4.10(a)), 1:12 (Figure 4.10(b)) and 1:16 (Figure 4.10(c))) have similar morphology of spherical structure. These ZIF-7 shows the rough surface structure, showing the structure is still ongoing crystal growth as this is might due to the synthesis period (Zhou, 2019). This also due to the solvent used and no modulator used to help in crystallization. ZIF-7 with a ratio concentration of 1:16 also shows some defects as there are holes on the particle surface. Cai W. et al (2014) reported that ZIF-7 that using $Zn(NO_3)_2$ metal ion as precursor form spherical structure in DMF solvent during synthesis (Cai et al., 2014). This report shows similar with the result of the ZIF-7 structure in this study that synthesis in water solvent and using $Zn(NO_3)_2$ metal ion precursor.

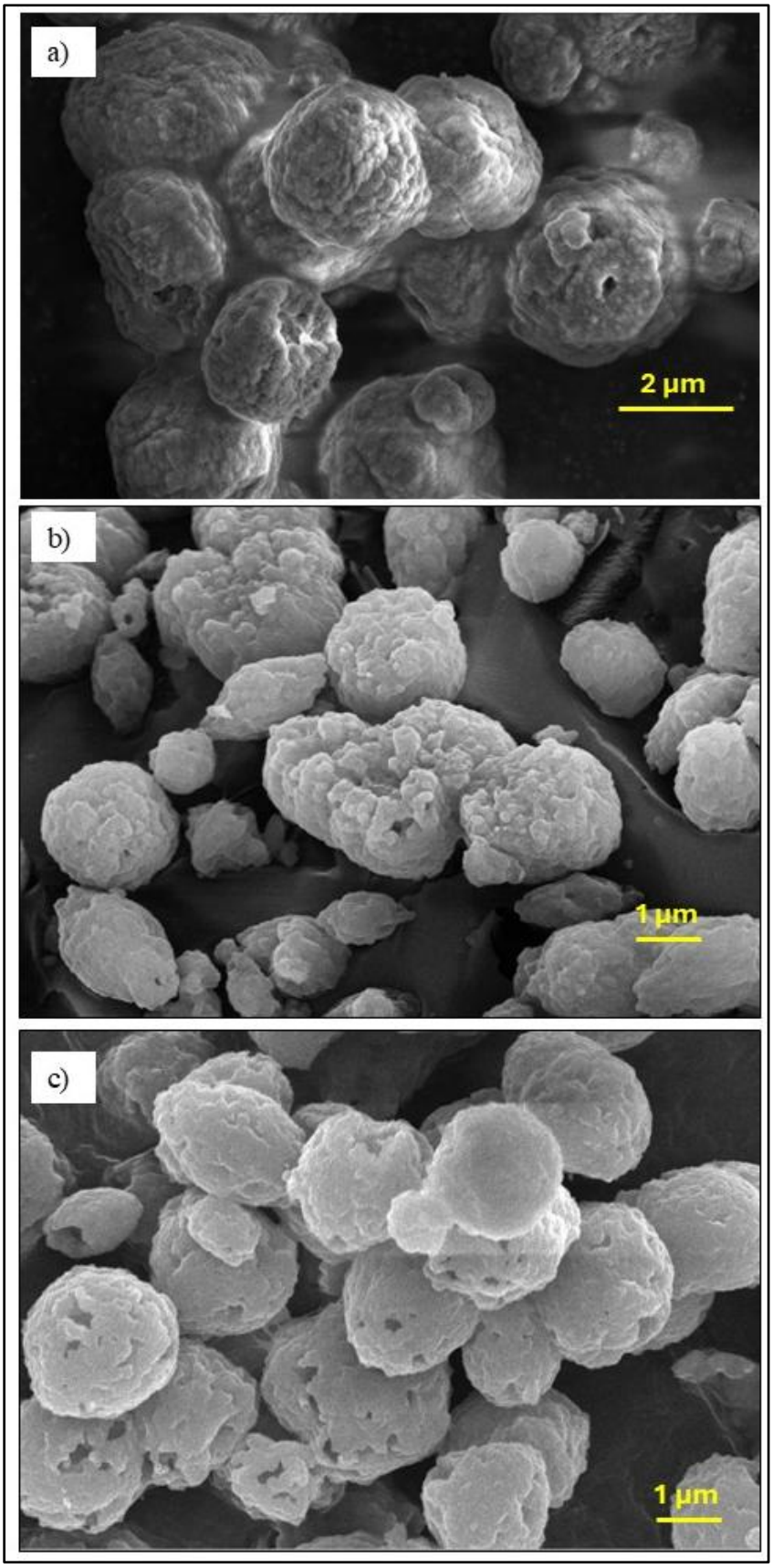

Figure 4.10 FESEM Images of ZIF-7 (Magnification x10k) with Respective Metal:Ligand ratio; (a) 1:8 (b) 1:12 (c) 1:16.

The modulator can be use during synthesis ZIF-7 in water to improve the crystallization. Conventionally, DMF is used in synthesis ZIF-7 to produce standard rhombic dodecahedron (Xiao & Liu, 2019). By using water as solvent (to promote eco-friendly), water polarity reduces the interaction benzimidazole to zinc ion as zinc will interact with hydroxide ion to become zinc hydroxide. The benzimidazole is also not ready to interact with zinc ion due to the water pH which is neutral (not reduce the amine to positively charged nitrogen to bind with zinc ion). Furthermore, benzimidazole itself is a sparing soluble (only small quantity dissolve in water) in room temperature, promoting this structure in Figure 4.10 produce. The modulator such as amine related compound (such as dieathanolamine (DEA)) can be use in constructing the ZIF-7 crystal as ZIF-7 need base to deprotonating benzimidazole (Goesten et al., 2013).

The ZIF-7 XRD patterns in Figure 4.11 have a combination peak of ZIF-7 immersed in water for 48 hours and in ethanol and DMF for 48 hours as reported by Ming He et al. (He et al., 2013). The ZIF-7 diffraction peak at 2θ like when immerse in water are 9.0°, 17.04°, 19.44°, 22.46°, 26.94°, 33.74°, 35.5°, 37.88°. The diffraction peak at ZIF-7 2θ like when immerse in ethanol and DMF are 13.2°, 14.74°, 18.36°, 23.8°, 26.3°, 29.0°. ZIF-7 is a MOF that can transform its morphology based on the temperature, therefore, the structure of the ZIF-7 can differ from other (Deacon et al., 2022). ZIF-7 also can become dense when using water as a solvent or immersed in water. Traditionally, ZIF-7 is synthesized by using DMF as a solvent. Ming He et al. (2013) (He et al., 2013) stated that immersing ZIF-7 np-phase in water causes the ZIF-7 np-phase framework to change to a more stable structure and the pore become smaller compared to ZIF-7 np-phase (He et al., 2013). This dense structure is the most stable of ZIF-7 (P. Zhao et al., 2014). In this study, the ZIF-7 is synthesized at 35℃ as the benzimidazole is hard to dissolve in room temperature water and the temperature is suitable for in-situ encapsulation for laccase in MOF as the optimum temperature for free laccase is at 40℃ (Liu et al., 2023; Mazlan & Hanifah, 2017). This XRD pattern also show similar to report of Ebrahimi M. and Mansournia M. (2017) (Ebrahimi & Mansournia, 2017).

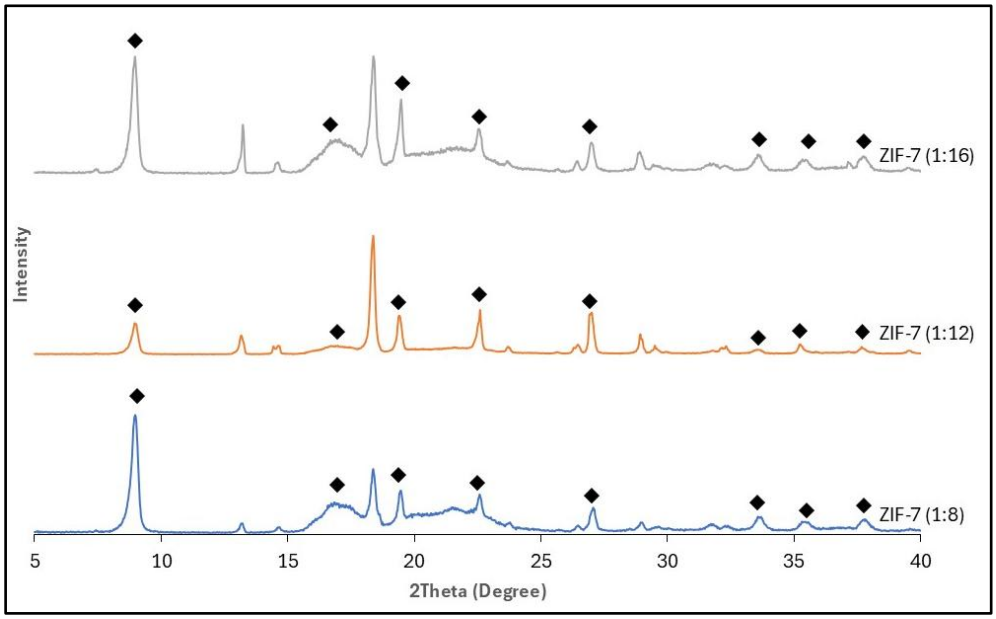

Figure 4.11 XRD Pattern for ZIF7 with Different Concentration of Metal to Organic Ligand Ratio.

FTIR spectra pattern of ZIF-7 with different concentration ratios shown in Figure 4.12. This spectra pattern shows that there no significant difference between these ZIF-7s even though different concentration ratios between metal ion and organic ligands, which show the interaction of the precursor are the same. Like ZIF-8 and ZIF-67, peak shown in range of 515cm^{-1} to 2000cm^{-1}. There is no wide N-H stretch bond of raw benzimidazole at range of 2500 to 3250 cm^{-1} (Yoon et al., 2021). At peak of 738 cm^{-1} show the imidazole in-plane ring bending (Jia et al., 2022). The peak of 1285 cm^{-1} and 1446 cm^{-1} show the entire benzimidazole ring stretching and C-C bond of benzimidazole stretching, respectively (Anwar et al., 2024). The peak of aromatic C=C appear at 1589 cm^{-1} (Yoon et al., 2021).

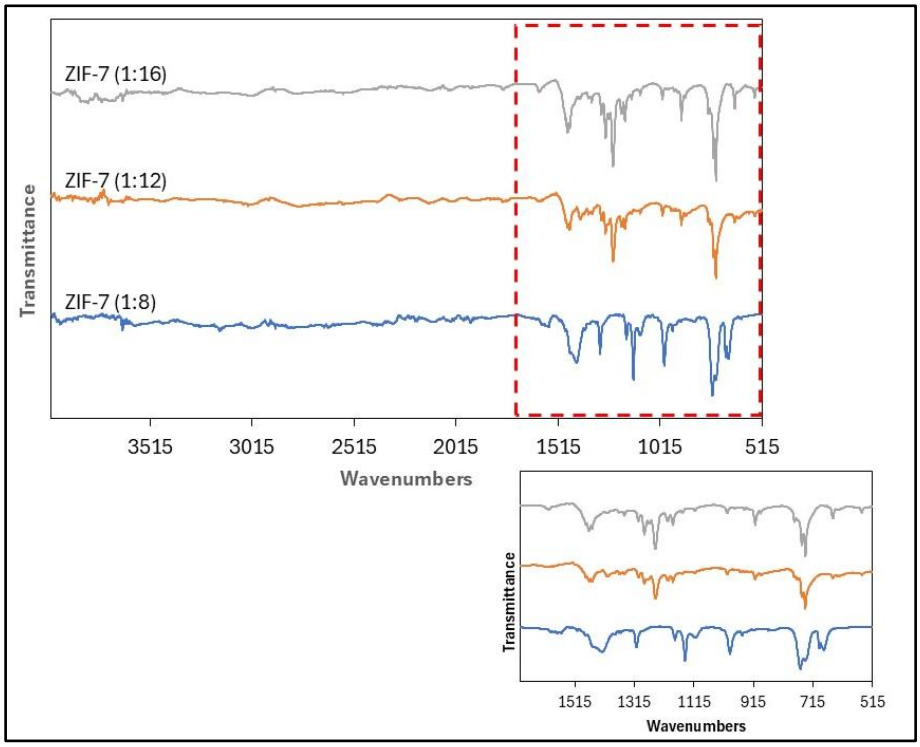

Figure 4.12 FTIR Spectra Pattern of ZIF-7 with Concentration Ratios of Metal:Ligand

The thermogram of ZIF-7 in different concentrations ratio of metal ion to organic ligand during synthesis is shown in Figure 4.13 and the total weight loss of the ZIF-7 in different concentrations ratio is shown in Table 4.5. ZIF-7 go through first thermal degradation at 120 ℃ for ZIF-7 (1:8) and 179 ℃ for ZIF-7 (1:12) and (1:16). This happens because of the removal of water and benzimidazole residue. Benzimidazole degrade above the melting point which at 170-172 ℃ ("BENZIMIDAZOLE," 1939). During this first degradation, ZIF-7 (1:12) drop very low to 30 weight percent, showing there are a lot of benzimidazole residue compared to other concentration ratio (ZIF-7 (1:8) and ZIF-7 (1:16) have hole defect make the benzimidazole less in the structure). After first degradation, all ZIF-7 have a long plateau, showing a stable structure of ZIF-7 throughout the temperature. For ZIF-7 (1:8), second thermal degradation occurs at 500 ℃, showing the ZIF-7 (1:8) structure start to collapse. This is because of the lack of benzimidazole ratio that reduce the crystal formation and reduce the ZIF structure integrity. Compared to ZIF-7 (1:12) and (1:16) the structure starts to collapse at temperature near to 700℃. These structures show better integration that prevent it to destruct early compared to ZIF-7 (1:8). ZIF-7 (1:16) have lowest weight loss (55%) because it has low benzimidazole impurity in ZIF-7 structure

(due to have hole of defect as shown in FESEM) in first degradation drop even though have same long and high temperature stability with ZIF-7 (1:12) (78.6%).

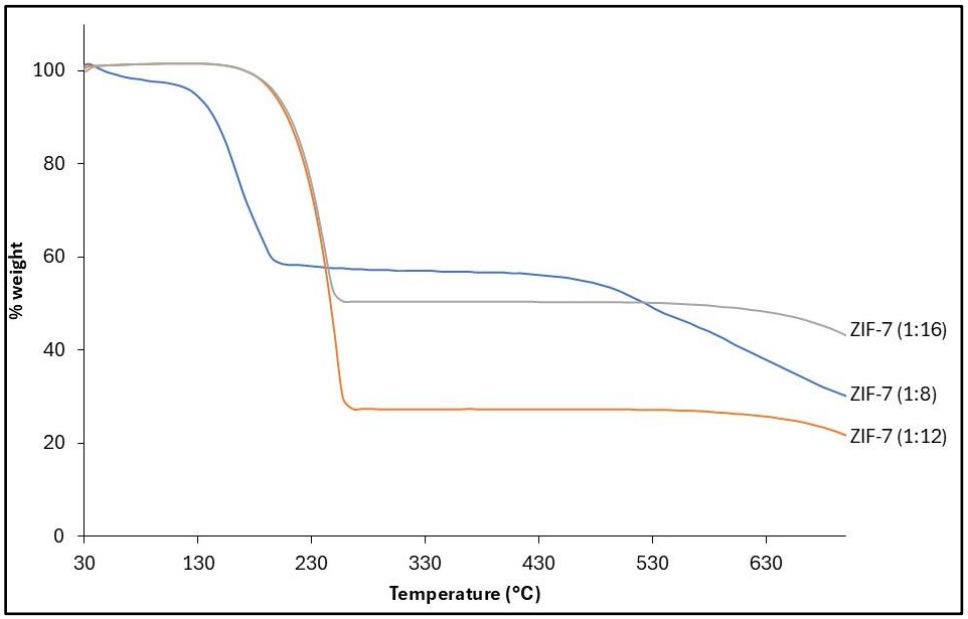

Figure 4.13 The Thermogram of ZIF-7 with Different Concentration ratio of Metal:Ligand

Table 4.5
The Total Weight Loss of ZIF-7 with Different Concentration Ratio of Metal:Organic Ligand

ZIF	Ratio metal to ligand	Total weight loss (%)
ZIF-7	1:8	70.0
	1:12	78.6
	1:16	55.0

Table 4.6 show the BET surface area, pore volume, pore size and particle size of ZIF-7 with different concentration ratio of precursor. These BET surface area and the pore volume show nearly similar to report by Ebrahimi M. and Mansournia M. (2017) (Ebrahimi & Mansournia, 2017). The low surface areas of ZIF-7 (1:8) and (1:12) is suggesting the insufficient organic ligand to coordinate zinc ions, leads to incomplete framework formation, or amorphization (as shown in the FESEM image in Figure 4.10). ZIF-7 (1:16) show high surface area, due to the structure defect even though show amorphous structure in FESEM image in Figure 4.10(c). This is due to the sparing soluble of benzimidazole in water and needing high pH to deprotonation. Small value

of pore volume suggests that these ZIF-7s (1:8, 1:12 and 1:16) have poor porosity (due to amorphization), as reported by Ebrahimi M. and Mansournia M. (2017) (Ebrahimi & Mansournia, 2017). For the pore size, ZIF-7 (1:16) have lowest pore size compared to 1:8 and 1:12, indicated higher ligand concentrations promoting better crystallinity, resulting in microporosity. The particle size of these ZIF-7s show the agglomerates except for the ratio 1:16. Agglomerates of 1:8 and 1:12 happen to the lack of nucleation site which lack organic ligand presence (dissolve in water), meanwhile, 1:16 have higher organic ligand presence, resulting more uniform crystallization.

Table 4.6
The BET Surface Area, Pore Volume, Pore Size and Particle Size of ZIF-7 with Different Concentration Ratios

ZIF-7 (metal:ligand)	BET surface area (m^2/g)	Pore volume (cm^3/g)	Pore size (nm)	Particle size (μm)
1:8	2.135	0.010	18.393	120.23
1:12	2.394	0.015	25.844	478.63
1:16	27.568	0.035	10.387	5.01

4.3 Physicochemical Properties of Enzyme-MOF (E-MOF) Complexes

From the Section 4.2 of characterization of ZIFs (ZIF-8, ZIF-67 and ZIF-7) with different concentrations ratio, each of the ZIFs will be selected based on their characteristics for enzyme encapsulation for further study. The MOF structure will not change its characteristic and its stability when enzyme embedded into it (Cui et al., 2017; Ren et al., 2018). ZIF-8 (1:16) from ZIF-8 group, ZIF-67(1:12) from ZIF-67 group and ZIF-7(1:16) from ZIF-7 group will be selected for enzyme encapsulation.

For ZIF-8 (1:16), the FESEM image show the structure is nearly to standard structure of ZIF-8 of rhombic dodecahedron (truncated rhombic dodecahedron). For XRD, the ZIF-8 (1:16) also show all peak of standard ZIF-8 (JCPDS card of ZIF-8) compared to other concentration ratio of ZIF-8. For TGA, ZIF-78 (1:16) show better thermal stability (the plateau) up to 700℃ compared to other ZIF-8s. The ZIF-8 (1:16) also has the highest surface area, and larger pore volume compared to others, showing these characteristics assisting in increasing the enzyme immobilization by providing huge space for enzyme stay inside. The lower pore size of ZIF-8 (1:16) also help to reduce enzyme leaching.

For ZIF-67 (1:12), the FESEM image show the consistent structure of ZIF-67 with no significant different size compared to ZIF-67 (1:8) and ZIF-67 (1:16). XRD for ZIF-67 have no significant difference for all concentration ratios as all ZIF-67 XRD patterns show all peak of ZIF-L. ZIF-67 (1:12) show the smallest pore size compared to other ZIF-67s, share same pore volume to ZIF-67 (1:16) and have surface area in between ZIF-67(1:8) and ZIF-67 (1:16). Even though ZIF-67 (1:12) have small pore volume, but it has the lowest weight loss of thermal degradation in TGA compared to ZIF-67 (1:8) and (1:16) and has a long plateau of thermal stability in TGA that slowly degrade at third thermal degradation compare to ZIF-67 (1:16) albeit the range temperature of plateau same to ZIF-67 (1:16) (but ZIF-67 (1:16) steep drop of third degradation of crystal structure collapse). Like ZIF-8 (1:16), ZIF-67 (1:12) also have lowest pore size compared to others to reduce enzyme leaching even though the surface area not the largest as ZIF-67 (1:8) have leafy-like structure, but the structure of ZIF-67 (1:8) itself might induce the enzyme leaching especially on high force. Other than that, the pore volume of all ZIF-67s have slightly same volume, which enzyme compaction may happen.

For ZIF-7 (1:16), FESEM image show standard shape structure of spherical shape even though it has little defect and still in amorphous condition like ZIF-7 (1:8) and (1:12). Like ZIF-67, XRD of ZIF-7 also have no significant difference as all ZIF-7 XRD pattern show same for all peaks. Same as ZIF-8 (1:16) and ZIF-67 (1:12), ZIF-7 (1:16) have better thermal stability compared to other ZIF-7 with different concentration ratios as it has long plateau of crystal structure stability, lower weight loss and slow in third degradation. Like ZIF-8 (1:16), ZIF-7 (1:16) have the largest surface area, largest pore volume and the lowest pore size, which helping in increase the chances of enzyme encapsulation and reduce the enzyme leaching.

4.3.1 Enzyme Immobilization in E-MOF Complexes

In encapsulating the laccase in the ZIF, the laccase solution of 1mg/mL in buffer solution (pH 7) is added together with the ZIF's precursors solution by using *in situ* encapsulation/one pot synthesis. The concentration during pristine ZIF synthesis remain the same in this encapsulation synthesis. The ZIF that used for laccase as embedding matrix support are selected as explained in Section 4.3.

The laccase from *Trametes versicolor* is used embedded in the selected ZIFs producing L@ZIFs (L@ZIF-8, L@ZIF-67 and L@ZIF-7). The enzyme loading into the ZIFs is observed by using UV-vis spectrometer. These E-MOF go through characterization of FESEM, XRD, TGA, FTIR, BET, and particle analysis.

These L@ZIFs show different enzyme loading as shown in Table 4.7. The average of laccase loading for L@ZIF-8 load 65.15% laccase, L@ZIF-67 load 81.01% laccase and L@ZIF-7 load 61.2% laccase. This different enzyme loading on different ZIFs is due to the pore volume and the particle morphologies. The L@ZIF-8 have high loss of enzyme during centrifuge compared to others L@ZIFs that is 6.55%. High enzyme leakage of L@ZIF-8 during centrifuge is due to the ZIF-8 high pore size (Table 4.8) and centrifugal force causing the laccase leak out from the ZIF-8. High loading of enzyme of L@ZIF-67 can happen due to enzyme adsorption on the ZIF-67 which can happen during synthesis *in situ* encapsulation, as reported by Wang Z. et al. (2020) as the pore volume of ZIF-67 lower compared to other ZIFs in this study (Z. Wang et al., 2020). The other reason might be the high amount of the laccase in small volume of L@ZIF-67 that cause compaction (Nadar et al., 2020; Pu et al., 2019). Meanwhile, L@ZIF-7 have that amount laccase loading because the laccase left with residue in the benzimidazole which laccase might stick together with benzimidazole particle residue with average 17.83%. Benzimidazole sparingly dissolve in water in 35℃, therefore the residue particle left at the wall of the bottle/beaker.

ZIFs are traditionally synthesized with organic solvent such methanol or DMF. However, for laccase immobilization, *in-situ* encapsulation method is not suitable to use organic solvent due to enzyme denaturation during synthesis (Dai et al., 2010; Knedel et al., 2019). The organic solvent usually used in enzyme infiltration, adsorption or chemically linked method which the enzyme immobilized in readymade ZIFs (synthesis using organic solvent). For example, Laccase immobilized on the ZIF-8 (ZIF-8 prepared using methanol) through chemical linking (amine functionalization) have loading ratio enzyme to ZIF-8 1:1 (Mahmoodi & Abdi, 2019). In other literature, mesoporous ZIF-8 (synthesized using methanol and trimethyl acetic acid as template) have laccase loading of 0.4 g/g through infiltration (Sun et al., 2023). This has higher laccase loading because it has large pores which promote enzyme infiltrate the pore, plus using glutaraldehyde as linking agent during immobilization increase the enzyme stay inside pore. The chemical linking and glutaraldehyde reduce the enzyme activity by covering the active site from reaction (Saddique et al., 2023). Furthermore, these

methods required extra time, and expensive chemical compared to *in-situ* encapsulation (Saddique et al., 2023). Infiltration method lacking in heat and mass transfer due to enzyme compaction (high enzyme loading) causing low enzyme activity (Liang et al., 2020).

Table 4.7
Mass Balance Calculations Leading to Enzyme Loading Percentage

	Feed amount (mg)	**During synthesis (mg)**	**After centrifuge (mg)**	**Enzyme loading (%)**
L@ZIF-8	1	0.71	0.65	65.44
L@ZIF-67	1	0.86	0.81	81.02
L@ZIF-7	1	0.91	0.89	70.74

The FESEM images of the L@ZIFs are show in the Figure 4.14. From the images, all L@ZIFs (L@ZIF-8 and L@ZIF-7) show same morphology and structure with pristine ZIFs except for the ZIF-67 (Figure 4.14(b)) which more flowery, needley and flat. For L@ZIF-8 (Figure 4.14.(a)), its result corresponds to report by Cui J. et al. (2017), which ZIF-8 will not change it structure and morphology when embedded with macromolecules through in-situ encapsulation (Cui et al., 2017).

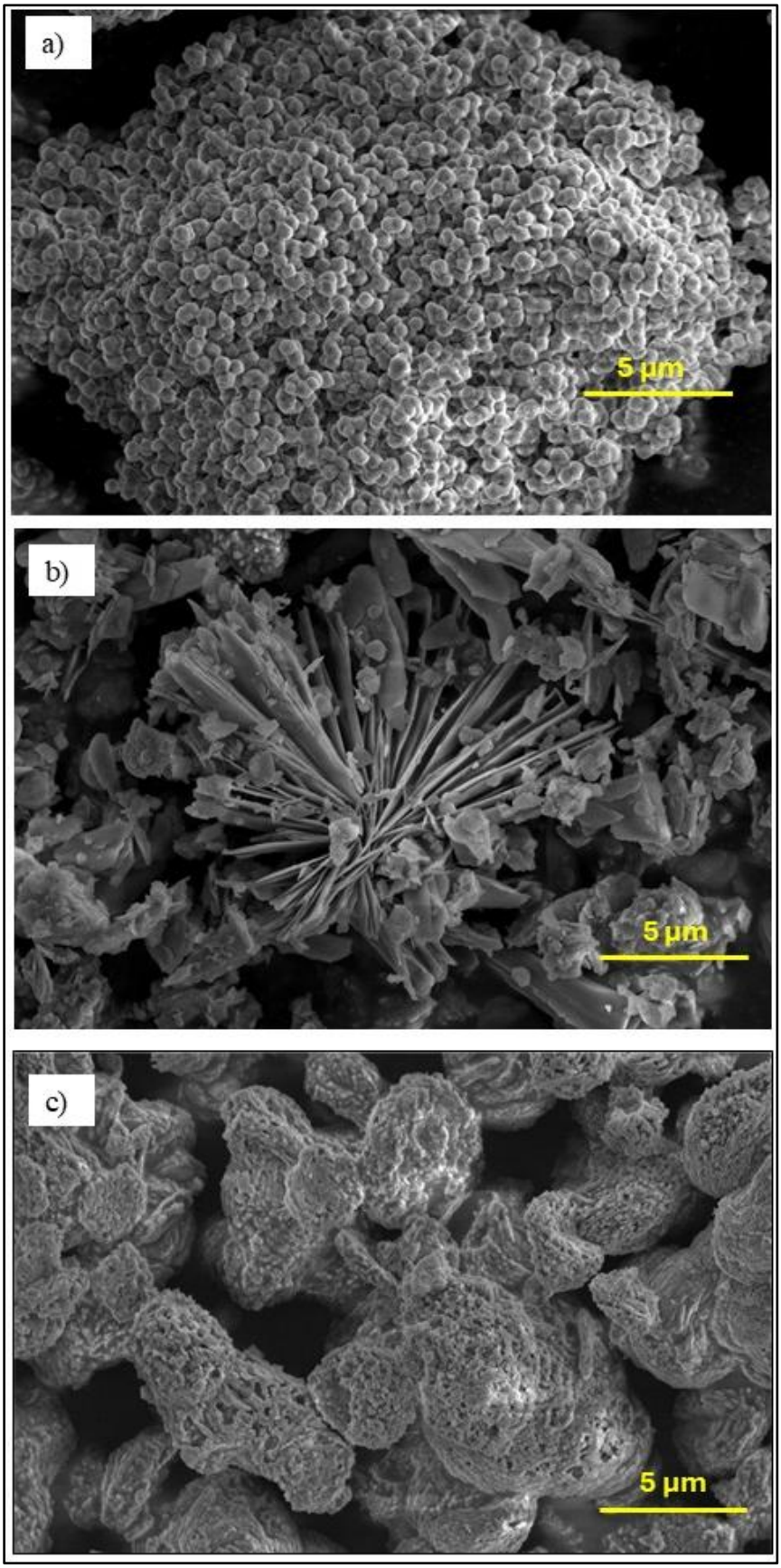

Figure 4.14 The FESEM Images (Magnification x5k) of a) L@ZIF-8, b) L@ZIF-67, and c) L@ZIF-7

Figure 4.15 show FTIR spectra comparison in between L@ZIF-8 and ZIF-8 (Figure 4.15(a)), L@ZIF-67 and ZIF-67 (Figure 4.15(b)) and L@ZIF-7 and ZIF-7 (Figure 4.15(c)). The FTIR of the L@ZIF-8 and L@ZIF-7 have shown not significant difference compared to their pristine ZIFs in Figure 4.15 (a) and (c) but they show a small peak of laccase at 1560 cm^{-1} of L@ZIF8 and 1590 cm^{-1} of L@ZIF-7 for amine II band. For amine I band, L@ZIF-7 at peak 1648 cm^{-1}. L@ZIF-8 and L@ZIF-7 show C-O band at 991 cm^{-1} and 1000 cm^{-1}, respectively. For L@ZIF-67, the FTIR pattern showing the peak of the laccase at wavelength of 1638 cm^{-1} showing amine I band and C=O bending, and 1558 cm^{-1} showing amine II band, N-H bending and C-N bending (Mansor et al., 2015; S. Zhang et al., 2018). The peak of 1015 cm^{-1} show the C-O bond of the laccase (Mansor et al., 2015). These peaks show the characteristic bond of the protein. This FTIR pattern of L@ZIF-67 is due to the method during the synthesis which the synthesis solution was let unstirred overnight. During that time, laccase that not encapsulated adsorb on the ZIF-67 structure. Figure 4.16 show the FTIR spectra of all L@ZIFs after laccase immobilization. The FTIR show that L@ZIF-8 and L@ZIF-7 have similarity FTIR spectra compared to L@ZIF-67 which show obvious laccase peak. This is due to the synthesis method which L@ZIF go through unstirred overnight before centrifuge and drying.

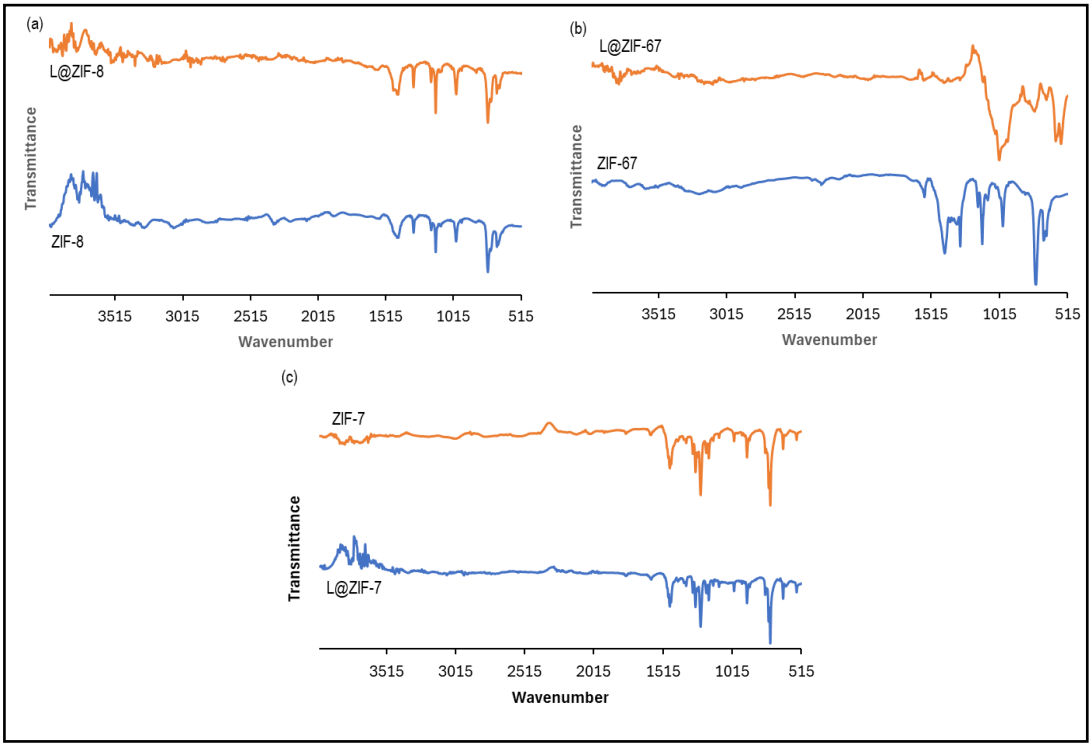

Figure 4.15 The FTIR Pattern of a) L@ZIF-8 and ZIF-8, b) L@ZIF-67 and ZIF-67 and c) L@ZIF-7 and ZIF-7

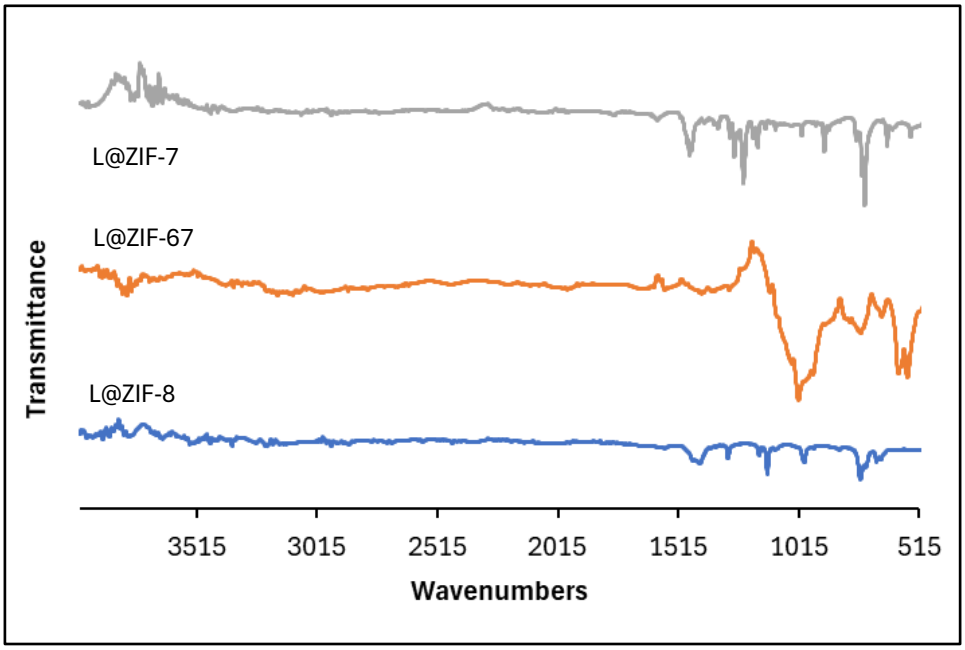

Figure 4.16 FTIR Spectra of L@ZIF-8, L@ZIF-67 and L@ZIF-7

The XRD pattern of the comparison of the L@ZIFs and pristine ZIFs shown in Figure 4.17. The peak of L@ZIFs in XRD pattern have no significant different with the pristine of ZIFs in Figure 4.17(a) and Figure 4.179(c) (for ZIF-7) except for the L@ZIF-67 (Figure 4.17(b)), the first peak of the XRD so high that make the other peak small and the first peak shift to the left. The XRD pattern corresponds to the FESEM images, showing the morphology of L@ZIF-8 and L@ZIF-7 does not change with its pristine. The L@ZIF-67 changes might due the different interaction of ZIF-67 precursors (as explained in Section 4.2.2). When adding enzyme for immobilization, the ZIF crystal nucleation changes to achieve the enzyme encapsulation (Liang et al., 2015). Figure 4.18 show the XRD pattern of all L@ZIFs. This Figure show that the different ZIFs have different XRD patterns after laccase immobilization, which corresponding to their different morphology from the FESEM images.

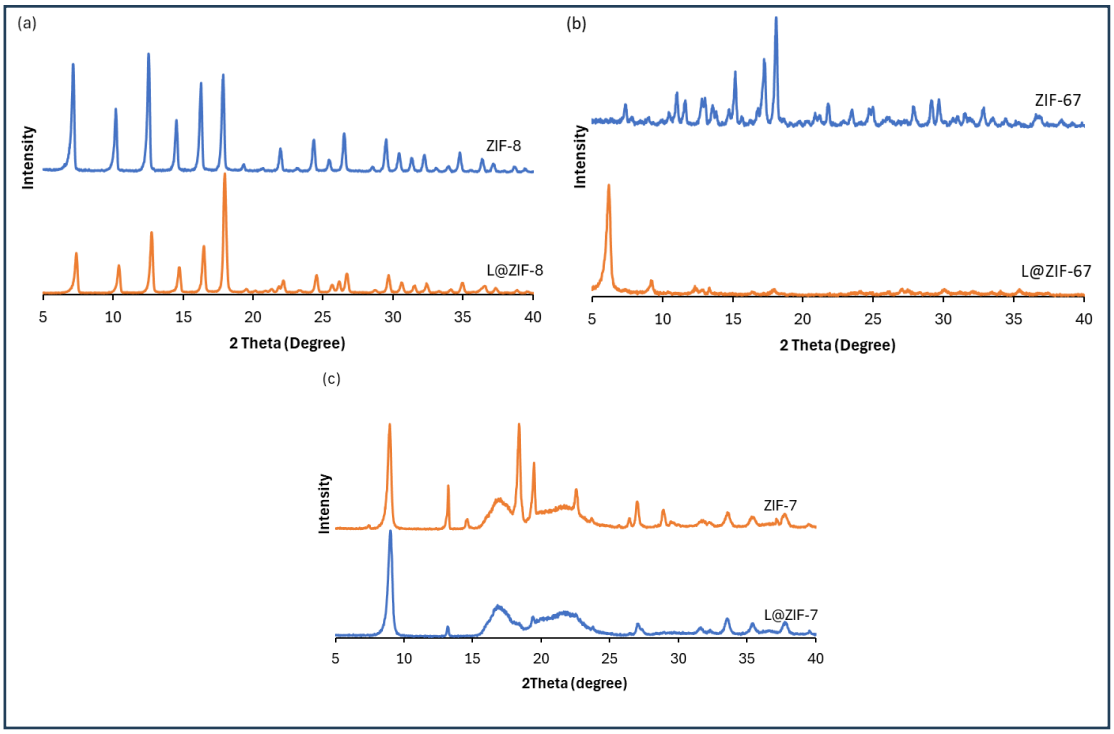

Figure 4.17 The XRD Pattern of a) ZIF-8 and L@ZIF-8, b) ZIF-67 and L@ZIF-67 and c) ZIF-7 and L@ZIF-7

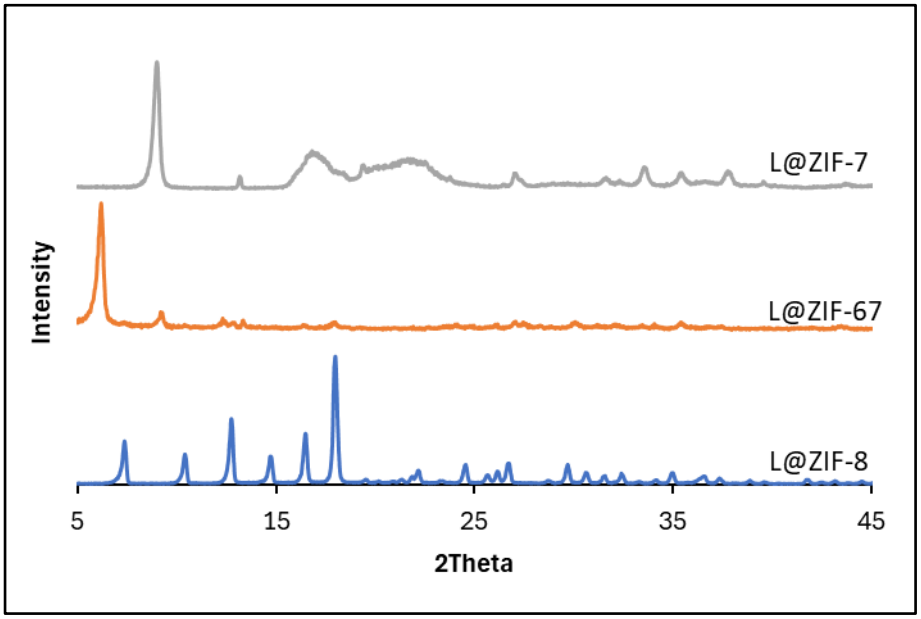

Figure 4.18 XRD Pattern of L@ZIF-8, L@ZIF-67, and L@ZIF-7

The comparison of L@ZIFs and pristine ZIFs for TGA thermogram is shown in Figure 4.19 and the TGA thermogram of the L@ZIFs is shown in the Figure 4.20. For Figure 4.19, all L@ZIFs have lower thermal structure stability (the TGA plateau) compare its ZIFs respectively. This result happens due to the enzyme incorporation in

the MOF causing the crystal arrangement disrupted thus reduce the structure stability. The high weight loss of first drop for L@ZIF-8 (Figure 4.19(a)) and L@ZIF-7 (Figure 4.19(c)) and second drop for L@ZIF-67 (Figure 4.19(b)) is due to higher guest molecules (enzyme, water and imidazole) compared to pristine ZIF (only water and imidazole) (Tu et al., 2022; Z. Wang et al., 2020). Figure 4.19(c) show the L@ZIF-7 have lower weight loss after first drop, showing less guest molecule inside L@ZIF-7 compared to others.

From Figure 4.20, L@ZIF-8 show very significant plateau after first thermal degradation (guest molecules removals) compared to L@ZIF-67 and L@ZIF-7 which show very small plateau. This show that L@ZIF-8 have better structure stability toward elevated temperature compared to others. These thermogram shows that L@ZIFs still can withstand high temperatures.

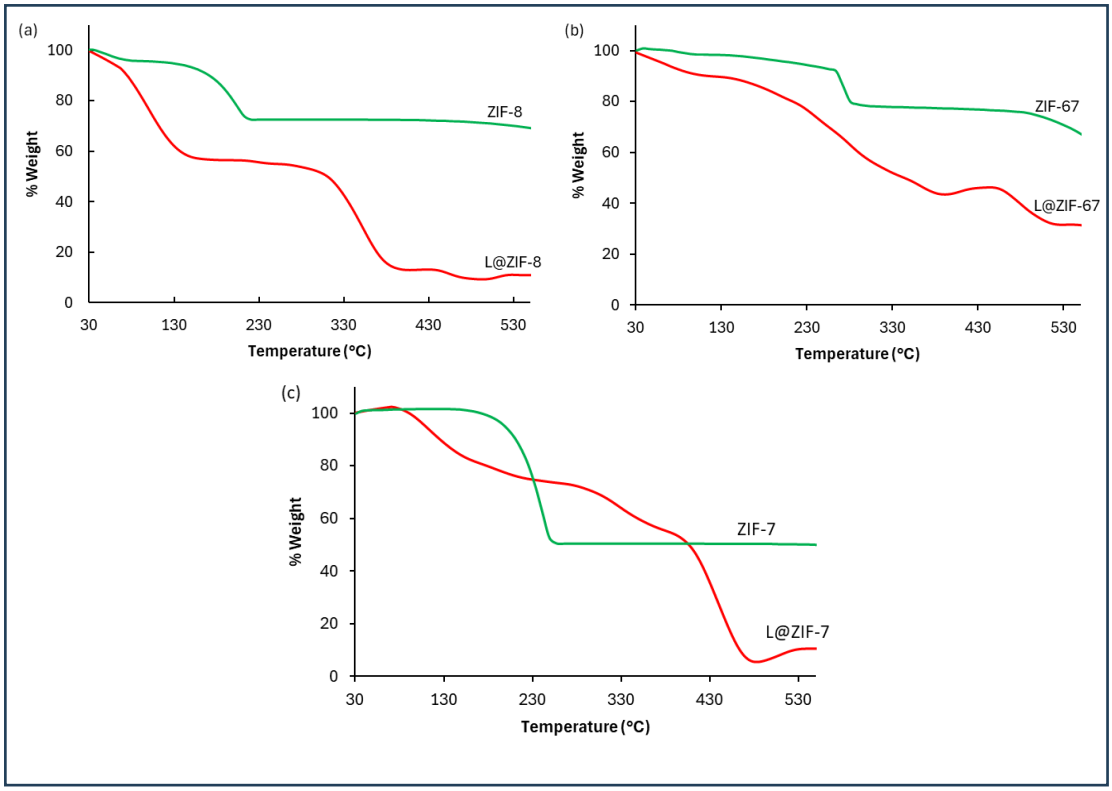

Figure 4.19 The TGA Thermogram of a) ZIF-8 and L@ZIF-8, b) ZIF-67 and L@ZIF-67 and c) ZIF-7 and L@ZIF-7

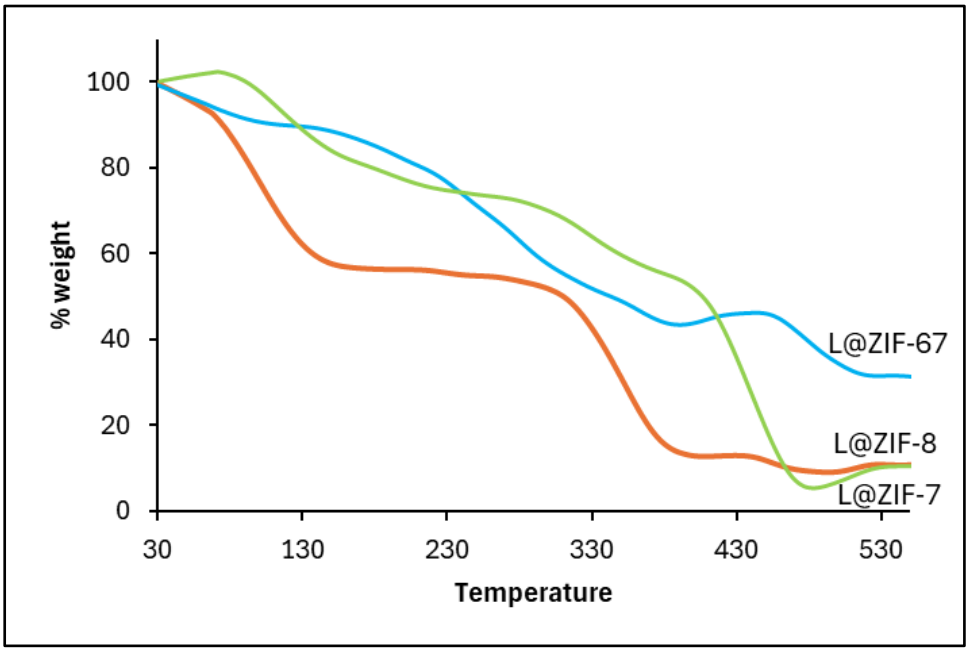

Figure 4.20 The Thermogram of TGA L@ZIF-8, L@ZIF-67, and L@ZIF-7

The BET surface area, pore volume, pore size and particle size of the L@ZIFs is shown in the Table 4.8. For the L@ZIF-8 and L@ZIF-7, the surface area and pore volume are reduce compared to the pristine ZIF-8 and ZIF-7 (552.59 m^2/g and 27.568 m^2/g for surface area and 0.312 cm^3/g and 0.035 cm^3/g for pore volume). These reductions show the presence of laccase embedded into the ZIF-8 and ZIF-7 which attribute to pore blocking and framework filling which inaccessible by nitrogen. For ZIF-67, there are different which increase of surface area and pore volume to the pristine ZIF-67, 1.71 m^2/g and 0.002 cm^3/g due to the morphology and structure changing during the synthesis as the result corresponds to FESEM image of L@ZIF-67 (Figure 4.14(b)).

For the pore size, the L@ZIF-8 and L@ZIF-67 shown the increment compared to their pristine, demonstrate the formation of mesoporous structures caused by the enzyme encapsulation and crystallization simultaneously. Meanwhile, L@ZIF-7 show reduction of pore size, which consistence with dense structure of ZIF-7 and microporous. However, the microporous of L@ZIF-7 can causing unfavourable enzyme diffusion, which can reduce the biocatalytic reaction.

For particle size, L@ZIF-67 show severe agglomeration and L@ZIF-8 show moderate agglomeration. This due to strong coordination between cobalt ion, ligands and protein induced nucleation. In this case, the enzyme work as nucleation site, the crystal aggregation occurs and causing large composite. The agglomeration also might

happen due to the interaction between the ZIFs itself (Van Der Waals forces). Meanwhile L@ZIF-7 produces the smallest particles, showing more controlling nucleation (due to the benzimidazole that sparing soluble).

Table 4.8
The BET Surface Area, Pore Volume, Pore Size and Particle Size of L@ZIF-8, L@ZIF-67, and L@ZIF-7

ZIF	BET surface area (m^2/g)	Pore volume (cm^3/g)	Pore size (nm)	Particle size (μm)
L@ZIF-8	2.992	0.012	16.012	104.71
L@ZIF-67	59.748	0.163	10.917	1096.48
L@ZIF-7	7.106	0.001	0.650	10.00

4.4 Laccase Kinetic Study

The catalytic performance of *Trametes versicolor* laccase was evaluated through kinetic analysis, applying the Michaelis–Menten model in three types of plots: Lineweaver-Burk, Hanes-Woolf and Eadie-Hofstie plots. Enzyme activity was determined at varying substrate concentrations of ABTS from 0.2 mM to 1.0 mM. For the Lineweaver-Burk plot, the reciprocal of reaction velocity ($1/V_o$) was plotted against the reciprocal of substrate concentration (1/[S]). From the linear regression, the y-intercept corresponds to $1/V_{max}$ and the x-intercept to $-1/K_m$. For Hanes-Woolf plot, [S]/ V_o was plotted against the substrate ([S]). From the linear plot, y-intercept correlated with (K_m/V_{max}) and $1/V_{max}$ is a slope. Meanwhile, Eadie-Hofstie plot was plotted V_o versus V_o/[S], which the y-intercept is V_{max} and the slope is $-K_m$.

Figure 4.21 illustrates three types of plots to determine the K_m and V_{max} of the free laccase: (a) Lineweaver-Burk, (b) Hanes-Woolf and (c) Eadie-Hofstie. These plots are used to determine the Michaelis-Menten constant (K_m) and the maximum reaction rate (V_{max}). The value of K_m and V_{max} of free Laccase used in this study is 0.27 mM and 0.0031 mM/min respectively which from the Hanes-Woolf plot. The Hanes-Woolf plot (Figure 4.21(b)) shows better R^2 of 0.9431 which have better accuracy compared to other plots. This result has slightly higher K_m and slightly lower V_{max} to report of Z. Li et. al (2024) of 0.22 mM and 0.00378 mM/min respectively (Zixuan Li et al., 2024). This can be due to the different conditions; room temperature at pH 7 while the report

at 30℃ at pH 6. The Michaelis constant (K_m) represents the substrate concentration at which the reaction rate reaches half of its maximum velocity. For free *T. versicolor* laccase, the measured K_m value reflects the intrinsic affinity between the enzyme's active site and the substrate. A lower Km indicates higher substrate affinity, implying that the enzyme can achieve significant catalytic rates even at low substrate levels. Conversely, a higher K_m suggests weaker binding, requiring higher substrate concentrations to approach saturation. In the context of biocatalysis for micropollutant degradation, a low K_m is advantageous as it ensures effective catalysis even at trace pollutant concentrations. The maximum reaction velocity (V_{max}) represents the catalytic turnover rate when the enzyme's active sites are fully saturated with substrate. It reflects the rate at which the enzyme–substrate complex converts to product under optimal conditions. A high V_{max} indicates efficient catalytic capability, directly influencing the throughput of pollutant degradation processes. From this, the result of K_m and V_{max} is slightly less enzyme affinity and catalytic turnover compared to reported.

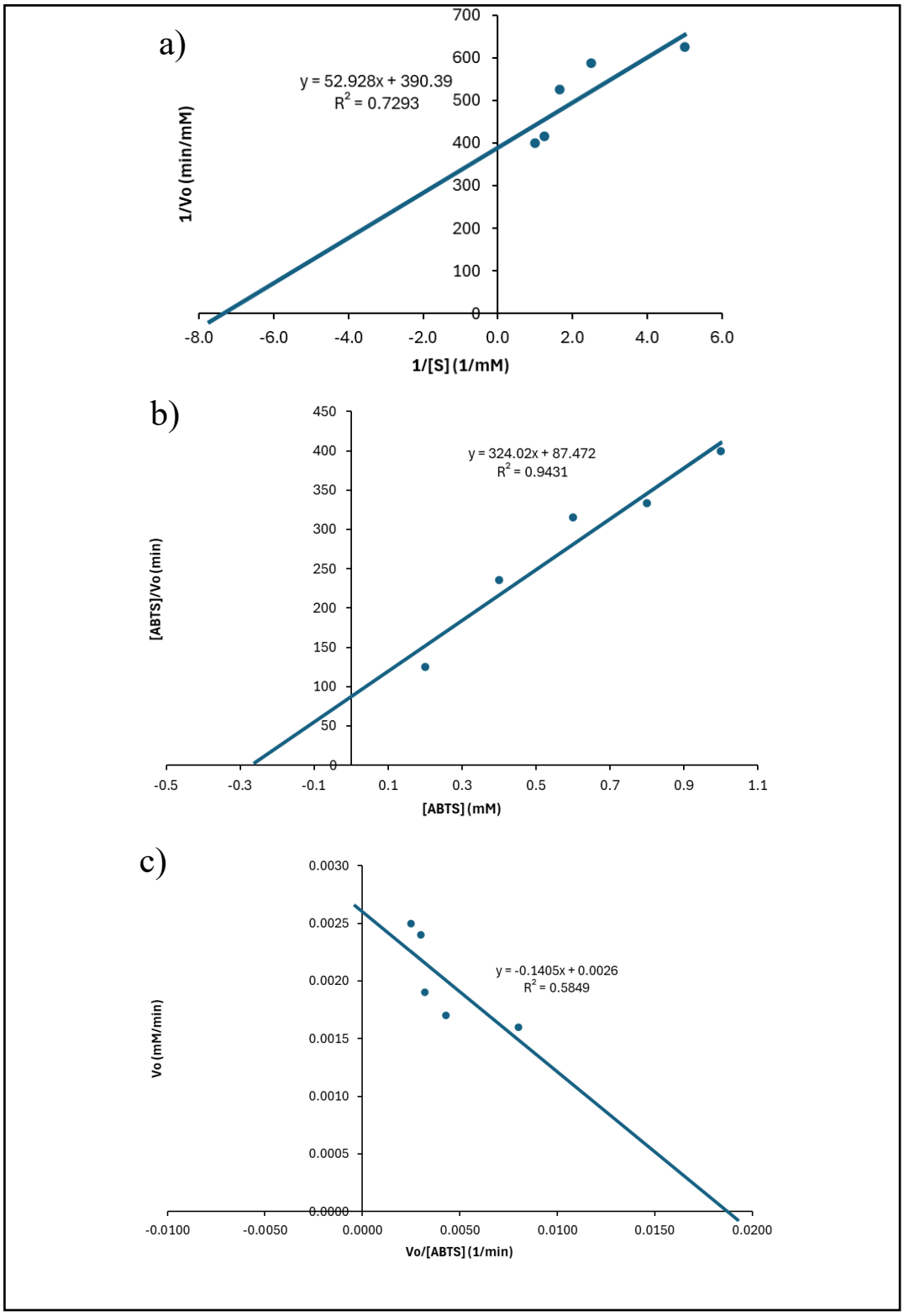

Figure 4.21 a) Lineweaver-Burk Plot b) Hanes-Woolf Plot and c) Eadie-Hofstee for Free Laccase.

In this study, the kinetic parameters for free *T. versicolor* laccase were successfully determined using the Hanes-Woolf plot, providing clear values for K_m and

V_{max} that reflected the enzyme's intrinsic substrate affinity and catalytic capacity. However, for the L@ZIFs, accurate determination of K_m and V_{max} was not possible. This limitation may arise from several factors, including the strong adsorption of the substrate onto the MOF's porous surface, which interferes with the accurate measurement of substrate concentration in the reaction medium; mass-transfer resistance within the MOF channels that prevents the enzyme from reaching true saturation; and potential light-scattering effects of the particulate MOF during spectrophotometric assays (Bolivar et al., 2022; Knedel et al., 2019; Rybarczyk et al., 2025; Xia et al., 2020). In addition, the heterogeneous nature of the immobilized system, where enzyme activity is influenced by both catalytic turnover and substrate diffusion into the framework, complicates direct application of the classical Michaelis–Menten model (Bolivar et al., 2022).

The heterogeneous nature of the E-MOF system means that catalytic performance is not governed solely by enzyme–substrate interactions, as in a free enzyme, but also by the influence of the solid support. In this dual-phase environment, the substrate must first diffuse through the MOF pores, where mass-transfer resistance and spatial confinement may restrict access to the active site. At the same time, substrate molecules can adsorb onto the MOF surface, altering their effective concentration near the enzyme. Furthermore, enzyme molecules immobilized within the MOF may adopt different orientations and experience distinct microenvironments compared to those in bulk solution, leading to variations in activity (Knedel et al., 2019; Patil & Yadav, 2018; Xu et al., 2023). These combined factors complicate the direct application of Michaelis–Menten kinetics, making K_m and V_{max} values for the E-MOF difficult to measure. Instead, adsorption and absorption studies of the MOF are more appropriate to elucidate how substrate–MOF interactions govern the observed catalytic behavior. Consequently, further insight into the E-MOF's performance can be better obtained through adsorption/absorption studies, which will elucidate how substrate–MOF interactions contribute to the overall catalytic behavior and pollutant removal efficiency.

4.5 Adsorption Studies of Pristine Particles (ZIF-8, ZIF-67 and ZIF-7)

Adsorption studies are an essential step in assessing the performance of ZIF materials for pollutant removal and for understanding their potential as E-MOF supports. Owing to their large surface area, tunable pore structure, and diverse surface

chemistry, ZIFs can interact strongly with organic micropollutants such as MB. The adsorption capacity and mechanism of a ZIF provide critical insights into how pollutants diffuse, interact, and localize within the porous framework. These studies are particularly relevant because the adsorption behaviour directly influences how substrates are delivered to active enzyme sites when ZIFs are later employed as immobilization matrices in E-MOF systems.

In this study, adsorption of MB onto pristine ZIF-8 and ZIF-67 was examined under controlled conditions at a range of dye concentrations from 16 to 30 ppm. These two frameworks, which share the sodalite topology but differ in their metal centres (Zn^{2+} in ZIF-8 and Co^{2+} in ZIF-67), were selected to enable a comparative evaluation of how the metal node affects MB adsorption. Meanwhile, ZIF-7 with different organic ligand demonstrate differently in adsorption study. because ZIF-7 exhibits surface chemistry that is less compatible with cationic dye adsorption. Unlike ZIF-8, whose imidazolate linkers display localized negative polarization that promotes electrostatic attraction with MB, the benzimidazolate linkers and Zn^{2+} centres in ZIF-7 produce a more neutral and hydrophobic surface (Sun et al., 2018). Such characteristics reduce electrostatic affinity and, in some cases, may even lead to repulsive interactions with MB molecules especially at pH neutral (Kiwaan et al., 2021).

The importance of evaluating adsorption behaviour extends beyond the physicochemical characterization of pristine ZIFs. When enzymes such as laccase are encapsulated within ZIF frameworks, the pollutant first interacts with the MOF surface before reaching the active enzyme site. Therefore, adsorption studies on pristine ZIFs provide a foundation for understanding how substrates accumulate, diffuse, and concentrate within the porous network. In the case of MB, its adsorption onto ZIF-8 or ZIF-67 directly influences the efficiency of subsequent biocatalytic oxidation by laccase in E-MOF systems. By clarifying the adsorption properties of these frameworks, this study establishes a mechanistic link between pollutant capture by the MOF and pollutant transformation by the enzyme, thus highlighting the dual contribution of adsorption and catalysis in achieving efficient MB degradation.

4.5.1 Adsorption Kinetics

The adsorption kinetics of MB onto ZIF-8 and ZIF-67 were evaluated using the pseudo-first-order (PFO) and pseudo-second-order (PSO) models in order to understand the underlying adsorption mechanisms and the rate-controlling steps. The experimental data, as shown in Figures 4.22 and 4.23, reveal distinct kinetic behaviours between the two ZIFs. In Table 4.9, ZIF-8, the PFO model provided a better correlation (R^2 = 0.9566) compared to the PSO model (R^2 = 0.8575), indicating that the adsorption process was predominantly governed by physical interactions and surface diffusion. The equilibrium adsorption capacity predicted by the PFO model was relatively low (Q_e = 1.32 mg/g), but the model's strong correlation suggests that diffusion onto external surfaces plays the most significant role in the initial uptake of MB by ZIF-8. The PSO model, however, predicted a much higher equilibrium capacity (Q_e = 31.95 mg/g), suggesting that chemisorption may also contribute to the adsorption process, although not as the dominant mechanism. The small pseudo-second-order rate constant (K_2 = 0.0004 g/mg·min) reflects a relatively slow adsorption rate, which is consistent with the gradual penetration of MB molecules into the microporous cavities of ZIF-8. After 5 hours of adsorption, ZIF-8 adsorb 58.1% of 16ppm of methylene blue.

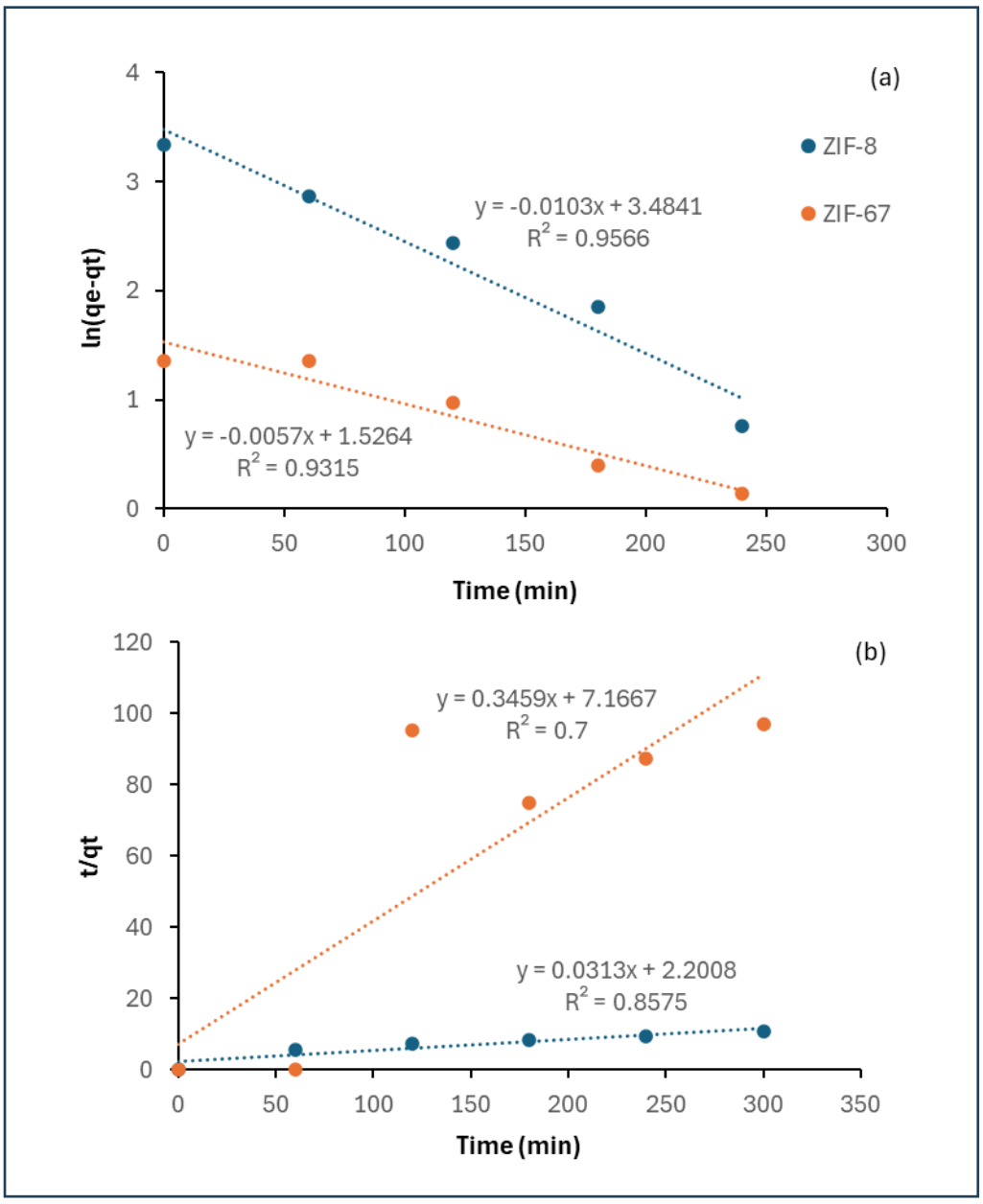

Figure 4.22 The Adsorption Graph of ZIF-8 and ZIF-67 of Methylene Blue (16ppm) with Best Fitted Line a) Pseudo-First Order Model and b) Pseudo-Second Order Model

Table 4.9
Pseudo-First Order and Pseudo-Second Order Kinetic Parameter in Methylene Blue (16ppm) Removal by Pristine ZIF-8 and ZIF-67

MOF	Pseudo-First Order Model			Pseudo-Second Order Model		
	K_1 (1/min)	Qe (mg/g)	R^2	K_2 (g/mg.min)	Qe (mg/g)	R^2
ZIF-8	0.0136	1.3208	0.9566	0.0004	31.9489	0.8575
ZIF-67	0.0058	0.4282	0.9315	0.0167	2.8910	0.7

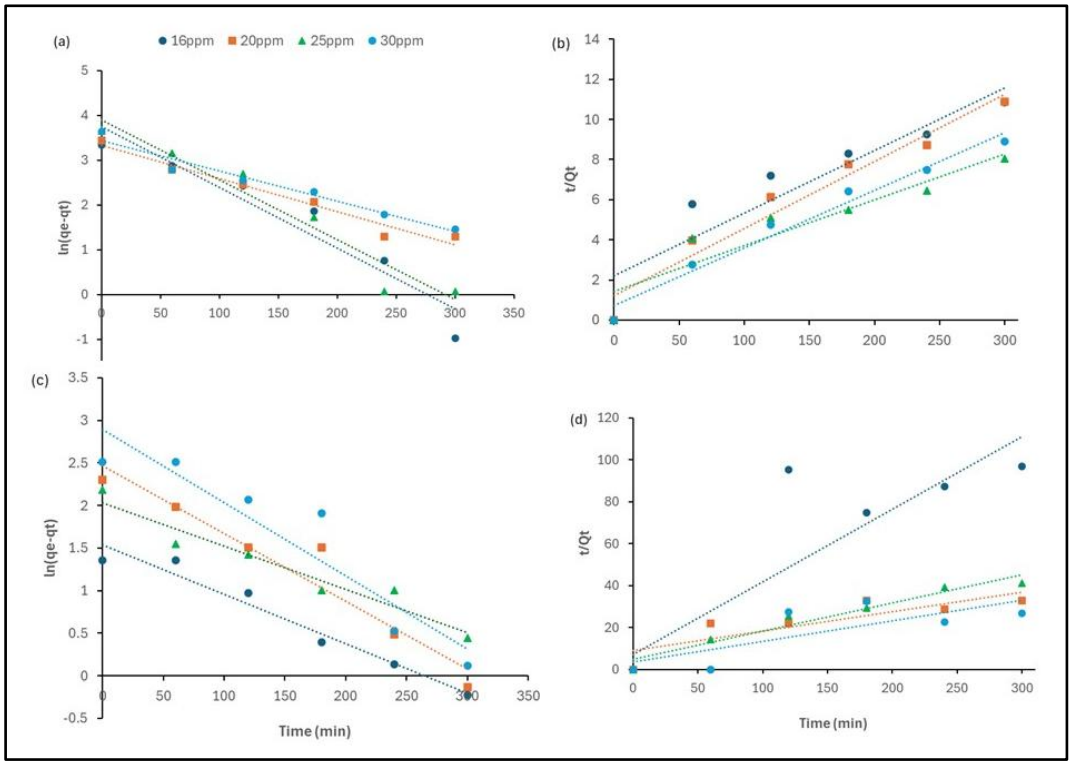

Figure 4.23 The Adsorption Graph of ZIF-8 and ZIF-67 of Methylene Blue with Best Fitted Line a) Pseudo-First Order Model ZIF-8, b) Pseudo-Second Order Model ZIF-8, c) Pseudo-First Order Model ZIF-67 and d) Pseudo-Second Order Model ZIF-67

For ZIF-67 in Table 4.9, the kinetic profile was markedly different. The PFO model again provided a stronger correlation ($R^2 = 0.9315$) compared to the PSO model ($R^2 = 0.700$), confirming that the adsorption of MB onto ZIF-67 was also dominated by weak physisorption processes. The calculated equilibrium adsorption capacity from the PFO model was only 0.43 mg/g, which is significantly lower than that of ZIF-8, reflecting the poor uptake ability of ZIF-67. The PSO model predicted a slightly higher capacity ($Q_e = 2.89$ mg/g), but its weak correlation coefficient ($R^2 = 0.700$) indicates that chemisorption was not a significant contributor. Interestingly, ZIF-67 exhibited a much larger pseudo-second-order rate constant ($K_2 = 0.0167$ g/mg·min) compared to ZIF-8, suggesting that the few adsorption sites available on ZIF-67 interacted relatively quickly with MB molecules. However, the overall adsorption was limited by the material's low capacity and structural instability in aqueous solution. After 5 hours of adsorption, ZIF-67 adsorbs 6.3% of 16ppm of methylene blue.

Meanwhile, ZIF-7 also conducted adsorption study with result show extremely low R^2 values (0.0532 for PFO and 0.005 for PSO) and unrealistic Qe values (-36.63 mg/g), indicating the conventional kinetics models are not applicable. Desorption

during the process associated with this result. Other attributes to this result are the instability structure of ZIF-7 in aqueous solution due to amorphous structure that can causing hydrolysis due to OH^- attack on benzimidazole and dynamic rearrangement of structure in water (Dahnum et al., 2019; He et al., 2013). Furthermore, ZIF-7 activity depends on pH of environment. The higher the pH, ZIF-7 become negatively charge. Since the adsorption study done in ultrapure water, there some of OH^- ion presence, causing ZIF-7 slightly negative charge thus interact with cationic dye (Kiwaan et al., 2021). But due to OH^- can attack benzimidazole-zinc binding, desorption happens.

The predominance of the pseudo-first-order model for both ZIF-8 and ZIF-67 suggests that external surface adsorption and diffusion are the primary rate-limiting steps, rather than strong chemical bonding. Nevertheless, the higher Q_e values predicted by the pseudo-second-order model, especially for ZIF-8, indicate that possible weak chemisorption effects cannot be completely ruled out. These findings are consistent with Younis S. et al. (2025) who emphasized that the suitability of PFO and PSO models typically indicates the coexistence of both physical and chemical mechanisms in dye adsorption processes (Younis et al., 2025). In the case of ZIF-8, both physisorption and chemisorption appear to act synergistically, whereas in ZIF-67, adsorption is largely restricted to weak physical interactions with limited surface accessibility.

Overall, the kinetic data demonstrate that ZIF-8 exhibits both higher adsorption capacity and more versatile adsorption mechanisms compared to ZIF-67. While both materials follow pseudo-first-order kinetics, ZIF-8 benefits from additional chemisorption contributions, resulting in significantly better performance for MB removal. These results further support the conclusion that ZIF-8 is a superior adsorbent for dye remediation applications, as it combines higher stability, larger pore accessibility, and stronger interaction sites relative to ZIF-67.

4.5.2 Adsorption Isotherm Analysis

The adsorption isotherm models were applied to further elucidate the equilibrium adsorption behaviour of methylene blue (MB) onto ZIF-8 and ZIF-67. Both the Langmuir and Freundlich models were tested, as shown in Figure 4.24 and Table 4.10. The Langmuir isotherm assumes monolayer adsorption on a homogeneous surface with identical adsorption sites and no lateral interactions between adsorbed molecules, whereas the Freundlich isotherm accounts for heterogeneous surface adsorption and

multilayer formation (Younis et al., 2025). The fitting of the experimental data to these models thus provides insight into the nature of dye–MOF interactions.

For ZIF-8, the adsorption data exhibited an excellent fit with the Langmuir isotherm, yielding a high correlation coefficient ($R^2 = 0.961$), a maximum adsorption capacity (Q_{max}) of 50.51 mg/g, and a Langmuir constant (K_L) of 0.1898 L/mg (Figure 4.24). These results clearly indicate that the adsorption of MB onto ZIF-8 occurs predominantly as a monolayer process on well-defined, energetically equivalent sites. The positive value of Q_{max} reflects strong affinity and effective uptake, suggesting that ZIF-8 provides uniform active sites accessible to MB molecules. The relatively high Langmuir constant further confirms the strong interaction between ZIF-8 and MB, which can be attributed to electrostatic attraction, π–π interactions with imidazolate linkers, and the large accessible pore volume of the ZIF-8 framework (Yu & Wu, 2020).

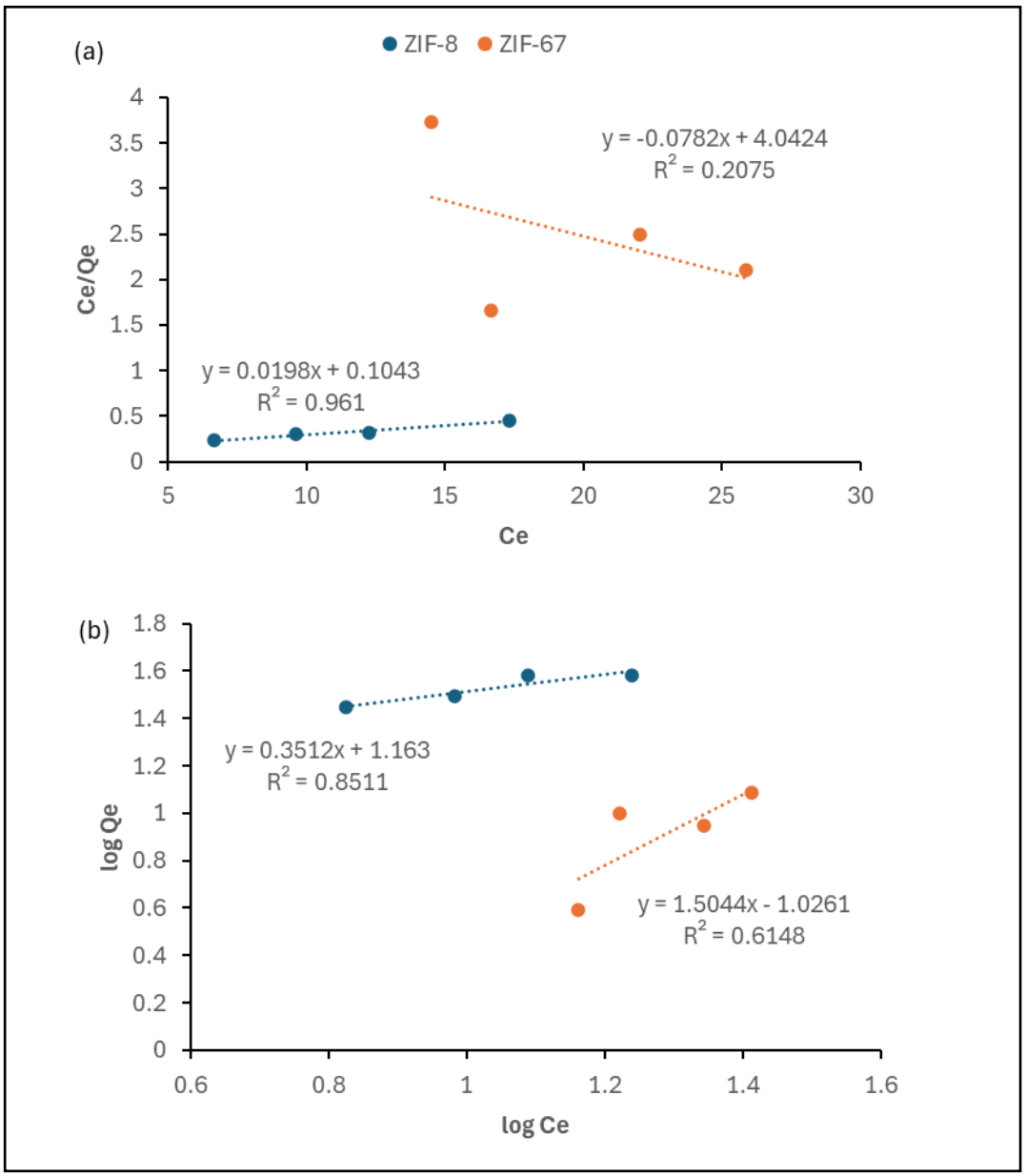

Figure 4.24 The a) Langmuir and b) Freundlich Isotherm of Pristine ZIF-8 and ZIF-67

Table 4.10
The Adsorption Parameter of Langmuir Isotherm and Freundlich Isotherm for ZIF-8

MOF	Langmuir Isotherm			Freundlich Isotherm		
	K_L (L/mg)	Qmax (mg/g)	R^2	K_F (mg/g)(L/mg)$^{(1/n)}$	1/n (mg/g)	R^2
ZIF-8	0.1898	50.5051	0.961	0.0656	0.3512	0.8511
ZIF-67	-0.01934	-12.7877	0.2075	0.0119	1.5044	0.6148

In contrast, the Langmuir isotherm was poorly fitted for ZIF-67, with a very low correlation coefficient (R^2 = 0.2075) and negative parameter values (Q_{max} = –12.79

mg/g; K_L = –0.0193 L/mg). A negative Q_{max} is physically meaningless and strongly suggests that the Langmuir model does not adequately describe the adsorption process in ZIF-67. Instead, the Freundlich isotherm provided a relatively better fit, with R^2 = 0.6148, a Freundlich consant (K_F) of 0.0119 mg/g$(L/mg)^{(1/n)}$, and a heterogeneity factor (1/n) of 1.5044. The high value of 1/n (>1) indicates unfavourable adsorption, implying that as MB concentration increases, the adsorption efficiency of ZIF-67 decreases. This behaviour is consistent with the framework instability of ZIF-67 in aqueous media, which reduces the number of active sites available and leads to heterogeneous, non-uniform adsorption (Qian et al., 2018).

The comparison between the two MOFs clearly highlights the superior adsorption characteristics of ZIF-8. Its adsorption conforms well to the Langmuir model, confirming monolayer coverage and efficient utilization of adsorption sites, while ZIF-67 shows only weak and irregular adsorption that cannot be explained by monolayer theory. The poor performance of ZIF-67 under the Langmuir model is further supported by literature findings where ZIF-67 has been reported to undergo partial structural collapse in aqueous solutions, thereby reducing pore accessibility (Qian et al., 2018).

Interestingly, the Freundlich model for ZIF-8 yielded a lower correlation coefficient (R^2 = 0.8511) compared to Langmuir, with K_F = 0.0656 and 1/n = 0.3512. The value of 1/n between 0 and 1 indicates favourable adsorption, suggesting that while ZIF-8 primarily follows monolayer adsorption, it also exhibits some degree of heterogeneous adsorption behaviour, possibly due to surface roughness, defect sites, or secondary interactions on external surfaces. This duality is common in porous materials where both internal pore surfaces and external particle surfaces contribute to overall adsorption capacity.

Taken together, the isotherm analysis reinforces the conclusion that ZIF-8 exhibits strong, uniform adsorption sites conducive to high-capacity MB uptake, whereas ZIF-67 provides weak, non-uniform interactions that are unfavourable for effective adsorption. The Langmuir-type monolayer adsorption of ZIF-8 is advantageous for dye removal applications as it implies predictable adsorption behaviour and efficient utilization of adsorbent material.

4.5.3 Mechanistic Adsorption Behaviour of ZIF-8 and ZIF-67

The adsorption studies revealed that ZIF-8 exhibits significantly superior adsorption performance compared to ZIF-67, a difference that can be attributed to both structural and chemical factors. In ZIF-8, Zn^{2+} ions coordinate with 2-methylimidazole linkers to form a chemically stable and moderately hydrophilic framework, enabling strong electrostatic attraction between the positively charged MB molecules (Feng et al., 2016). In contrast, ZIF-67, with Co^{2+} as its coordination centre, exhibits less favourable electronic interactions with MB (Tables 4.9 and 4.10). This fundamental difference in framework chemistry alters the surface charge distribution, thereby lowering the affinity of ZIF-67 toward cationic dye molecules.

The interactions governing MB adsorption on ZIF-8 are multifaceted and synergistic. Electrostatic attraction provides the primary driving force, supported by π-π stacking between the aromatic rings of MB and the imidazolate linkers, hydrogen bonding with nitrogen sites, and van der Waals forces within the pore walls (Darweesh et al., 2026; Yu & Wu, 2020). These combined interactions stabilize the adsorption process and result in efficient pollutant capture. By comparison, the same interactions are much weaker in ZIF-67, where reduced electrostatic compatibility of the Co-imidazolate framework and compromised aqueous stability limit effective dye uptake (Qian et al., 2018).

This mechanistic interpretation is consistent with the adsorption isotherm analysis, where ZIF-8 conformed well to the Langmuir model ($R^2 = 0.961$), indicating uniform monolayer adsorption, while ZIF-67 aligned more closely with the Freundlich model ($R^2 = 0.6148$), reflecting heterogeneous adsorption on partially collapsed surfaces (Qian et al., 2018). Overall, the adsorption mechanism of ZIF-8 is characterized by structured monolayer uptake and strong surface interactions, establishing it as a robust and effective platform for pollutant capture, whereas ZIF-67 relies on weak and irregular adsorption processes with limited practical effectiveness.

Importantly, these findings provide a foundation for understanding how ZIF-based supports govern substrate accumulation and diffusion, which in turn directly influences the efficiency of enzyme-MOF systems in the subsequent biocatalytic oxidation of methylene blue.

4.6 Biocatalytic Oxidation of Methylene Blue

The biocatalytic oxidation of MB by E-MOFs represents a complex-synergistic mechanisms of adsorption, absorption, and enzymatic catalysis that collectively determines pollutant removal efficiency. The assessment involved L@ZIF-8, L@ZIF-67 and L@ZIF-7. Even though L@ZIF-7 demonstrates the principle of laccase encapsulation, its poor porosity and severe diffusion limitations due to surface chemistry that is less compatible with cationic dye adsorption.

E-MOF complexes contain about 1 mg of laccase is added into 10 mL of 0.05 mM methylene blue and the colour of methylene blue is observed and analysed for every 7 days by using UV-Vis spectrophotometer. Figure 4.25 show the biocatalytic reduction of methylene blue for a duration of 4 weeks. As shown in Figures 4.25 and 4.26, L@ZIF-8 exhibited superior performance compared to L@ZIF-67 and their pristine analogues. This is because L@ZIF-8 have larger surface area compared to other ZIFs. The L@ZIF-8 also have larger pore size that helping the enzyme expose to the substrate better (as shown in the Table 4.8). Even though L@ZIF-67 have highest enzyme loading among other L@ZIFs, the biocatalytic oxidation of MB by L@ZIF-67 is not rapid as L@ZIF-8. This might be due to the high amount laccase in small volume of L@ZIF-67 that cause compaction and the laccase's active site cannot be expose to the substrate. Furthermore, the laccase that absorb on the ZIF-67 might be degraded due to the drying process during L@ZIF-67 preparation (60℃).

L@ZIF-7 go through same procedure of methylene blue reduction like L@ZIF-8 and L@ZIF-67 but L@ZIF-7 gain the lowest reduction of 13.68% over 4 weeks. The reduction show adsorption at week 1 and week 2 of 13.79% and 14.22% respectively. However, desorption happens in week 3 and continue desorption until week 4 with 13.95% and 13.68% respectively. This situation happens due to the amorphous structure and presence of OH^- in ultrapure water that can attack to benzimidazole-zinc binding causing hydrolysis (mention in Section 4.5.1) (Dahnum et al., 2019; He et al., 2013). Other function of OH- is to negatively charge of neutral ZIF-7 to promote adsorption of methylene blue (Kiwaan et al., 2021). Due to this desorption, biocatalysis impossible because the result of adsorption of ZIF-7 throughout 4 weeks also obtained similar results.

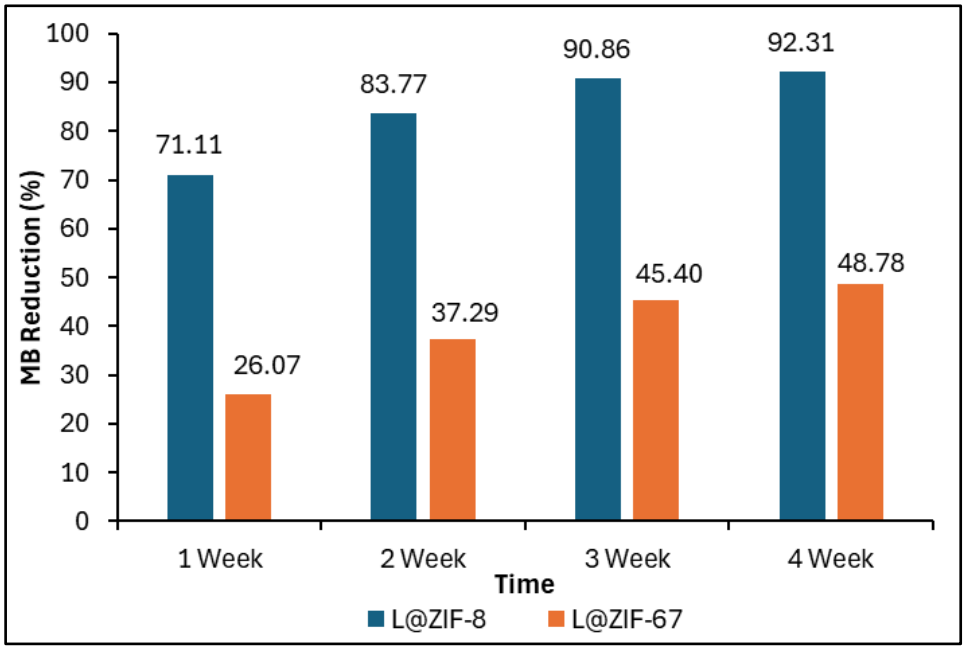

Figure 4.25 The Biocatalytic of Methylene Blue by Using Different L@ZIF Throughout 4 weeks

At the adsorption stage, MB molecules are initially concentrated onto the external and internal surfaces of the MOF via electrostatic attraction and π–π interactions. The cationic MB interacts with the negatively polarized imidazolate linkers of ZIFs, while aromatic stacking stabilizes MB uptake within pore channels. ZIF-8, with larger pore openings provided more accessible sites than ZIF-67, resulting in faster adsorption kinetics (Figure 4.22 and 4.23). Similar adsorption-assisted catalytic enhancement was reported by Zhou et al. (2022), where laccase immobilization improved micropollutant removal by coupling sorptive concentration with biocatalysis (Zhou et al., 2022).

Following adsorption, MB diffuses (adsorption) into the porous framework where immobilized laccase molecules are confined yet accessible. This microenvironment increases the local substrate concentration near the catalytic sites. The more open porosity of ZIF-8 thus maintained a balance between enzyme loading, substrate diffusion, and product release, while in L@ZIF-67, steric crowding limited substrate access and led to eventual pore blockage (Figure 4.25). The catalytic step proceeds via the multicopper oxidase mechanism of laccase. The Type 1 (T1) copper site oxidizes MB into a radical cation, which can undergo N-demethylation or aromatic cleavage to form decolorized intermediates (Arregui et al., 2019; Sánchez-Álvarez et al., 2024; Wu et al., 2022). Electrons are then transferred internally to the Type 2/Type

3 (T2/T3) trinuclear copper cluster, reducing O_2 to H_2O (Arregui et al., 2019). This redox cascade is highly dependent on substrate access to T1, which is facilitated by adsorption within MOF pores (Arregui et al., 2019).

In other literature, laccase immobilized through chemical linking on ZIF-8 (readymade, synthesized using methanol as solvent) have 90% Acid Blue 92 removal for 120 minutes (Mahmoodi & Abdi, 2019). Using organic solvent during *in-situ* enzyme encapsulation method can causing enzyme to denature and reduce its activity (Farnet Da Silva et al., 2007; Knedel et al., 2019). Therefore, the organic solvent for enzyme immobilization can be done by using adsorption, infiltration and chemical linking method. Even though chemical linking method in immobilizing laccase has better result in dye degradation but using non environmentally chemical during the synthesis of E-MOF (laccase on ZIF-8) less appropriate as not supporting in creating wastewater treatment solution.

A comparison of pristine versus laccase-loaded MOFs (Figure 4.26) illustrates the essential synergy of dual mechanisms. Pristine ZIF-8 and ZIF-67 achieved high initial adsorption but plateaued as pores became saturated. In contrast, L@ZIF-8 sustained MB removal over four weeks by continuously oxidizing adsorbed MB into smaller products, which diffused out of the pores. Although the overall biocatalytic contribution was modest (~6.5% by week 4), this catalytic turnover prevented complete pore saturation, maintaining long-term activity. The weaker performance of L@ZIF-67, despite higher enzyme loading, might be due to excessive enzyme confinement in cobalt-based MOFs reduces activity due to steric hindrance and mass-transfer limitations.

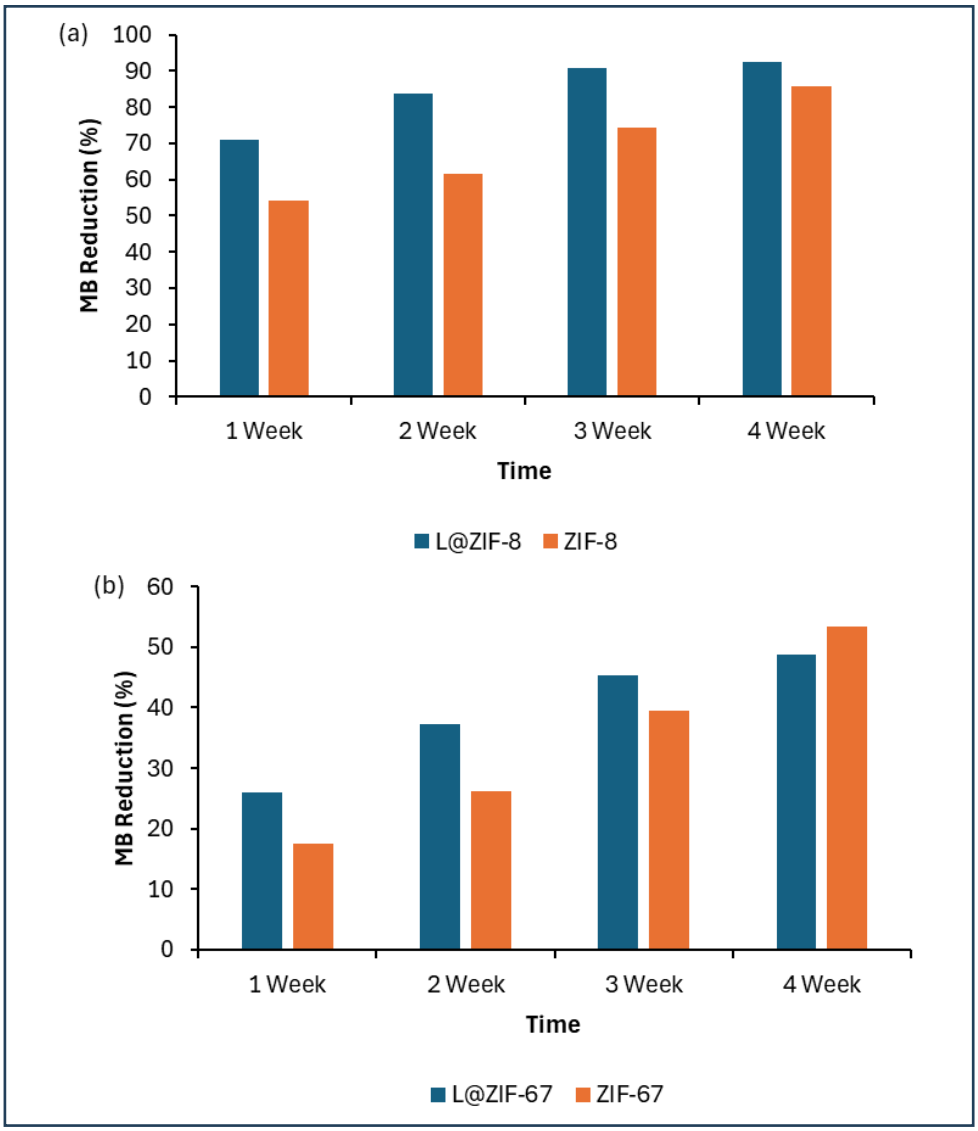

Figure 4.26 The Different Biocatalytic of L@ZIFs and Adsorption of Pristine ZIFs a) L@ZIF-8 and ZIF-8 b) L@ZIF-67 and ZIF-67

Recent advances demonstrate that tuning the porosity of metal-organic frameworks (MOFs) is critical for achieving an optimal balance between adsorption capacity and catalytic performance. Specifically, mesoporous or defect-rich ZIF-8 frameworks substantially improve the encapsulation efficiency, stability, and catalytic turnover of immobilized laccase enzymes compared to conventional microporous ZIF-8. For example, Sun et al. (2023) and Xu et al. (2023) reported that hierarchically structured or mesoporous ZIF-8 materials facilitate better enzyme loading and enhanced biodegradation activity under various conditions (Sun et al., 2023; Xu et al., 2023). Additionally, earlier research by Knedel et al. (2018) showed that *in situ* encapsulation of laccase within ZIF-8 improved both thermal and chemical stability, while also

conferring substrate selectivity (Knedel et al., 2019). These findings collectively underscore the importance of framework architecture and porosity design in modulating enzyme functionality and increasing the efficacy of laccase-based biocatalysts.

Taken together, the results in Figures 4.25 and 4.26 highlight that the superior catalytic performance of laccase encapsulated in ZIF-8 (L@ZIF-8) is not solely due to maximizing enzyme loading. Instead, it arises from a synergistic balance of three mechanisms: (i) adsorption of methylene blue (MB) through electrostatic and π–π interactions, (ii) absorption of MB into the porous ZIF-8 framework, which ensures close proximity to immobilized laccase, and (iii) efficient biocatalytic oxidation via laccase's copper redox centers, coupled with unrestricted product release. This mechanistic synergy explains why enzyme-metal-organic frameworks (E-MOFs), especially L@ZIF-8, outperform pristine MOFs and free enzymes in dye degradation. These observations align with broader studies highlighting the benefits of enzyme-MOF composites for wastewater remediation (Aguila-Rosas et al., 2025).

CHAPTER 5
CONCLUSION

5.1 Conclusions

This study successfully addressed the critical challenge of micropollutant persistence in aquatic environments by developing laccase–metal–organic framework (L@ZIF) composites as sustainable biocatalytic systems. The aqueous synthesis of ZIF-8, ZIF-67, and ZIF-7 provided a green and scalable approach to MOF fabrication, eliminating hazardous solvents and ensuring compatibility with enzyme encapsulation.

In relation to Research Objective 1, the synthesized ZIFs and their enzyme–MOF composites were systematically characterized using FESEM, XRD, FTIR, TGA, BET, and particle size analysis. These analyses confirmed that water-based synthesis produced high-quality frameworks with distinct morphologies such as truncated edge rhombic dodecahedra for ZIF-8 and rod-like crystals for ZIF-67 demonstrating that the choice of metal-to-ligand ratios governs crystallization pathways, porosity, and surface area. Importantly, the characterization validated that the *in-situ* encapsulation strategy successfully incorporated laccase within the frameworks without compromising structural integrity.

In relation to Research Objective 2, adsorption studies of pristine ZIFs revealed significant uptake of methylene blue, with kinetic modelling showing that ZIF-8 followed pseudo-first-order behaviour and Langmuir isotherm adsorption, while ZIF-67 conformed to Freundlich isotherm behaviour. These results indicate distinct mechanisms of dye uptake, with ZIF-8 favouring monolayer adsorption on homogeneous sites and ZIF-67 favouring multilayer adsorption on heterogeneous sites. The adsorption phase thus played a critical role in preconcentrating methylene blue near the catalytic sites. When related to enzyme kinetics, the free laccase displayed slight high K_m (0.27 mM) and a moderate Vmax (0.0031 mM/min) than values reported elsewhere (0.22 mM and 0.00378 mM/min). This suggests slight lower substrate affinity and catalytic turnover relative to the literature. The adsorption-driven enrichment of dye molecules by ZIFs effectively complemented these enzyme characteristics by ensuring a higher local substrate concentration, thereby enhancing the overall degradation efficiency once the enzyme was encapsulated.

In relation to Research Objective 3, the catalytic performance of the enzyme–MOF composites demonstrated that laccase activity was successfully preserved and, in some cases, enhanced by encapsulation. Among the composites, L@ZIF-8 achieved the highest catalytic efficiency, degrading more than 90% of methylene blue within four weeks. This superior performance can be attributed to the synergistic effects of MOF porosity, which facilitated substrate diffusion, and the protective microenvironment provided to laccase, which maintained its redox activity under aqueous conditions. Comparatively, L@ZIF-67 showed lower but still significant degradation capacities, highlighting how MOF topology and pore chemistry influence biocatalytic outcomes. These findings validate that enzyme immobilization within ZIFs not only extends the enzyme's operational stability but also enables sustained pollutant degradation over prolonged periods, fulfilling the ultimate aim of this research.

By fulfilling all three objectives, the research demonstrated that enzyme immobilization in ZIFs not only preserved but enhanced biocatalytic activity under environmentally relevant conditions. The integration of adsorption kinetics, enzyme kinetics, enzyme loading, and degradation performance established a comprehensive understanding of enzyme–MOF interactions, bridging the gap between material design and pollutant remediation.

Overall, this work contributes a sustainable platform for micropollutant treatment by combining eco-friendly MOF synthesis with high-efficiency biocatalysis. Beyond methylene blue, the approach holds promise for a broad range of dyes, pharmaceuticals, and endocrine-disrupting chemicals, offering a versatile solution to emerging water contaminants. From a broader perspective, the study advances the alignment of green chemistry with global sustainability efforts, directly supporting SDG 6 (Clean Water and Sanitation), SDG 12 (Responsible Consumption and Production), and SDG 14 (Life Below Water). The insights gained from this research provide a strong foundation for scaling enzyme–MOF composites toward practical wastewater treatment technologies, enabling cleaner water production and long-term environmental protection.

5.2 Recommendations

In improvise the E-MOF especially by using Zeolitic Imidazolate Framework (ZIFs) for future research and development are stated as below:

a) Modify and improvise the formulation of the ZIF-67 and ZIF-67 structure to make sure the structure suitable with the enzyme encapsulation and enzyme activity

b) Modify and improvise the formulation of the ZIF-67 and ZIF-7 structure to get standard structure of rhombic dodecahedron by using water as solvent

c) Improvise by optimizing the enzyme concentration in immobilizing inside the MOF

d) Conduct the enzyme activity & kinetics of free laccase and E-MOF using methylene blue as substrate

REFERENCES

Aghajani Hashjin, M., Zarshad, S., Motejadded Emrooz, H. B., & Sadeghzadeh, S. (2023). Enhanced atmospheric water harvesting efficiency through green-synthesized MOF-801: a comparative study with solvothermal synthesis. *Scientific Reports*, *13*(1). https://doi.org/10.1038/s41598-023-44367-1

Aguila-Rosas, J., Cano, F. J., Nagaya, A., Quirino-Barreda, C. T., de Jesús Martínez Ortiz, M., Vargas, A. G., Ibarra, I. A., & Lima, E. (2025). MOF-Composites for adsorption and degradation of contaminants in wastewater [10.1039/D5CC02843D]. *Chemical Communications*, *61*(63), 11706-11731. https://doi.org/10.1039/D5CC02843D

Ahmad, M. F., Ahmad, F. A., Alsayegh, A. A., Zeyaullah, M., AlShahrani, A. M., Muzammil, K., Saati, A. A., Wahab, S., Elbendary, E. Y., Kambal, N., Abdelrahman, M. H., & Hussain, S. (2024). Pesticides impacts on human health and the environment with their mechanisms of action and possible countermeasures. In *Heliyon* (Vol. 10): Elsevier Ltd.

Ahmadi, M., Ayyoubzadeh, S. M., Ghorbani-Bidkorbeh, F., Shahhosseini, S., Dadashzadeh, S., Asadian, E., Mosayebnia, M., & Siavashy, S. (2021). An investigation of affecting factors on MOF characteristics for biomedical applications: A systematic review. In *Heliyon* (Vol. 7): Elsevier Ltd.

Akhundzadeh Tezerjani, A., Halladj, R., & Askari, S. (2021). Different view of solvent effect on the synthesis methods of zeolitic imidazolate framework-8 to tuning the crystal structure and properties. *RSC Advances*, *11*(32), 19914-19923. https://doi.org/10.1039/d1ra02856a

Al-Tohamy, R., Ali, S. S., Li, F., Okasha, K. M., Mahmoud, Y. A. G., Elsamahy, T., Jiao, H., Fu, Y., & Sun, J. (2022). A critical review on the treatment of dye-containing wastewater: Ecotoxicological and health concerns of textile dyes and possible remediation approaches for environmental safety. In *Ecotoxicology and Environmental Safety* (Vol. 231): Academic Press.

Aldana, J. C., Agudelo, C., Álvarez, P. M., & Acero, J. L. (2024). Removal of Micropollutants in Water Reclamation by Membrane Filtration: Impact of Pretreatments and Adsorption. *Membranes*, *14*(7). https://doi.org/10.3390/membranes14070146

Alkhathami, N. D., Alamrani, N. A., Hameed, A., Al-Qahtani, S. D., Shah, R., & El-

Metwaly, N. M. (2023). Adsorption of pharmaceutical ibuprofen over functionalized zirconium metal-organic frameworks; Batch experiment and mechanism of interaction. *Polyhedron*, *235*. https://doi.org/10.1016/j.poly.2023.116349

Allegretto, J. A., Onna, D., Bilmes, S. A., Azzaroni, O., & Rafti, M. (2024). Unified Roadmap for ZIF-8 Nucleation and Growth: Machine Learning Analysis of Synthetic Variables and Their Impact on Particle Size and Morphology. *Chemistry of Materials*, *36*(11), 5814-5825. https://doi.org/10.1021/acs.chemmater.4c01069

Amari, A., Alzahrani, F. M., Alsaiari, N. S., Katubi, K. M., Rebah, F. B., & Tahoon, M. A. (2021). Magnetic metal organic framework immobilized laccase for wastewater decolorization. *Processes*, *9*(5). https://doi.org/10.3390/pr9050774

Anwar, F., Varghese, A. M., Kuppireddy, S., Khaleel, M., Wang, K., & Karanikolos, G. N. (2024). Functionalized and Hybridized ZIF-7 Adsorbents for Ethane-Ethylene Separation. *Industrial and Engineering Chemistry Research*. https://doi.org/10.1021/acs.iecr.4c02431

Arregui, L., Ayala, M., Gómez-Gil, X., Gutiérrez-Soto, G., Hernández-Luna, C. E., Herrera De Los Santos, M., Levin, L., Rojo-Domínguez, A., Romero-Martínez, D., Saparrat, M. C. N., Trujillo-Roldán, M. A., & Valdez-Cruz, N. A. (2019). Laccases: structure, function, and potential application in water bioremediation. *Microbial Cell Factories*, *18*(1), 1-33. https://doi.org/10.1186/s12934-019-1248-0

Aziz, S., Mazhar, A. R., Ubaid, A., Shah, S. M. H., Riaz, Y., Talha, T., & Jung, D. W. (2024). A comprehensive review of membrane-based water filtration techniques. In *Applied Water Science* (Vol. 14): Springer Science and Business Media Deutschland GmbH.

Babaei, H., Ghobadi Nejad, Z., Yaghmaei, S., & Farhadi, F. (2023). Co-immobilization of multi-enzyme cascade system into the metal–organic frameworks for the removal of Bisphenol A. *Chemical Engineering Journal*, *461*(November 2022), 142050-142050. https://doi.org/10.1016/j.cej.2023.142050

Bakar, B., Dik, G., Ulu, A., & Ateş, B. (2024). Immobilization of Xylanase into Zeolitic Imidazolate Framework-67 (ZIF-67) and Manganese-Doped ZIF-67 (Mn/ZIF-67): A Comparison Study. *Topics in Catalysis*, *67*(9-12), 698-713. https://doi.org/10.1007/s11244-023-01898-1

Barrios, J. A., Becerril, E., De León, C., Barrera-Díaz, C., & Jiménez, B. (2015). Electrooxidation treatment for removal of emerging pollutants in wastewater sludge. *Fuel*, *149*, 26-33. https://doi.org/https://doi.org/10.1016/j.fuel.2014.10.055

Barrios, J. A., Cano, A., Becerril, J. E., & Jiménez, B. (2016). Influence of solids on the removal of emerging pollutants in electrooxidation of municipal sludge with boron-doped diamond electrodes. *Journal of Electroanalytical Chemistry*, *776*, 148-151. https://doi.org/https://doi.org/10.1016/j.jelechem.2016.07.018

Belete, B., Desye, B., Ambelu, A., & Yenew, C. (2023). Micropollutant Removal Efficiency of Advanced Wastewater Treatment Plants: A Systematic Review. In *Environmental Health Insights* (Vol. 17): SAGE Publications Inc.

BENZIMIDAZOLE. (1939). *Organic Syntheses*, *19*, 12-12. https://doi.org/10.15227/orgsyn.019.0012

Bergaoui, M., Khalfaoui, M., Awadallah-F, A., & Al-Muhtaseb, S. (2021). A review of the features and applications of ZIF-8 and its derivatives for separating CO2 and isomers of C3- and C4- hydrocarbons. *Journal of Natural Gas Science and Engineering*, *96*(June), 104289-104289. https://doi.org/10.1016/j.jngse.2021.104289

Bhatt, P., Bhandari, G., & Bilal, M. (2022). Occurrence, toxicity impacts and mitigation of emerging micropollutants in the aquatic environments: Recent tendencies and perspectives. *Journal of Environmental Chemical Engineering*, *10*(3). https://doi.org/10.1016/j.jece.2022.107598

Bilal, M., Adeel, M., Rasheed, T., & Iqbal, H. M. N. (2019). Multifunctional metal-organic frameworks-based biocatalytic platforms: Recent developments and future prospects. *Journal of Materials Research and Technology*, *8*(2), 2359-2371. https://doi.org/10.1016/j.jmrt.2018.12.001

Bilal, M., Iqbal, H. M. N., & Barceló, D. (2019). Mitigation of bisphenol A using an array of laccase-based robust bio-catalytic cues – A review. *Science of the Total Environment*, *689*, 160-177. https://doi.org/10.1016/j.scitotenv.2019.06.403

Bilal, M., Lam, S. S., & Iqbal, H. M. N. (2022). Biocatalytic remediation of pharmaceutically active micropollutants for environmental sustainability. In *Environmental Pollution* (Vol. 293): Elsevier Ltd.

Binaeian, E., Nabipour, H., Ahmadi, S., & Rohani, S. (2023). The green synthesis and applications of biological metal-organic frameworks for targeted drug delivery

and tumor treatments. In *Journal of Materials Chemistry B* (Vol. 11, pp. 11426-11459): Royal Society of Chemistry.

Bolivar, J. M., Woodley, J. M., & Fernandez-Lafuente, R. (2022). Is enzyme immobilization a mature discipline? Some critical considerations to capitalize on the benefits of immobilization. In *Chemical Society Reviews* (Vol. 51, pp. 6251-6290): Royal Society of Chemistry.

Cai, W., Lee, T., Lee, M., Cho, W., Han, D. Y., Choi, N., Yip, A. C. K., & Choi, J. (2014). Thermal structural transitions and carbon dioxide adsorption properties of zeolitic imidazolate framework-7 (ZIF-7). *Journal of the American Chemical Society*, *136*(22), 7961-7971. https://doi.org/10.1021/ja5016298

Chaturvedi, P., Shukla, P., Giri, B. S., Chowdhary, P., Chandra, R., Gupta, P., & Pandey, A. (2021). Prevalence and hazardous impact of pharmaceutical and personal care products and antibiotics in environment: A review on emerging contaminants. In *Environmental Research* (Vol. 194): Academic Press Inc.

Chen, J., Liu, J., Chen, B., Yang, F., Li, B., Li, H., Jiang, Z., & Song, H. (2023). Effective biodegradation of chlorophenols, sulfonamides, and their mixtures by bacterial laccase immobilized on chitin. *Ecotoxicology and Environmental Safety*, *256*. https://doi.org/10.1016/j.ecoenv.2023.114856

Chen, S., Pang, H., Sun, J., & Li, K. (2023). Research advances and applications of ZIF-90 metal-organic framework nanoparticles in the biomedical field. In *Materials Chemistry Frontiers* (Vol. 8, pp. 1195-1211): Royal Society of Chemistry.

Chen, Z., Oh, W. D., & Yap, P. S. (2022). Recent advances in the utilization of immobilized laccase for the degradation of phenolic compounds in aqueous solutions: A review. In *Chemosphere* (Vol. 307): Elsevier Ltd.

Chen, Z., Wang, X., Cao, R., Idrees, K. B., Liu, X., Wasson, M. C., & Farha, O. K. (2020). Water-Based Synthesis of a Stable Iron-Based Metal-Organic Framework for Capturing Toxic Gases. *ACS Materials Letters*, *2*(9), 1129-1134. https://doi.org/10.1021/acsmaterialslett.0c00264

Chen, Z., Wang, X., Islamoglu, T., & Farha, O. K. (2019). Green synthesis of a functionalized zirconium-based metal-organic framework for water and ethanol adsorption. *Inorganics*, *7*(5). https://doi.org/10.3390/inorganics7050056

Chowdhary, P., Bharagava, R. N., Mishra, S., & Khan, N. (2020). Role of Industries in Water Scarcity and Its Adverse Effects on Environment and Human Health. In *Environmental Concerns and Sustainable Development* (pp. 235-256). Springer

Singapore. https://doi.org/10.1007/978-981-13-5889-0_12

Chu, Y., Ma, Q., Hou, X., Zhang, Y., Zhang, J., Ni, X., & Wang, Y. (2023). Enhancement of electrocatalytic activity for micropollutant removal by CeO2@CNT-based membranes: The influences of the structure and morphology of CeO2. In *Journal of Cleaner Production* (Vol. 425): Elsevier Ltd.

Cibati, A., Gonzalez-Olmos, R., Rodriguez-Mozaz, S., & Buttiglieri, G. (2022). Unravelling the performance of UV/H2O2 on the removal of pharmaceuticals in real industrial, hospital, grey and urban wastewaters. *Chemosphere*, *290*. https://doi.org/10.1016/j.chemosphere.2021.133315

Cui, J., Feng, Y., Lin, T., Tan, Z., Zhong, C., & Jia, S. (2017). Mesoporous Metal-Organic Framework with Well-Defined Cruciate Flower-Like Morphology for Enzyme Immobilization. *ACS Applied Materials and Interfaces*, *9*(12), 10587-10594. https://doi.org/10.1021/acsami.7b00512

da Silva, L. C. A., Honorato, T. L., Cavalcante, R. S., Franco, T. T., & Rodrigues, S. (2012). Effect of pH and Temperature on Enzyme Activity of Chitosanase Produced Under Solid Stated Fermentation by Trichoderma spp. *Indian Journal of Microbiology*, *52*(1), 60-65. https://doi.org/10.1007/s12088-011-0196-0

Dahnum, D., Seo, B., Cheong, S. H., Lee, U., Ha, J. M., & Lee, H. (2019). Formation of defect site on ZIF-7 and its effect on the methoxycarbonylation of aniline with dimethyl carbonate. *Journal of Catalysis*, *380*, 297-306. https://doi.org/10.1016/j.jcat.2019.09.039

Dai, S., Tissot, A., & Serre, C. (2021). Metal-Organic Frameworks: From Ambient Green Synthesis to Applications. In *Bulletin of the Chemical Society of Japan* (Vol. 94, pp. 2623-2636): Chemical Society of Japan.

Dai, Y., Niu, J., Liu, J., Yin, L., & Xu, J. (2010). In situ encapsulation of laccase in microfibers by emulsion electrospinning: Preparation, characterization, and application. *Bioresource Technology*, *101*(23), 8942-8947. https://doi.org/10.1016/j.biortech.2010.07.027

Darweesh, R. F. H., Zaki, R. M., Mahdy, A., & Ahmed, A. S. A. (2026). Enhanced adsorption of methylene blue (MB) dye by the MoS2/ZIF-8 composite: isotherm and kinetics studies. *Materials Advances*, *7*(1), 338-350. https://doi.org/10.1039/d5ma00636h

Deacon, A., Briquet, L., Malankowska, M., Massingberd-Mundy, F., Rudić, S., Hyde,

T. l., Cavaye, H., Coronas, J., Poulston, S., & Johnson, T. (2022). Understanding the ZIF-L to ZIF-8 transformation from fundamentals to fully costed kilogram-scale production. *Communications Chemistry*, *5*(1). https://doi.org/10.1038/s42004-021-00613-z

Devaisy, S., Kandasamy, J., Aryal, R., Johir, M. A. H., Ratnaweera, H., & Vigneswaran, S. (2023). Removal of Organics with Ion-Exchange Resins (IEX) from Reverse Osmosis Concentrate. *Membranes*, *13*(2). https://doi.org/10.3390/membranes13020136

Dhankhar, N., & Kumar, J. (2023). Impact of increasing pesticides and fertilizers on human health: A review. *Materials Today: Proceedings*. https://doi.org/10.1016/j.matpr.2023.03.766

Diab, K. E., Salama, E., Hassan, H. S., Abd El-moneim, A., & Elkady, M. F. (2021). Biocompatible MIP-202 Zr-MOF tunable sorbent for cost-effective decontamination of anionic and cationic pollutants from waste solutions. *Scientific Reports*, *11*(1), 6619. https://doi.org/10.1038/s41598-021-86140-2

Ding, M., Cai, X., & Jiang, H. L. (2019). Improving MOF stability: Approaches and applications. In *Chemical Science* (Vol. 10, pp. 10209-10230): Royal Society of Chemistry.

Dlamini, M. L., Lesaoana, M., Kotze, I., & Richards, H. (2023). An oxidoreductase enzyme, fungal laccase immobilized on zeolitic imidazolate frameworks for the biocatalytic degradation of an endocrine-disrupting chemical, dimethyl phthalate. *Journal of Environmental Chemical Engineering*, *11*(3). https://doi.org/10.1016/j.jece.2023.109810

Dogruel, S., Zuhal, Atesci, C., Aydin, E., & Pehlivanoglu-Mantas, E. (2020). Ozonation in advanced treatment of secondary municipal wastewater effluents for the removal of micropollutants. https://doi.org/10.1007/s11356-020-10339-5/Published

Ebrahimi, M., & Mansournia, M. (2017). Rapid room temperature synthesis of zeolitic imidazolate framework-7 (ZIF-7) microcrystals. *Materials Letters*, *189*, 243-247. https://doi.org/10.1016/j.matlet.2016.12.025

Ebrahimipour, S. Y., Shahsavari, M., Sheikhshoaei, M., & Sheikhshoaie, I. (2025). Zeolitic imidazolate frameworks (ZIFs): Versatile materials for sensing and mitigating diverse food contaminants. *Journal of Food Composition and Analysis*, *146*, 107825.

https://doi.org/https://doi.org/10.1016/j.jfca.2025.107825

El Hammoudani, Y., Dimane, F., Haboubi, K., Benaissa, C., Benaabidate, L., Bourjila, A., Achoukhi, I., El Boudammoussi, M., Faiz, H., Touzani, A., Moudou, M., & Esskifati, M. (2024). Micropollutants in wastewater treatment plants: A bibliometric - bibliographic study. In *Desalination and Water Treatment* (Vol. 317): Elsevier B.V.

Ezike, T. C., Udeh, J. O., Joshua, P. E., Ezugwu, A. L., Isiwu, C. V., Eze, S. O. O., & Chilaka, F. C. (2021). Substrate specificity of a new laccase from Trametes polyzona WRF03. *Heliyon*, *7*(1). https://doi.org/10.1016/j.heliyon.2021.e06080

Ezugbe, E. O., & Rathilal, S. (2020). Membrane technologies in wastewater treatment: A review. In *Membranes* (Vol. 10): MDPI AG.

Farnet Da Silva, A. M., Gil, G., Ferré, E., Farnet, A. M., & Ferre, E. (2007). Effects of pollutants on laccase activities of Marasmius quercophilus, a white-rot fungus isolated from a Mediterranean schlerophyllous litter. https://doi.org/10.1016/j.chemosphere.2007.06.086ï

Feng, Y., Li, Y., Xu, M., Liu, S., & Yao, J. (2016). Fast adsorption of methyl blue on zeolitic imidazolate framework-8 and its adsorption mechanism. *RSC Advances*, *6*(111), 109608-109612. https://doi.org/10.1039/c6ra23870j

Gamoń, F., Żabczyński, S., Szopińska, M., Pierpaoli, M., Zych, D., Bogdanowicz, R., Artichowicz, W., Łuczkiewicz, A., & Fudala-Książek, S. (2024). Electrochemical Oxidation of Selected Micropollutants from Environment Matrices Using Boron-Doped Diamond Electrodes: Process Efficiency and Transformation Product Detection. *Water*, *16*(24).

Gao, J., Mao, H., Jin, H., Chen, C., Feldhoff, A., & Li, Y. (2020). Functionalized ZIF-7/Pebax® 2533 mixed matrix membranes for CO2/N2 separation. *Microporous and Mesoporous Materials*, *297*. https://doi.org/10.1016/j.micromeso.2020.110030

Gao, X., Pan, H., Yang, K., Dang, J., Qiao, C., Liu, Y., & Zhou, C. (2023). Immobilization of horseradish peroxidase on hierarchically porous magnetic metal-organic frameworks for visual detection and efficient degradation of 2,4-dichlorophenol in simulated wastewater. *Biochemical Engineering Journal*, *190*, 108760. https://doi.org/https://doi.org/10.1016/j.bej.2022.108760

Ghosh, T. K., Singh, D. L., Mishra, V., Sahoo, M. K., & Ranga Rao, G. (2022). Design of ZIF-67 nanoflake derived NiCo-LDH/rGO hybrid nanostructures for aqueous

symmetric supercapattery application under alkaline condition. *Nanotechnology*, *33*(41). https://doi.org/10.1088/1361-6528/ac7fa4

Goesten, M., Stavitski, E., Pidko, E. A., Gücüyener, C., Boshuizen, B., Ehrlich, S. N., Hensen, E. J. M., Kapteijn, F., & Gascon, J. (2013). The molecular pathway to ZIF-7 microrods revealed by in situ time-resolved small- and wide-angle x-ray scattering, quick-scanning extended X-ray absorption spectroscopy, and DFT calculations. *Chemistry - A European Journal*, *19*(24), 7809-7816. https://doi.org/10.1002/chem.201204638

Guillossou, R., Le Roux, J., Mailler, R., Pereira-Derome, C. S., Varrault, G., Bressy, A., Vulliet, E., Morlay, C., Nauleau, F., Rocher, V., & Gasperi, J. (2020). Influence of dissolved organic matter on the removal of 12 organic micropollutants from wastewater effluent by powdered activated carbon adsorption. *Water Research*, *172*. https://doi.org/10.1016/j.watres.2020.115487

Gulia, J., Lath, A., Saharan, B. S., Singh, N. P., & Santal, A. R. (2024). Removal of Micropollutants from Industrial Wastewater: Conventional and Advanced Methods. In (pp. 33-47). https://doi.org/10.1021/bk-2024-1475.ch002

Han, J., Zhang, X., Jiang, J., & Li, W. (2021). How Much of the Total Organic Halogen and Developmental Toxicity of Chlorinated Drinking Water Might Be Attributed to Aromatic Halogenated DBPs? *Environmental Science and Technology*, *55*(9), 5906-5916. https://doi.org/10.1021/acs.est.0c08565

Han, Z., Fan, X., Yu, S., Li, X., Wang, S., & Lu, L. (2022). Metal-organic frameworks (MOFs): A novel platform for laccase immobilization and application. *Journal of Environmental Chemical Engineering*, *10*(6). https://doi.org/10.1016/j.jece.2022.108795

He, M., Yao, J., Li, L., Wang, K., Chen, F., & Wang, H. (2013). Synthesis of zeolitic imidazolate framework-7 in a water/ethanol mixture and its ethanol-induced reversible phase transition. *ChemPlusChem*, *78*(10), 1222-1225. https://doi.org/10.1002/cplu.201300193

Heo, J., Joseph, L., Yoon, Y., Park, Y. G., Her, N., Sohn, J., & Yoon, S. H. (2011). Removal of micropollutants and NOM in carbon nanotube-UF membrane system from seawater. *Water Science and Technology*, *63*(11), 2737-2744. https://doi.org/10.2166/wst.2011.602

Hu, Y., Dai, L., Liu, D., Du, W., & Wang, Y. (2018). Progress & prospect of metal-organic frameworks (MOFs) for enzyme immobilization (enzyme/MOFs).

Renewable and Sustainable Energy Reviews, *91*(April), 793-801. https://doi.org/10.1016/j.rser.2018.04.103

Hu, Y., Song, X., Zheng, Q., Wang, J., & Pei, J. (2019). Zeolitic imidazolate framework-67 for shape stabilization and enhanced thermal stability of paraffin-based phase change materials. *RSC Advances*, *9*(18), 9962-9967. https://doi.org/10.1039/c9ra00874h

Huang, G., Yan, Y., Xu, D., Wu, J., Xu, C., Fu, L., & Lin, B. (2021). Curcumin-loaded nanoMOFs@CMFP: A biological preserving paste with antibacterial properties and long-acting, controllable release. *Food Chemistry*, *337*. https://doi.org/10.1016/j.foodchem.2020.127987

Hübner, U., Spahr, S., Lutze, H., Wieland, A., Rüting, S., Gernjak, W., & Wenk, J. (2024). Advanced oxidation processes for water and wastewater treatment - Guidance for systematic future research. *Heliyon*, *10*(9). https://doi.org/10.1016/j.heliyon.2024.e30402

Ibrahim, A. A., Ali, S. L., Adly, M. S., El-Hakam, S. A., Samra, S. E., & Ahmed, A. I. (2021). Green construction of eco-friendly phosphotungstic acid Sr-MOF catalysts for crystal violet removal and synthesis of coumarin and xanthene compounds. *RSC Advances*, *11*(59), 37276-37289. https://doi.org/10.1039/d1ra07160b

Iriarte-Mesa, C., Díaz-Castañón, S., & Abradelo, D. G. (2019). Facile immobilization of Trametes versicolor laccase on highly monodisperse superparamagnetic iron oxide nanoparticles. *Colloids and Surfaces B: Biointerfaces*, *181*, 470-479. https://doi.org/10.1016/j.colsurfb.2019.05.012

Isanapong, J., Suwannoi, K., Lertlattanapong, S., & Panchal, S. (2024). Purification, characterization of laccase from Pleurotus ostreatus HK35, and optimization for congo red biodecolorization using Box–Behnken design. *3 Biotech*, *14*(3). https://doi.org/10.1007/s13205-024-03926-7

Islam, T., Repon, M. R., Islam, T., Sarwar, Z., & Rahman, M. M. (2023). Impact of textile dyes on health and ecosystem: a review of structure, causes, and potential solutions. In *Environmental Science and Pollution Research* (Vol. 30, pp. 9207-9242): Springer Science and Business Media Deutschland GmbH.

Jamil, N., Othman, N. H., Alias, N. H., Shahruddin, M. Z., Roslan, R. A., Lau, W. J., & Ismail, A. F. (2019). Mixed matrix membranes incorporated with reduced graphene oxide (rGO) and zeolitic imidazole framework-8 (ZIF-8) nanofillers

for gas separation. *Journal of Solid State Chemistry*, *270*(June 2018), 419-427. https://doi.org/10.1016/j.jssc.2018.11.028

Jia, Q., Lasseuguette, E., Lozinska, M. M., Ferrari, M. C., & Wright, P. A. (2022). Hybrid Benzimidazole-Dichloroimidazole Zeolitic Imidazolate Frameworks Based on ZIF-7 and Their Application in Mixed Matrix Membranes for CO2/N2Separation. *ACS Applied Materials and Interfaces*, *14*(41), 46615-46626. https://doi.org/10.1021/acsami.2c12908

Jian, M., Liu, B., Liu, R., Qu, J., Wang, H., & Zhang, X. (2015). Water-based synthesis of zeolitic imidazolate framework-8 with high morphology level at room temperature. *RSC Advances*, *5*(60), 48433-48441. https://doi.org/10.1039/c5ra04033g

Jiang, S., Ren, D., Wang, Z., Zhang, S., Zhang, X., & Chen, W. (2022). Improved stability and promoted activity of laccase by One-Pot encapsulation with Cu (PABA) nanoarchitectonics and its application for removal of Azo dyes. *Ecotoxicology and Environmental Safety*, *234*. https://doi.org/10.1016/j.ecoenv.2022.113366

Jofrishal, Fajri, R., Ediati, R., & Amri, Y. (2020). Synthesis of ZIF-8 at room temperature and reuse filtrate. *Journal of Physics: Conference Series*, *1460*(1). https://doi.org/10.1088/1742-6596/1460/1/012086

Johnson, P. I., Favela, K., Jarin, J., Le, A. M., Clark, P. Y., Fu, L., Gillis, A. D., Morga, N., Nguyen, C., & Harley, K. G. (2022). Chemicals of concern in personal care products used by women of color in three communities of California. *Journal of Exposure Science and Environmental Epidemiology*, *32*(6), 864-876. https://doi.org/10.1038/s41370-022-00485-y

Julien, P. A., Mottillo, C., & Friščić, T. (2017). Metal-organic frameworks meet scalable and sustainable synthesis. In *Green Chemistry* (Vol. 19, pp. 2729-2747): Royal Society of Chemistry.

Kabir, M. F., & Ju, L. K. (2023). On optimization of enzymatic processes: Temperature effects on activity and long-term deactivation kinetics. *Process Biochemistry*, *130*, 734-746. https://doi.org/10.1016/j.procbio.2023.05.031

Khan, F. S. A., Mubarak, N. M., Khalid, M., Tan, Y. H., Abdullah, E. C., Rahman, M. E., & Karri, R. R. (2021). A comprehensive review on micropollutants removal using carbon nanotubes-based adsorbents and membranes. In *Journal of Environmental Chemical Engineering* (Vol. 9): Elsevier Ltd.

Kim, M. K., & Zoh, K. D. (2016). Occurrence and removals of micropollutants in water environment. *Environmental Engineering Research*, *21*(4), 319-332. https://doi.org/10.4491/eer.2016.115

Kiwaan, H. A., Sh. Mohamed, F., El-Bindary, A. A., El-Ghamaz, N. A., Abo-Yassin, H. R., & El-Bindary, M. A. (2021). Synthesis, identification and application of metal organic framework for removal of industrial cationic dyes. *Journal of Molecular Liquids*, *342*. https://doi.org/10.1016/j.molliq.2021.117435

Knedel, T. O., Ricklefs, E., Schlüsener, C., Urlacher, V. B., & Janiak, C. (2019). Laccase Encapsulation in ZIF-8 Metal-Organic Framework Shows Stability Enhancement and Substrate Selectivity. *ChemistryOpen*, *8*(11), 1337-1344. https://doi.org/10.1002/open.201900146

Kołodziejczak-Radzimska, A., & Jesionowski, T. (2020). A novel cysteine-functionalized MxOy material as support for laccase immobilization and a potential application in decolorization of Alizarin Red S. *Processes*, *8*(8). https://doi.org/10.3390/PR8080885

Kumar, S., Jain, S., Nehra, M., Dilbaghi, N., Marrazza, G., & Kim, K. H. (2020). Green synthesis of metal–organic frameworks: A state-of-the-art review of potential environmental and medical applications. *Coordination Chemistry Reviews*, *420*, 213407-213407. https://doi.org/10.1016/j.ccr.2020.213407

Kumar, V., Kumar, R., Singh, J., & Kumar, P. (2019). *Contaminants in Agriculture and Environment: Health Risks and Remediation*. Agro Environ Media, Publication Cell of AESA, Agriculture and Environmental Science Academy. https://books.google.com.my/books?id=a3ykDwAAQBAJ

Kurtuldu, A., Eşgin, H., Yetim, N. K., & Semerci, F. (2022). Immobilization Horseradish Peroxidase onto UiO-66-NH2 for Biodegradation of Organic Dyes. *Journal of Inorganic and Organometallic Polymers and Materials*, *32*(8), 2901-2909. https://doi.org/10.1007/s10904-022-02310-3

Kushch, O. V., Hordieieva, I. O., Sirobaba, S. I., & Shendrik, A. N. (2024). Selection of organic solvents as reaction media for laccase from Trametes versicolor. *Biocatalysis and Biotransformation*, *42*(6), 775-791. https://doi.org/10.1080/10242422.2024.2377556

Ladole, M. R., Pokale, P. B., Patil, S. S., Belokar, P. G., & Pandit, A. B. (2020). Laccase immobilized peroxidase mimicking magnetic metal organic frameworks for industrial dye degradation. *Bioresource Technology*, *317*(June), 124035-

124035. https://doi.org/10.1016/j.biortech.2020.124035

Lei, Y., Yang, H., Xie, J., Chen, Q., Quan, W., & Wang, A. (2023). Synthesis of strong magnetic response ZIF-67 for rapid adsorption of Cu2+. *Frontiers in Chemistry*, *11*. https://doi.org/10.3389/fchem.2023.1135193

Li, H., Zhao, K., Zhang, X., Yu, H., Wang, J., & Niu, J. (2024). Electrochemical Anodic Oxidation-Based Membrane System for Micropollutant Removal. In *ACS ES and T Engineering* (Vol. 4, pp. 224-249): American Chemical Society.

Li, J., Chang, H., Li, Y., Li, Q., Shen, K., Yi, H., & Zhang, J. (2020). Synthesis and adsorption performance of La@ZIF-8 composite metal-organic frameworks. *RSC Advances*, *10*(6), 3380-3390. https://doi.org/10.1039/c9ra10548d

Li, K., Chen, M., Chen, L., Zhao, S., Pan, W., Li, P., & Han, Y. (2024). Adsorption of tetracycline from aqueous solution by ZIF-8: Isotherms, kinetics and thermodynamics. *Environmental Research*, *241*. https://doi.org/10.1016/j.envres.2023.117588

Li, S. F., Zhai, X. J., Zhang, C., Mo, H. L., & Zang, S. Q. (2020). Enzyme immobilization in highly ordered macro-microporous metal-organic frameworks for rapid biodegradation of hazardous dyes. *Inorganic Chemistry Frontiers*, *7*(17), 3146-3153. https://doi.org/10.1039/d0qi00489h

Li, X., Li, A., Li, Z., Sun, H., Shi, P., Zhou, Q., & Shuang, C. (2021). Organic micropollutants and disinfection byproducts removal from drinking water using concurrent anion exchange and chlorination process. *Science of the Total Environment*, *752*. https://doi.org/10.1016/j.scitotenv.2020.141470

Li, Y., Tao, L., Wang, Q., Wang, F., Li, G., & Song, M. (2023). Potential Health Impact of Microplastics: A Review of Environmental Distribution, Human Exposure, and Toxic Effects. In *Environment and Health* (Vol. 1, pp. 249-257): American Chemical Society.

Li, Z., Bhowmik, S., Sagresti, L., Brancato, G., Smith, M., Benson, D. E., Li, P., & Merz, K. M. (2024). Simulating Metal-Imidazole Complexes. *Journal of Chemical Theory and Computation*, *20*(15), 6706-6716. https://doi.org/10.1021/acs.jctc.4c00581

Li, Z., Shi, Q., Dong, X., & Sun, Y. (2024). Co-Immobilization of Laccase and Mediator into Fe-Doped ZIF-8 Significantly Enhances the Degradation of Organic Pollutants. *Molecules*, *29*(2). https://doi.org/10.3390/molecules29020307

Liang, J., & Liang, K. (2020). Biocatalytic Metal–Organic Frameworks: Prospects

Beyond Bioprotective Porous Matrices. *Advanced Functional Materials*, *30*(27), 1-24. https://doi.org/10.1002/adfm.202001648

Liang, J., Ning, X. a., Song, J., Lu, X., Sun, J., & Zhang, Y. (2019). Treatment of 3,3′-dimethoxybenzidine in sludge by advance oxidation process: Degradation products and toxicity evaluation. *Journal of Environmental Management*, *238*, 102-109. https://doi.org/10.1016/j.jenvman.2018.11.135

Liang, K., Ricco, R., Doherty, C. M., Styles, M. J., Bell, S., Kirby, N., Mudie, S., Haylock, D., Hill, A. J., Doonan, C. J., & Falcaro, P. (2015). Biomimetic mineralization of metal-organic frameworks as protective coatings for biomacromolecules. *Nature Communications*, *6*, 4-11. https://doi.org/10.1038/ncomms8240

Liang, S., Wu, X. L., Xiong, J., Zong, M. H., & Lou, W. Y. (2020). Metal-organic frameworks as novel matrices for efficient enzyme immobilization: An update review. *Coordination Chemistry Reviews*, *406*, 213149-213149. https://doi.org/10.1016/j.ccr.2019.213149

Liu, S., Bilal, M., Rizwan, K., Gul, I., Rasheed, T., & Iqbal, H. M. N. (2021). Smart chemistry of enzyme immobilization using various support matrices – A review. *International Journal of Biological Macromolecules*, *190*(July), 396-408. https://doi.org/10.1016/j.ijbiomac.2021.09.006

Liu, S., Jassby, D., Mandler, D., & Schäfer, A. I. (2024). Differentiation of adsorption and degradation in steroid hormone micropollutants removal using electrochemical carbon nanotube membrane. *Nature Communications*, *15*(1). https://doi.org/10.1038/s41467-024-52730-7

Liu, S., Liu, J., Wang, Z., Wu, Z., Wei, Y., Liu, P., Lan, X., Liao, Y., & Lan, P. (2023). In situ embedding of glucose oxidase in amorphous ZIF-7 with high catalytic activity and stability and mechanism investigation. *International Journal of Biological Macromolecules*, *242*. https://doi.org/10.1016/j.ijbiomac.2023.124806

Liu, W., Shen, X., Han, Y., Liu, Z., Dai, W., Dutta, A., Kumar, A., & Liu, J. (2019). Selective adsorption and removal of drug contaminants by using an extremely stable Cu(II)-based 3D metal-organic framework. *Chemosphere*, *215*, 524-531. https://doi.org/10.1016/j.chemosphere.2018.10.075

Liu, Y., Liu, Y., Gu, L., Han, J., Zhi, W., Wang, Y., & Wang, L. (2021). Modulating the biofunctionality of enzyme-MOF nanobiocatalyst through structure-

switching aptamer for continuous degradation of BPA. *Colloids and Surfaces B: Biointerfaces*, *208*. https://doi.org/10.1016/j.colsurfb.2021.112099

Liu, Z., Solliec, M., Papineau, I., Lompe, K. M., Mohseni, M., Bérubé, P. R., Sauvé, S., & Barbeau, B. (2022). Elucidating the removal of organic micropollutants on biological ion exchange resins. *Science of the Total Environment*, *808*. https://doi.org/10.1016/j.scitotenv.2021.152137

Ma, L., Qiu, X., Li, Y., Tang, S., Shen, W., Xing, C., Kong, D., & Sheng, J. (2020). Carboxypeptidase A immobilization with zeolitic imidazolate framework for enhancement of ochratoxin A degradation ability. *Food and Agricultural Immunology*, *31*(1), 587-599. https://doi.org/10.1080/09540105.2020.1749570

Mahfudz, M. K., Jaikhan, S., Phirom-on, K., & Apiraksakorn, J. (2024). Cost-Effective Strategy and Feasibility for Amylase Production from Okara by Bacillus subtilis J12. *Fermentation*, *10*(11).

Mahmoodi, N. M., & Abdi, J. (2019). Metal-organic framework as a platform of the enzyme to prepare novel environmentally friendly nanobiocatalyst for degrading pollutant in water. *Journal of Industrial and Engineering Chemistry*, *80*, 606-613. https://doi.org/10.1016/j.jiec.2019.08.036

Mailler, R., Gasperi, J., Coquet, Y., Derome, C., Buleté, A., Vulliet, E., Bressy, A., Varrault, G., Chebbo, G., & Rocher, V. (2016). Removal of emerging micropollutants from wastewater by activated carbon adsorption: Experimental study of different activated carbons and factors influencing the adsorption of micropollutants in wastewater. *Journal of Environmental Chemical Engineering*, *4*(1), 1102-1109. https://doi.org/10.1016/j.jece.2016.01.018

Malvestiti, J. A., Cruz-Alcalde, A., López-Vinent, N., Dantas, R. F., & Sans, C. (2019). Catalytic ozonation by metal ions for municipal wastewater disinfection and simulataneous micropollutants removal. *Applied Catalysis B: Environmental*, *259*. https://doi.org/10.1016/j.apcatb.2019.118104

Mandal, S., Ishak, S., Mohd Ariffin, M. A., Lee, D.-E., & Park, T. (2023). Effect of pore structure on the thermal stability of shape-stabilized phase change materials. *Journal of Materials Research and Technology*, *25*, 465-479. https://doi.org/https://doi.org/10.1016/j.jmrt.2023.05.217

Mansor, A. F., Mohidem, N. A., Wan Mohd Zawawi, W. N. I., Othman, N. S., Endud, S., & Mat, H. (2015). Preparation and characterization of in situ entrapment of laccase in silica microparticles via an ambient drying procedure. *Journal of Sol-*

Gel Science and Technology, *75*(2), 323-335. https://doi.org/10.1007/s10971-015-3703-7

Marszałek, A., Kamińska, G., & Abdel Salam, N. F. (2022). Simultaneous adsorption of organic and inorganic micropollutants from rainwater by bentonite and bentonite-carbon nanotubes composites. *Journal of Water Process Engineering*, *46*. https://doi.org/10.1016/j.jwpe.2021.102550

Mayolo-Deloisa, K., González-González, M., & Rito-Palomares, M. (2020). Laccases in Food Industry: Bioprocessing, Potential Industrial and Biotechnological Applications. In *Frontiers in Bioengineering and Biotechnology* (Vol. 8): Frontiers Media S.A.

Mazlan, S. Z., & Hanifah, S. A. (2017). Effects of Temperature and pH on Immobilized Laccase Activity in Conjugated Methacrylate-Acrylate Microspheres. *International Journal of Polymer Science*, *2017*(2002). https://doi.org/10.1155/2017/5657271

Mehta, J., Bhardwaj, N., Bhardwaj, S. K., Kim, K. H., & Deep, A. (2016). Recent advances in enzyme immobilization techniques: Metal-organic frameworks as novel substrates. *Coordination Chemistry Reviews*, *322*, 30-40. https://doi.org/10.1016/j.ccr.2016.05.007

Moreno, A. D., Ibarra, D., Eugenio, M. E., & Tomás-Pejó, E. (2020). Laccases as versatile enzymes: from industrial uses to novel applications. In *Journal of Chemical Technology and Biotechnology* (Vol. 95, pp. 481-494): John Wiley and Sons Ltd.

Mu, R., Wang, Z., Wamsley, M. C., Duke, C. N., Lii, P. H., Epley, S. E., Todd, L. C., & Roberts, P. J. (2020). Application of enzymes in regioselective and stereoselective organic reactions. *Catalysts*, *10*(8). https://doi.org/10.3390/catal10080832

Murtaza, S. Z. M., Shomal, R., Sabouni, R., & Ghommem, M. (2022). Facile metal organic framework composites as photocatalysts for lone/simultaneous photodegradation of naproxen, ibuprofen and methyl orange. *Environmental Technology and Innovation*, *27*. https://doi.org/10.1016/j.eti.2022.102751

Mutzner, L., Furrer, V., Castebrunet, H., Dittmer, U., Fuchs, S., Gernjak, W., Gromaire, M. C., Matzinger, A., Mikkelsen, P. S., Selbig, W. R., & Vezzaro, L. (2022). A decade of monitoring micropollutants in urban wet-weather flows: What did we learn? *Water Research*, *223*(April).

https://doi.org/10.1016/j.watres.2022.118968

Nadar, S. S., Vaidya, L., & Rathod, V. K. (2020). Enzyme embedded metal organic framework (enzyme–MOF): De novo approaches for immobilization. *International Journal of Biological Macromolecules*, *149*, 861-876. https://doi.org/10.1016/j.ijbiomac.2020.01.240

Nazir, M. A., Ullah, S., Shahid, M. U., Hossain, I., Najam, T., Ismail, M. A., Rehman, A. u., Karim, M. R., & Shah, S. S. A. (2025). Zeolitic imidazolate frameworks (ZIF-8 & ZIF-67): Synthesis and application for wastewater treatment. *Separation and Purification Technology*, *356*, 129828. https://doi.org/https://doi.org/10.1016/j.seppur.2024.129828

Nimbalkar, M. N., & Bhat, B. R. (2019). Facile Green Synthesis of Zirconium Based Metal-Organic Framework having Carboxylic Anchors. *Materials Today: Proceedings*, *9*(April 2018), 522-527. https://doi.org/10.1016/j.matpr.2018.10.371

Oladoye, P. O., Ajiboye, T. O., Omotola, E. O., & Oyewola, O. J. (2022). Methylene blue dye: Toxicity and potential elimination technology from wastewater. In *Results in Engineering* (Vol. 16): Elsevier B.V.

Owen, M. P., Schauwers, W., Hugh-Jones, M. E., Kiernan, J. A., Turnbull, P. C. B., & Beyer, W. (2013). A simple, reliable M'Fadyean stain for visualizing the Bacillus anthracis capsule. *Journal of Microbiological Methods*, *92*(3), 264-269. https://doi.org/10.1016/j.mimet.2013.01.009

Panwar, V., Lzaod, S., & Dutta, T. (2023). Thermostable Bacterial Laccase: Catalytic Properties and Its Application in Biotransformation of Emerging Pollutants. *ACS Omega*, *8*(38), 34710-34719. https://doi.org/10.1021/acsomega.3c03627

Patel, M., Kumar, R., Kishor, K., Mlsna, T., Pittman, C. U., & Mohan, D. (2019). Pharmaceuticals of emerging concern in aquatic systems: Chemistry, occurrence, effects, and removal methods. In *Chemical Reviews* (Vol. 119, pp. 3510-3673): American Chemical Society.

Patil, P. D., & Yadav, G. D. (2018). Rapid In Situ Encapsulation of Laccase into Metal-Organic Framework Support (ZIF-8) under Biocompatible Conditions. *ChemistrySelect*, *3*(17), 4669-4675. https://doi.org/10.1002/slct.201702852

Peng, J., Wu, E., Lou, X., Deng, Q., Hou, X., Lv, C., & Hu, Q. (2021). Anthraquinone removal by a metal-organic framework/polyvinyl alcohol cryogel-immobilized laccase: Effect and mechanism exploration. *Chemical Engineering Journal*,

418(March). https://doi.org/10.1016/j.cej.2021.129473

Pérez-Cejuela, H. M., Mon, M., Ferrando-Soria, J., Pardo, E., Armentano, D., Simó-Alfonso, E. F., & Herrero-Martínez, J. M. (2020). Bio-metal-organic frameworks for molecular recognition and sorbent extraction of hydrophilic vitamins followed by their determination using HPLC-UV. *Microchimica Acta*, *187*(4). https://doi.org/10.1007/s00604-020-4185-z

Pu, S., Zhang, X., Yang, C., Naseer, S., Zhang, X., Ouyang, J., Li, D., & Yang, J. (2019). The effects of NaCl on enzyme encapsulation by zeolitic imidazolate frameworks-8. *Enzyme and Microbial Technology*, *122*, 1-6. https://doi.org/10.1016/j.enzmictec.2018.12.003

Qian, X., Ren, Q., Wu, X., Sun, J., Wu, H., & Lei, J. (2018). Enhanced Water Stability in Zn-Doped Zeolitic Imidazolate Framework-67 (ZIF-67) for CO2 Capture Applications. *ChemistrySelect*, *3*(2), 657-661. https://doi.org/10.1002/slct.201702114

Rafiei, S., Tangestaninejad, S., Horcajada, P., Moghadam, M., Mirkhani, V., Mohammadpoor-Baltork, I., Kardanpour, R., & Zadehahmadi, F. (2018). Efficient biodiesel production using a lipase@ZIF-67 nanobioreactor. *Chemical Engineering Journal*, *334*, 1233-1241. https://doi.org/10.1016/j.cej.2017.10.094

Raptopoulou, C. P. (2021). Metal-organic frameworks: Synthetic methods and potential applications. In *Materials* (Vol. 14, pp. 1-32): MDPI AG.

Rego, R. M., Kuriya, G., Kurkuri, M. D., & Kigga, M. (2021). MOF based engineered materials in water remediation: Recent trends. *Journal of Hazardous Materials*, *403*(June 2020), 123605-123605. https://doi.org/10.1016/j.jhazmat.2020.123605

Ren, S., Feng, Y., Wen, H., Li, C., Sun, B., Cui, J., & Jia, S. (2018). Immobilized carbonic anhydrase on mesoporous cruciate flower-like metal organic framework for promoting CO2 sequestration. *International Journal of Biological Macromolecules*, *117*, 189-198. https://doi.org/10.1016/j.ijbiomac.2018.05.173

Rogacka, J., & Labus, K. (2024). Metal–organic frameworks as highly effective platforms for enzyme immobilization–current developments and future perspectives. *Brazilian Journal of Chemical Engineering*. https://doi.org/10.1007/s43153-024-00513-4

Rovira, J., & Domingo, J. L. (2019). Human health risks due to exposure to inorganic and organic chemicals from textiles: A review. In *Environmental Research* (Vol. 168, pp. 62-69): Academic Press Inc.

Rybarczyk, A., Smułek, W., Ejsmont, A., Goscianska, J., Jesionowski, T., & Zdarta, J. (2025). The role of metal–organic framework (MOF) in laccase immobilization for advanced biocatalyst formation for use in micropollutants removal. *Environmental Pollution*, *371*. https://doi.org/10.1016/j.envpol.2025.125954

Saddique, Z., Imran, M., Javaid, A., Rizvi, N. B., Akhtar, M. N., Iqbal, H. M. N., & Bilal, M. (2023). Enzyme-Linked Metal Organic Frameworks for Biocatalytic Degradation of Antibiotics. *Catalysis Letters*. https://doi.org/10.1007/s10562-022-04261-3

Salgaonkar, M., Nadar, S. S., & Rathod, V. K. (2019). Biomineralization of orange peel peroxidase within metal organic frameworks (OPP-MOFs) for dye degradation. *Journal of Environmental Chemical Engineering*, *7*(2). https://doi.org/10.1016/j.jece.2019.102969

Sánchez-Álvarez, A., Quintanilla-Villanueva, G. E., Rodríguez-Quiroz, O., Rodríguez-Delgado, M. M., Villarreal-Chiu, J. F., Sicardi-Segade, A., & Luna-Moreno, D. (2024). Use of Laccase Enzymes as Bio-Receptors for the Organic Dye Methylene Blue in a Surface Plasmon Resonance Biosensor. *Sensors*, *24*(24). https://doi.org/10.3390/s24248008

Sankar, S. S., Karthick, K., Sangeetha, K., Karmakar, A., & Kundu, S. (2020). Transition-Metal-Based Zeolite Imidazolate Framework Nanofibers via an Electrospinning Approach: A Review. In *ACS Omega* (Vol. 5, pp. 57-67): American Chemical Society.

Santhi, V. A., Sakai, N., Ahmad, E. D., & Mustafa, A. M. (2012). Occurrence of bisphenol A in surface water, drinking water and plasma from Malaysia with exposure assessment from consumption of drinking water. *Science of the Total Environment*, *427-428*, 332-338. https://doi.org/10.1016/j.scitotenv.2012.04.041

Sharma, P., Bano, A., Yadav, S., & Singh, S. P. (2023). Biocatalytic Degradation of Emerging Micropollutants. In *Topics in Catalysis* (Vol. 66, pp. 676-690): Springer.

Shaukat, R. A., Saqib, Q. M., Kim, J., Song, H., Khan, M. U., Chougale, M. Y., Bae, J., & Choi, M. J. (2022). Ultra-robust tribo- and piezo-electric nanogenerator based

on metal organic frameworks (MOF-5) with high environmental stability. *Nano Energy*, *96*. https://doi.org/10.1016/j.nanoen.2022.107128

Shen, C. H., Chuang, C. H., Gu, Y. J., Ho, W. H., Song, Y. D., Chen, Y. C., Wang, Y. C., & Kung, C. W. (2021). Cerium-Based Metal-Organic Framework Nanocrystals Interconnected by Carbon Nanotubes for Boosting Electrochemical Capacitor Performance. *ACS Applied Materials and Interfaces*, *13*(14), 16418-16426. https://doi.org/10.1021/acsami.1c02038

Sher, F., Hanif, K., Rafey, A., Khalid, U., Zafar, A., Ameen, M., & Lima, E. C. (2021). Removal of micropollutants from municipal wastewater using different types of activated carbons. *Journal of Environmental Management*, *278*. https://doi.org/10.1016/j.jenvman.2020.111302

Shi, Z., Yu, Y., Fu, C., Wang, L., & Li, X. (2017). Water-based synthesis of zeolitic imidazolate framework-8 for CO2 capture. *RSC Advances*, *7*(46), 29227-29232. https://doi.org/10.1039/c7ra04875k

Shortall, K., Otero, F., Bendl, S., Soulimane, T., & Magner, E. (2022). Enzyme Immobilization on Metal Organic Frameworks: The Effect of Buffer on the Stability of the Support. *Langmuir*, *38*(44), 13382-13391. https://doi.org/10.1021/acs.langmuir.2c01630

Shraddha, Shekher, R., Sehgal, S., Kamthania, M., & Kumar, A. (2011). Laccase: Microbial sources, production, purification, and potential biotechnological applications. *Enzyme Research*, *2011*(1). https://doi.org/10.4061/2011/217861

Solorio-Rodriguez, S. A., Williams, A. A.-O., Poulsen, S. S., Knudsen, K. A.-O., Jensen, K. A.-O., Clausen, P. A.-O., Danielsen, P. H., Wallin, H., Vogel, U. A.-O., & Halappanavar, S. Single-Walled vs. Multi-Walled Carbon Nanotubes: Influence of Physico-Chemical Properties on Toxicogenomics Responses in Mouse Lungs. LID - 10.3390/nano13061059 [doi] LID - 1059. (2079-4991 (Print)).

Soni, V., Bhatt, U., Tailor, P., & Strasser, R. J. (2025). Impact of synthetic and herbal dyes on photosynthesis and ROS scavenging enzyme activities in Spirodela polyrhiza. *Scientific Reports*, *15*(1). https://doi.org/10.1038/s41598-025-02038-3

Stamm, C., Räsänen, K., Burdon, F. J., Altermatt, F., Jokela, J., Joss, A., Ackermann, M., & Eggen, R. I. L. (2016). Unravelling the Impacts of Micropollutants in Aquatic Ecosystems: Interdisciplinary Studies at the Interface of Large-Scale

Ecology. *Advances in Ecological Research*, *55*, 183-223. https://doi.org/10.1016/bs.aecr.2016.07.002

Sun, H., Yuan, F., Jia, S., Zhang, X., & Xing, W. (2023). Laccase encapsulation immobilized in mesoporous ZIF-8 for enhancement bisphenol A degradation. *Journal of Hazardous Materials*, *445*. https://doi.org/10.1016/j.jhazmat.2022.130460

Sun, Y., Li, Y., & Tan, J. C. (2018). Liquid Intrusion into Zeolitic Imidazolate Framework-7 Nanocrystals: Exposing the Roles of Phase Transition and Gate Opening to Enable Energy Absorption Applications. *ACS Applied Materials and Interfaces*, *10*(48), 41831-41838. https://doi.org/10.1021/acsami.8b16527

Ta, D. N., Nguyen, H. K. D., Trinh, B. X., Le, Q. T. N., Ta, H. N., & Nguyen, H. T. (2018). Preparation of nano-ZIF-8 in methanol with high yield. *Canadian Journal of Chemical Engineering*, *96*(7), 1518-1531. https://doi.org/10.1002/cjce.23155

Tarigan, M., Raji, S., Al-Fatesh, H., Czermak, P., & Ebrahimi, M. (2025). The Occurrence of Micropollutants in the Aquatic Environment and Technologies for Their Removal. In *Processes* (Vol. 13): Multidisciplinary Digital Publishing Institute (MDPI).

Tran, U. P. N., Le, K. K. A., & Phan, N. T. S. (2011). Expanding applications of metal-organic frameworks: Zeolite imidazolate framework zif-8 as an efficient heterogeneous catalyst for the knoevenagel reaction. *ACS Catalysis*, *1*(2), 120-127. https://doi.org/10.1021/cs1000625

Tu, Y., Li, H., Tu, T., & Zhang, Q. (2022). Lamellar Enzyme-Metal-Organic Framework Composites Enable Catalysis on Large Substrates. *CCS Chemistry*, *4*(3), 872-879. https://doi.org/10.31635/ccschem.021.202000759

Tülek, A., Yıldırım, D., Aydın, D., & Binay, B. (2021). Highly-stable Madurella mycetomatis laccase immobilized in silica-coated ZIF-8 nanocomposites for environmentally friendly cotton bleaching process. *Colloids and Surfaces B: Biointerfaces*, *202*(December 2020). https://doi.org/10.1016/j.colsurfb.2021.111672

Uddin, M. J., Ampiaw, R. E., & Lee, W. (2021). Adsorptive removal of dyes from wastewater using a metal-organic framework: A review. *Chemosphere*, *284*(January), 131314-131314. https://doi.org/10.1016/j.chemosphere.2021.131314

Ulu, A. (2020). Metal–organic frameworks (MOFs): a novel support platform for ASNase immobilization. *Journal of Materials Science*, *55*(14), 6130-6144. https://doi.org/10.1007/s10853-020-04452-6

Upadhyay, P., Shrivastava, R., & Agrawal, P. K. (2016). Bioprospecting and biotechnological applications of fungal laccase. In *3 Biotech* (Vol. 6, pp. 1-12): Springer Verlag.

van Gijn, K., Zhao, Y., Balasubramaniam, A., de Wilt, H. A., Carlucci, L., Langenhoff, A. A. M., & Rijnaarts, H. H. M. (2022). The effect of organic matter fractions on micropollutant ozonation in wastewater effluents. *Water Research*, *222*. https://doi.org/10.1016/j.watres.2022.118933

Wang, B., Wang, L., Cen, W., Lyu, T., Jarvis, P., Zhang, Y., Zhang, Y., Han, Y., Wang, L., Pan, G., Zhang, K., & Fan, W. (2024). Exploring a chemical input free advanced oxidation process based on nanobubble technology to treat organic micropollutants. *Environmental Pollution*, *340*. https://doi.org/10.1016/j.envpol.2023.122877

Wang, C., Ying, Z., Ma, M., Huo, M., & Yang, W. (2019). Degradation of micropollutants by UV-Chlorine treatment in reclaimedwater: pH effects, formation of disinfectant byproducts, and toxicity assay. *Water (Switzerland)*, *11*(12). https://doi.org/10.3390/W11122639

Wang, H., Xi, H., Xu, L., Jin, M., Zhao, W., & Liu, H. (2021). Ecotoxicological effects, environmental fate and risks of pharmaceutical and personal care products in the water environment: A review. In *Science of the Total Environment* (Vol. 788): Elsevier B.V.

Wang, J., Yu, S., Feng, F., & Lu, L. (2019). Simultaneous purification and immobilization of laccase on magnetic zeolitic imidazolate frameworks: Recyclable biocatalysts with enhanced stability for dye decolorization. *Biochemical Engineering Journal*, *150*(26), 107285-107285. https://doi.org/10.1016/j.bej.2019.107285

Wang, Q., & Astruc, D. (2020). State of the Art and Prospects in Metal–Organic Framework (MOF)-Based and MOF-Derived Nanocatalysis. *Chemical Reviews*, *120*(2), 1438-1511. https://doi.org/10.1021/acs.chemrev.9b00223

Wang, Q., Zhang, X., Chai, X., Wang, T., Cao, T., Li, Y., Zhang, L., Fan, F., Fu, Y., & Qi, W. (2021). An Electrochemical Sensor for H2O2Based on Au Nanoparticles Embedded in UiO-66 Metal-Organic Framework Films. *ACS Applied Nano*

Materials, *4*(6), 6103-6110. https://doi.org/10.1021/acsanm.1c00915

Wang, X., Lan, P. C., & Ma, S. (2020). Metal-Organic Frameworks for Enzyme Immobilization: Beyond Host Matrix Materials. *ACS Central Science*, *6*(9), 1497-1506. https://doi.org/10.1021/acscentsci.0c00687

Wang, Z., Ren, D., Yu, H., Jiang, S., Zhang, S., & Zhang, X. (2020). Study on improving the stability of adsorption-encapsulation immobilized Laccase@ZIF-67. *Biotechnology Reports*, *28*, e00553-e00553. https://doi.org/10.1016/j.btre.2020.e00553

Wei, J. Z., Gong, F. X., Sun, X. J., Li, Y., Zhang, T., Zhao, X. J., & Zhang, F. M. (2019). Rapid and Low-Cost Electrochemical Synthesis of UiO-66-NH2 with Enhanced Fluorescence Detection Performance. *Inorganic Chemistry*, *58*(10), 6742-6747. https://doi.org/10.1021/acs.inorgchem.9b00157

Wu, E., Li, Y., Huang, Q., Yang, Z., Wei, A., & Hu, Q. (2019). Laccase immobilization on amino-functionalized magnetic metal organic framework for phenolic compound removal. *Chemosphere*, *233*, 327-335. https://doi.org/10.1016/j.chemosphere.2019.05.150

Wu, K., Shi, M., Pan, X., Zhang, J., Zhang, X., Shen, T., & Tian, Y. (2022). Decolourization and biodegradation of methylene blue dye by a ligninolytic enzyme-producing Bacillus thuringiensis: Degradation products and pathway. *Enzyme and Microbial Technology*, *156*. https://doi.org/10.1016/j.enzmictec.2022.109999

Xia, H., Li, N., Zhong, X., & Jiang, Y. (2020). Metal-Organic Frameworks: A Potential Platform for Enzyme Immobilization and Related Applications. *Frontiers in Bioengineering and Biotechnology*, *8*(June), 1-16. https://doi.org/10.3389/fbioe.2020.00695

Xiao, T., & Liu, D. (2019). Progress in the synthesis, properties and applications of ZIF-7 and its derivatives. In *Materials Today Energy* (Vol. 14): Elsevier Ltd.

Xu, G. R., An, Z. H., Xu, K., Liu, Q., Das, R., & Zhao, H. L. (2021). Metal organic framework (MOF)-based micro/nanoscaled materials for heavy metal ions removal: The cutting-edge study on designs, synthesis, and applications. *Coordination Chemistry Reviews*, *427*. https://doi.org/10.1016/j.ccr.2020.213554

Xu, R., Zhang, X., Zelekew, O. A., Schott, E., & Wu, Y. N. (2023). Improved stability and activity of laccase through de novo and post-synthesis immobilization on a

hierarchically porous metal-organic framework (ZIF-8). *RSC Advances*, *13*(25), 17194-17201. https://doi.org/10.1039/d3ra01571h

Xu, S., Liang, J., Mohammad, M. I. B., Lv, D., Cao, Y., Qi, J., Liang, K., & Ma, J. (2021). Biocatalytic metal–organic framework membrane towards efficient aquatic micropollutants removal. *Chemical Engineering Journal*, *426*. https://doi.org/10.1016/j.cej.2021.131861

Xue, S., Li, J., Zhou, L., Gao, J., Liu, G., Ma, L., He, Y., & Jiang, Y. (2019). Simple Purification and Immobilization of His-Tagged Organophosphohydrolase from Cell Culture Supernatant by Metal Organic Frameworks for Degradation of Organophosphorus Pesticides. *Journal of Agricultural and Food Chemistry*, *67*(49), 13518-13525. https://doi.org/10.1021/acs.jafc.9b05206

Yang, C., Zhu, Y., Wang, J., Sun, W., Yang, L., Lin, H., & Lv, S. (2021). A novel granular MOF composite with dense and ordered MIL-100(Fe) nanoparticles grown on porous alumina: Green synthesis and enhanced adsorption of tetracycline hydrochloride. *Chemical Engineering Journal*, *426*. https://doi.org/10.1016/j.cej.2021.131724

Yang, K., & He, Z. (2025). Integrating oxidation and reduction processes in electrochemical wastewater treatment for contaminant removal with byproduct control. *Water Research*, *282*, 123632. https://doi.org/https://doi.org/10.1016/j.watres.2025.123632

Yang, W., Wang, J., Han, Y., Luo, X., Tang, W., Yue, T., & Li, Z. (2021). Robust MOF film of self-rearranged UiO-66-NO2 anchored on gelatin hydrogel via simple thermal-treatment for efficient Pb(II) removal in water and apple juice. *Food Control*, *130*. https://doi.org/10.1016/j.foodcont.2021.108409

Yang, X., Zhao, J., Cavaco-Paulo, A., Su, J., & Wang, H. (2023). Encapsulated laccase in bimetallic Cu/Zn ZIFs as stable and reusable biocatalyst for decolorization of dye wastewater. *International Journal of Biological Macromolecules*, *233*. https://doi.org/10.1016/j.ijbiomac.2023.123410

Yang, Y., Zhang, X., Jiang, J., Han, J., Li, W., Li, X., Yee Leung, K. M., Snyder, S. A., & Alvarez, P. J. J. (2022). Which Micropollutants in Water Environments Deserve More Attention Globally? *Environmental Science and Technology*, *56*(1), 13-29. https://doi.org/10.1021/acs.est.1c04250

Yin, R., Zhang, Y., Wang, Y., Zhao, J., & Shang, C. (2024). Far-UVC Photolysis of Peroxydisulfate for Micropollutant Degradation in Water. *Environmental*

Science and Technology, *58*(13), 6030-6038. https://doi.org/10.1021/acs.est.3c09120

Yoon, S. S., Lee, H. K., & Hong, S. R. (2021). Co2/n2 gas separation using pebax/zif-7—psf composite membranes. *Membranes*, *11*(9). https://doi.org/10.3390/membranes11090708

Younis, S. R. A., Abdelmotallieb, M., & Ahmed, A. S. A. (2025). Facile synthesis of ZIF-8@GO composites for enhanced adsorption of cationic and anionic dyes from their aqueous solutions. *RSC Advances*, *15*(11), 8594-8608. https://doi.org/10.1039/d4ra08890e

Yu, R., & Wu, Z. (2020). High adsorption for ofloxacin and reusability by the use of ZIF-8 for wastewater treatment. *Microporous and Mesoporous Materials*, *308*. https://doi.org/10.1016/j.micromeso.2020.110494

Yuan, S., Zou, L., Qin, J. S., Li, J., Huang, L., Feng, L., Wang, X., Bosch, M., Alsalme, A., Cagin, T., & Zhou, H. C. (2017). Construction of hierarchically porous metal-organic frameworks through linker labilization. *Nature Communications*, *8*. https://doi.org/10.1038/ncomms15356

Yusuf, V. F., Malek, N. I., & Kailasa, S. K. (2022). Review on Metal–Organic Framework Classification, Synthetic Approaches, and Influencing Factors: Applications in Energy, Drug Delivery, and Wastewater Treatment. *ACS Omega*, *7*(49), 44507-44531. https://doi.org/10.1021/acsomega.2c05310

Zdarta, J., Jesionowski, T., Pinelo, M., Meyer, A. S., Iqbal, H. M. N., Bilal, M., Nguyen, L. N., & Nghiem, L. D. (2022). Free and immobilized biocatalysts for removing micropollutants from water and wastewater: Recent progress and challenges. *Bioresource Technology*, *344*(PB), 126201-126201. https://doi.org/10.1016/j.biortech.2021.126201

Zeraati, M., Rahdar, A., Medina, D. I., & Sargazi, G. (2021). Synthesis of Al-Based Metal-Organic Framework in Water With Caffeic Acid Ligand and NaOH as Linker Sources With Highly Efficient Anticancer Treatment. *Frontiers in Chemistry*, *9*. https://doi.org/10.3389/fchem.2021.784461

Zhang, H., Luo, J., Woodley, J. M., & Wan, Y. (2021). Confining the motion of enzymes in nanofiltration membrane for efficient and stable removal of micropollutants. *Chemical Engineering Journal*, *421*(P2), 127870-127870. https://doi.org/10.1016/j.cej.2020.127870

Zhang, J., Zhang, T., Yu, D., Xiao, K., & Hong, Y. (2015). Transition from ZIF-L-Co

to ZIF-67: A new insight into the structural evolution of zeolitic imidazolate frameworks (ZIFs) in aqueous systems. *CrystEngComm*, *17*(43), 8212-8215. https://doi.org/10.1039/c5ce01531f

Zhang, P., Li, Y., Tang, Y., Shen, H., Li, J., Yi, Z., Ke, Q., & Xu, H. (2020). Copper-Based Metal-Organic Framework as a Controllable Nitric Oxide-Releasing Vehicle for Enhanced Diabetic Wound Healing. *ACS Applied Materials and Interfaces*, *12*(16), 18319-18331. https://doi.org/10.1021/acsami.0c01792

Zhang, R., Wang, L., Han, J., Wu, J., Li, C., Ni, L., & Wang, Y. (2020). Improving laccase activity and stability by HKUST-1 with cofactor via one-pot encapsulation and its application for degradation of bisphenol A. *Journal of Hazardous Materials*, *383*(May 2019), 121130-121130. https://doi.org/10.1016/j.jhazmat.2019.121130

Zhang, S., Wu, Z., Chen, G., & Wang, Z. (2018). An improved method to encapsulate laccase from trametes versicolor with enhanced stability and catalytic activity. *Catalysts*, *8*(7). https://doi.org/10.3390/catal8070286

Zhang, Y., Hu, P., Muhammad, Y., Tang, Y., Shao, S., Gao, Z., Wang, J., Wang, R., Hu, Y., Kuang, L., Zhao, Z., & Zhao, Z. (2021). High-density immobilization of laccase on hollow nano-sphere NH2-MIL88(Fe) host with interfacial defects to improve enzyme activity and stability for remazol brilliant blue R decolorization. *Chemical Engineering Journal*, *405*. https://doi.org/10.1016/j.cej.2020.127003

Zhang, Y., Jia, Y., Li, M., & Hou, L. a. (2018). Influence of the 2-methylimidazole/zinc nitrate hexahydrate molar ratio on the synthesis of zeolitic imidazolate framework-8 crystals at room temperature. *Scientific Reports*, *8*(1), 1-8. https://doi.org/10.1038/s41598-018-28015-7

Zhang, Y., Lin, Z., He, Q., Deng, Y., Wei, F., Xu, C., Fu, L., & Lin, B. (2022). Enhanced aqueous stability and long-acting antibacterial of silver-based MOFs via chitosan-crosslinked for fruit fresh-keeping. *Applied Surface Science*, *571*. https://doi.org/10.1016/j.apsusc.2021.151351

Zhao, P., Lampronti, G. I., Lloyd, G. O., Wharmby, M. T., Facq, S., Cheetham, A. K., & Redfern, S. A. T. (2014). Phase transitions in zeolitic imidazolate framework 7: The importance of framework flexibility and guest-induced instability. *Chemistry of Materials*, *26*(5), 1767-1769. https://doi.org/10.1021/cm500407f

Zhao, X., Fang, X., Wu, B., Zheng, L., & Zheng, N. (2014). Facile synthesis of size-

tunable ZIF-8 nanocrystals using reverse micelles as nanoreactors. *Science China Chemistry*, *57*(1), 141-146. https://doi.org/10.1007/s11426-013-5008-4

Zheng, Z., Alawadhi, A. H., & Yaghi, O. M. (2023). Green Synthesis and Scale-Up of MOFs for Water Harvesting from Air. *Molecular Frontiers Journal*, *07*(01n02), 20-39. https://doi.org/10.1142/s2529732523400011

Zhou, H. C., Long, J. R., & Yaghi, O. M. (2012). Introduction to metal-organic frameworks. *Chemical Reviews*, *112*(2), 673-674. https://doi.org/10.1021/cr300014x

Zhou, W. (2019). Reversed crystal growth. In *Crystals* (Vol. 9): MDPI AG.

Zhou, W., Zhang, W., & Cai, Y. (2022). Enzyme-enhanced adsorption of laccase immobilized graphene oxide for micro-pollutant removal. *Separation and Purification Technology*, *294*, 121178. https://doi.org/https://doi.org/10.1016/j.seppur.2022.121178

Zhu, D., Wu, Q., & Wang, N. (2011). Industrial Enzymes. *Comprehensive Biotechnology, Second Edition*, *3*, 3-13. https://doi.org/10.1016/B978-0-08-088504-9.00182-3

Zulkifli, N. S., & Abd Manaf, L. (2024). Exploring the informal learning of zero waste lifestyle in Malaysia with big data analytics. *Cleaner and Responsible Consumption*, *12*, 100182. https://doi.org/https://doi.org/10.1016/j.clrc.2024.100182

APPENDICES

APPENDIX A

The Standard Curve of BSA Concentration

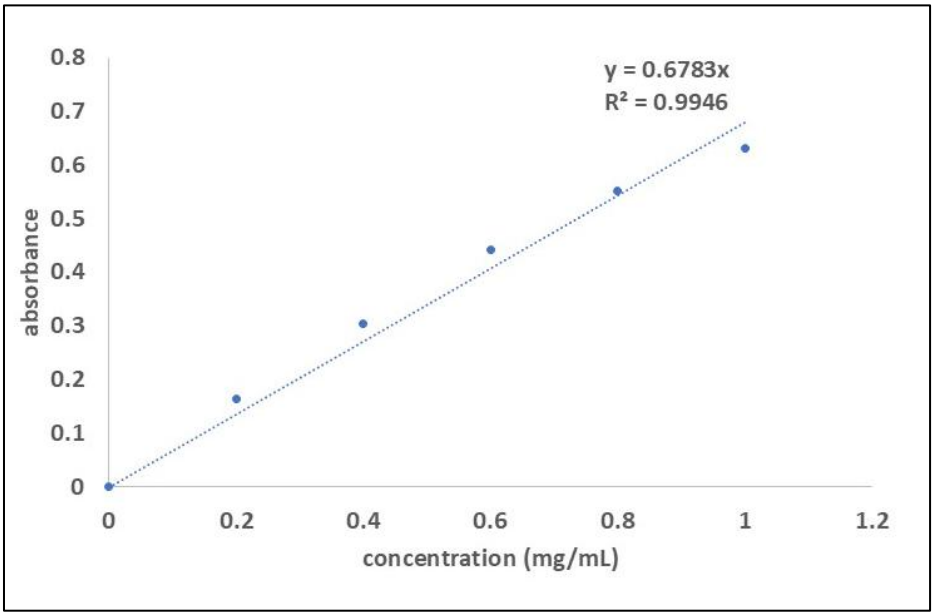

APPENDIX B

The Standard Curve of ABTS Concentration

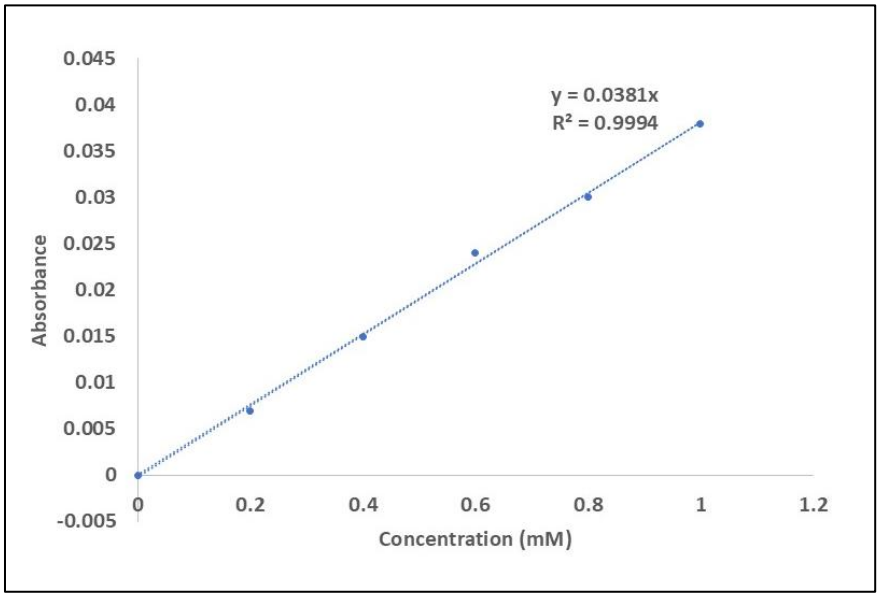

APPENDIX C

The Standard Curve of Methylene Blue Concentration

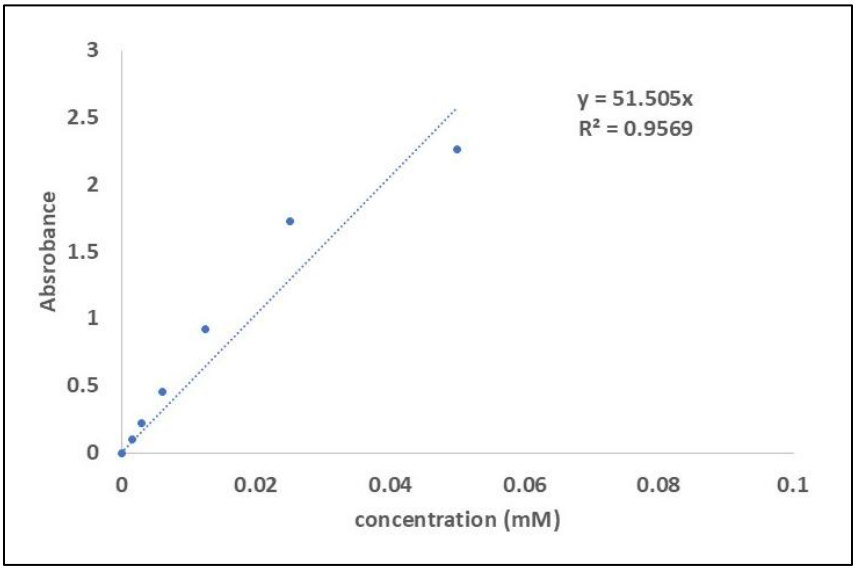

AUTHOR'S PROFILE

Amirah Syakirah Zahirulain obtained Bachelor of Engineering (Hons.) Chemical Engineering in 2020 from Universiti Teknologi MARA. Then, she continues her study in Master's in Science (Chemical Engineering) from Universiti Teknologi MARA. Her master's in science thesis involves the Metal-Organic Framework (MOF) synthesis specifically in Zeolitic Imidazolate Framework (ZIF) by using water solvent and enzyme technology by embedding enzyme into MOF for biocatalysis of water micropollutant.

LIST OF PUBLICATIONS

Marpani, F., Pauzi, S. M., Othman, F., Zahirulain, A. S., Alias, N. H., Shayuti, M. S. M., & Othman, N. H. Recent Approaches in Quantum Dots Application for Biological System. Chemical Engineering Transactions, 2023. 106,1207-1212. https://doi.org/10.3303/CET23106202

Zahirulain, A. S., Marpani, F., Him, N. R. N., Shayuti, M. S. M., Sharma, V., & Rahman, N. A., Influence of Different Solvents on the Structure of ZIF-67 for Enzyme Immobilization Matrices. Jurnal Kejuruteraan, 2025. 37(07), 3483-3492. https://dx.doi.org/10.17576/jkukm-2025-37(7)-27

LAMPIRAN MAKLUMAT BAHAN

JUDUL BAHAN (TESIS):

LACCASE IMMOBILIZATION IN ZEOLITIC IMIDAZOLATE METAL-ORGANIC FRAMEWORKS FOR WATER MICROPOLLUTANT REMOVAL VIA BIOCATALYSIS AND ADSORPTION